Mechanisms of Regulation and Fidelity in Tail-Anchored Membrane Protein Targeting

Thesis by

Meera Rao

In Partial Fulfillment of the Requirements for the

Degree of

Doctor of Philosophy

CALIFORNIA INSTITUTE OF TECHNOLOGY

Pasadena, California

2016

(Defended May 19, 2016)

Meera Rao

ORCID: 0000-0001-8650-6253

Acknowledgements

First, I would like to thank my advisor, Dr. Shu-ou Shan, for her valuable guidance during my graduate work. She has inspired me through her unrelenting pursuit of the truth in nature. I have benefited tremendously from her commitment to giving her students the best training she can. It has been an honor to work under her guidance.

I am grateful to my thesis committee, Dr. David Chan, Dr. William "Bil" Clemons, and Dr. Douglas Rees, for their supportive comments and suggestions over the years. In addition, I would like to acknowledge a few the many mentors in my undergraduate career that encouraged me in my pursuit of research: my academic advisor Dr. Ponzy Lu; my research advisor, Dr. Marni Falk; and Dr. Philip Nelson.

I am lucky to be a part of the sacred and rich community within the Shan Lab. Collectively, this group is bound by a strong commitment to science and to each other. Within the Shan Lab I have made numerous valuable friendships and collaborations. Thank you to David Akopian, Aileen Ariosa, Sowmya Chandrasekar, Yu-Hsien Hwang Fu, Peera Jaru-Ampornpan, Jae Ho Lee, George Liang, Vinh Lam, Camille McAvoy, Thang Nguyen, Nathan Pierce, Ishu Saraogi, Shuai Wang, Chien I Yang, and Xin Zhang.

Special thanks to the Shan Lab "GET Team": Un Seng Chio, Hyun Ju Cho, and Michael Rome. Their collaboration, support, and feedback were crucial

to the development of the work in this thesis.

Collaboration outside of the Shan lab has been an important part of my research experience at Caltech. Our collaboration with the Clemons lab has been incredibly valuable. In addition to Bil, I would like to thank Justin Chartron, Harry Gristick, Geoffrey Lin, Jeeyoung Mock, and Christian Suloway for their many structural insights and foundational work in the GET pathway. In addition, I would like to thank Voytek Okreglak and Dr. Peter Walter for their contributions to the work outlined in Chapter 3.

I would also like to thank the very supportive administration and staff at Caltech, whose support made it easier to do my work: Luz Castillo, Joe Drew, Margot Hoyt, Santiago Laparra, Blanca, Mariona, and Alison Ross.

I could not have finished my graduate work without the support from my friends. At Caltech, I am lucky to have had the friendship of Aileen Ariosa, Rebecca Rojansky, Jeeyoung Mock, and Sowmya Chandrasekar who have all contributed to my development as a scientist and friend. Outside Caltech, I would like to acknowledge Theresa Alog, Avery Berge, Laura King, Tanvi Rastogi, Adrienne Russman, and Tiffany Wang. Their friendship over the years has been wonderful; they have ushered me through many transitions at different stages throughout my life.

My family has also been strong support throughout my life. I thank my parents for their unconditional love and for inspiring a love of science in me at a

young age. I also thank my aunts (the other Drs. Rao) for their encouragement. Finally, I am grateful to my partner, Kayvon Namvar, for his love and support.

Abstract

Accurate protein localization is crucial to generate and to maintain cellular organization. Achieving accuracy is challenging, as the molecular signals that dictate a protein's destination are often promiscuous. The localization of tail-anchored (TA) proteins, whose transmembrane domain resides at its extreme C-terminus, presents major challenges to protein targeting machineries. This dissertation explores how TA capture and release are spatially and temporally regulated in the Guided Entry of Tail Anchored proteins (GET) pathway and how endoplasmic reticulum (ER) destined TAs are targeted with high fidelity.

A quantitative framework of the Get3 ATPase cycle reveals that ATP and GET pathway effector proteins specifically induce multiple conformational changes in Get3, which culminate in the ATPase activation that drives unidirectional targeting in the pathway. The Get4/5 TA loading complex locks Get3 in the ATP-bound state that is primed for TA protein capture, whereas the TA substrate induces tetramerization of Get3 and activates its ATPase reaction.

Additional analyses define multiple physicochemical features that distinguish TA proteins destined to different organelles. The GET pathway selects for these features at distinct stages using mechanisms such as differential binding, induced fit, and kinetic proofreading after ATP hydrolysis by Get3. These results reveal new roles for the cochaperone Sgt2 in providing key selection filters, and provide a biological logic for the complex cascade of substrate relay events during post-translational membrane protein targeting.

Published Content and Contributions

1. Rome, M.E., Rao, M., Clemons, W.M., and Shan, S.-O. (2013). Precise timing of ATPase activation drives targeting of tail-anchored proteins. Proc Natl Acad Sci USA *110*, 7666–7671.

   M.E. Rome and M.Rao contributed to this work equally. M. Rao. participated in the conception of the project, designed experiments, conducted experiments, and participated in the writing of the manuscript.

2. Rao, M., Okreglak, V., Chio, U., Cho, H., Shan, S. (2016) Multiple selection filters ensure accurate tail-anchored membrane protein targeting *In Preparation*

   M.Rao contributed to this work equally. M. Rao. participated in the conception of the project, designed experiments, conducted experiments, and participated in the writing of the manuscript.

Table of Contents

Chapter 1 : Introduction

How cells achieve and maintain a high level of internal organization in a dynamic and crowded inner environment is a fundamental question in biology. To maintain order within a cell, specific interactions between macromolecular complexes must be precisely controlled in space and time.

One of the major organizational challenges for the cell is efficient and accurate protein localization. Proteins destined for lipid membranes present a special challenge. When membrane proteins are synthesized by cytosolic ribosomes, their hydrophobic transmembrane domains (TMDs) must be shielded from the aqueous cytosol until their stable integration into their target membrane. If a membrane protein is not properly targeted, it is prone to irreversible aggregation that can result in mis-localization and proteostatic stress (Shao and Hegde, 2011).

While numerous membrane-protein targeting pathways have been identified in prokaryotes and eukaryotes (Cross et al., 2009) they share three fundamental features. (1) A molecularly encoded signal that determines cellular localization; (2) multi-state targeting machineries that recognize the signal and cycle between the cytosol and membrane; and (3) robust spatial and temporal coordination of substrate binding and release cycles (Akopian et al., 2013b).

One elegant way the cell prevents TMD aggregation during protein targeting is to use the co-translational signal recognition particle (SRP) pathway. Through a series of highly coordinated interactions with the SRP receptor (SR),

SRP recognizes an N-terminal hydrophobic signal sequence soon after it emerges from the ribosome and targets the nascent chain to the translocon at the endoplasmic reticulum (ER) membrane. Once the ribosome is docked on the translocon, the hydrophobic TMDs are translated directly into the membrane (Shao and Hegde, 2011).

Due to their topology, tail-anchored (TA) proteins, which contain a single TMD at their extreme C-terminus, are excluded from the SRP pathway and must be post-translationally targeted (Hegde and Keenan, 2011; Kutay et al., 1995). TAs comprise 3-5% of the membrane proteome (Hegde and Keenan, 2011) and mediate diverse cellular processes including protein translocation, vesicular transport, and protein quality control (Claessen et al., 2010; Hegde and Keenan, 2011). While TA proteins are found in nearly all eukaryotic membranes, they are post-translationally targeted to the ER, the mitochondrial outer membrane (OMM), and peroxisomes (Chen et al., 2014; Kutay et al., 1993). Regardless of target membrane, the C-terminal TMD is both necessary and sufficient to ensure the appropriate localization of TA proteins (Beilharz, 2003; Whitley et al., 1996).

In the TRC40/GET (Guided Entry of Tail-anchored proteins) pathway, a complex protein interaction cascade delivers TA proteins to the ER (Hegde and Keenan, 2011; Schuldiner et al., 2008; Stefanovic and Hegde, 2007). TA proteins are initially captured by the chaperone Sgt2 in yeast (Chartron et al., 2011; Wang et al., 2010) or the BAG6 complex in mammalian cells (Mariappan et al., 2010). The Get4/5 complex (or its mammalian homologue TRC35/Ubl4a), which binds both Sgt2 (or Bag6) and the Get3 ATPase (or its mammalian homologue

TRC40) (Jonikas et al., 2009; Schuldiner et al., 2008), then enables the loading of TA protein from Sgt2 onto Get3, the central dimeric ATPase in the pathway (Wang et al., 2010; 2011a). The Get3/TA complex then binds its receptor, the Get1/2 complex, on the ER membrane, upon which the TA protein is released from Get3 and inserted into the membrane (Mariappan et al., 2011; Schuldiner et al., 2008; Stefer et al., 2011). This dissertation aims to explore how TA substrate capture and release are spatially and temporally regulated in the GET pathway and how ER destined TA substrates are targeted with high fidelity.

Studies of spatial and temporal regulation in the GET pathway initially focused on Get3 for two reasons: (i) Get3 is a TA associated protein that cycles between the cytosol and the ER membrane and has been shown to interact with Get1, Get2, and Get4/5 (ii) Determining when and where ATP hydrolysis occurs provides insights into why ATP is required for TA targeting and what drives unidirectionality in the system.

An abundance of structural information highlights that the nucleotide state of Get3 leads to multiple conformations (Bozkurt et al., 2009; Hu et al., 2009; Mateja et al., 2009; Suloway et al., 2009; Yamagata et al., 2010). These range from an open state in apo-Get3 in which the helical subdomains within the dimer are separated, to more closed conformations in AMP-PNP or ADP•AlF_4^--bound Get3 in which the helical domains form a contiguous hydrophobic groove later shown to mediate TA protein binding (Mateja et al., 2015).

Biochemical and structural data also indicate that different GET pathway effector proteins have preferences for different nucleotide states of Get3

(Gristick et al., 2014; Kubota et al., 2012; Mariappan et al., 2011; Rome et al., 2014; Stefer et al., 2011). Data from multiple groups suggest that Get4 preferentially binds Get3 in an ATP-bound state, which is primed for substrate loading in the structure (Chartron et al., 2010; Gristick et al., 2014; Wang et al., 2010; 2011b). In contrast, the Get1 cytosolic domain preferentially binds apo-, open Get3 strongly suggesting that Get1 promotes the release of nucleotide and TA proteins from Get3 at the end of the targeting cycle (Kubota et al., 2012; Mariappan et al., 2011; Stefer et al., 2011).

Chapter 2 addresses many broad questions regarding how the Get3 ATPase cycle drives the efficient delivery of TA proteins: (i) When, where and how do ATP binding and hydrolysis occur in the GET pathway? (ii) What is the full range of conformations that Get3 can sample and to what extent do nucleotides and GET pathway effector proteins select for, or interact with, these conformations? (iii) Why is such a complex cascade of interactions necessary? Why is Get3 unable to directly capture the TA substrate and how does the Get4/5 complex drive the transfer of TA proteins to Get3? (iv) While the predominant model for TA protein binding invokes a closed Get3 dimer (Mateja et al., 2009; 2015), there is also evidence for a tetrameric Get3 complex: recombinant Get3/TA complexes are predominantly tetramers in size exclusion chromatography, and several archaeal Get3 homologues form obligate tetramers (Bozkurt et al., 2009; Suloway et al., 2011). Whether and how dimeric and tetrameric Get3 functions in TA protein targeting remain unclear.

As a result of establishing a quantitative framework for the ATPase cycle of *Saccharomyces cerevisiae (Sc)* Get3 we demonstrate that Get4/5 and the TA substrate actively regulate this cycle to ensure the precise timing of ATP hydrolysis. These results provide an explicit model for how Get3's ATPase cycle is coupled to conformational changes that drive TA protein targeting.

Chapter 3 addresses the molecular basis for substrate selection in the GET pathway. We address how a single C-terminal TMD provides sufficient molecular information to differentiate TA proteins destined to diverse organelles. While it has been established that the C-terminal TMD of a TA protein is sufficient for its association with both Sgt2 and Get3 (Wang et al., 2010), it is unclear how the GET pathway senses and selects for TAs destined to the ER. Previous work has noted that hydrophobicity of TMDs and basic residues at the extreme C-termini contribute to TA localization (Borgese et al., 2007; 2003; Rapaport, 2003). Our results rigorously define two properties that allow targeting machineries to discriminate TA proteins destined to different organelles. The GET pathway senses these properties at distinct stages and uses a variety of selection mechanisms including differential binding, induced fit, and kinetic proofreading after ATP hydrolysis by Get3. These results also reveal new roles for the cochaperone Sgt2 in providing key selection filters, and define a biological logic for the complex cascade of substrate relay events during post-translational membrane protein targeting.

Chapter 2 : Precise Timing of ATPase Activation Drives Targeting of Tail-anchored Proteins

A version of this chapter was first published as: Rome, M.E.*, Rao, M.*, Clemons, W.M., and Shan, S. O. (2013). Precise timing of ATPase activation drives targeting of tail-anchored proteins. Proc. Natl. Acad. Sci. *110*, 7666–7671

Abstract

The localization of tail-anchored (TA) proteins, whose transmembrane domain resides at the extreme C-terminus, presents major challenges to cellular protein targeting machineries. In eukaryotic cells, the highly conserved ATPase Get3 coordinates the delivery of TA proteins to the endoplasmic reticulum (ER). How Get3 uses its ATPase cycle to drive this fundamental process remains unclear. Here, we establish a quantitative framework for the Get3 ATPase cycle and show that ATP specifically induces multiple conformational changes in Get3 that culminate in its ATPase activation through tetramerization. Further, upstream and downstream components actively regulate the Get3 ATPase cycle to ensure the precise timing of ATP hydrolysis in the pathway: the Get4/5 TA loading complex locks Get3 in the ATP-bound state and primes it for TA protein capture, whereas the TA substrate induces tetramerization of Get3 and activates its ATPase reaction 100-fold. Our results establish a precise model for how Get3 harnesses the energy from ATP to drive the membrane localization of TA proteins, and provide new insights into how dimerization-activated nucleotide hydrolases regulate diverse cellular processes.

Introduction

Proper localization of membrane proteins is essential for the structure and function of all cells. Tail-anchored (TA) proteins, which contain a single transmembrane domain at their extreme C-terminus, comprise 3-5% of the membrane proteome (Hegde and Keenan, 2011) and mediate diverse cellular processes including protein translocation, vesicular transport, and protein quality control (Claessen et al., 2010; Hegde and Keenan, 2011). Due to their topology, TA proteins cannot engage co-translational protein targeting machineries, and instead must use post-translational mechanisms for efficient and accurate delivery to the target membrane (Hegde and Keenan, 2011; Kutay et al., 1995).

In the GET (Guided Entry of Tail-anchored proteins) pathway, a complex protein interaction cascade delivers TA proteins to the endoplasmic reticulum (ER) (Claessen et al., 2010; Hegde and Keenan, 2011; Schuldiner et al., 2008; Stefanovic and Hegde, 2007). TA proteins are initially captured by the chaperone Sgt2 in yeast (Chartron et al., 2011; Wang et al., 2010) or the BAG6 complex in mammalian cells (Mariappan et al., 2010). The Get4/5 complex (or its mammalian homologue TRC35/Ubl4a), which binds both Sgt2 (or Bag6) and the Get3 ATPase (or its mammalian homologue TRC40) (Jonikas et al., 2009; Schuldiner et al., 2008), then enables the loading of TA protein from Sgt2 onto Get3, the central ATPase in the pathway (Wang et al., 2010; 2011a). The Get3/TA complex then binds its receptor, the Get1/2 complex on the ER

membrane, upon which the TA protein is released from Get3 and inserted into the membrane (Mariappan et al., 2011; Schuldiner et al., 2008; Stefer et al., 2011). TA protein insertion is an ATP-dependent process (Kutay et al., 1995) driven by Get3/TRC40, an obligate ATPase homodimer (Chartron et al., 2012b; Mateja et al., 2009; Schuldiner et al., 2008; Stefanovic and Hegde, 2007; Suloway et al., 2009). Twenty-one Get3 structures, solved in various nucleotide states, show that nucleotide occupancy in the Get3 ATPase domain allows adjustments at its dimer interface that are amplified into larger displacements of its helical domains. This leads to various structures, from open conformations in apo-Get3 in which the helical subdomains are separated, to more closed conformations in AMPPNP- or ADP•AlF_4^--bound Get3 in which the helical domains form a contiguous hydrophobic groove proposed to mediate TA protein binding (Bozkurt et al., 2009; Hunter, 2009; Mateja et al., 2009; Suloway et al., 2009; Yamagata et al., 2010). Further, the Get1 cytosolic domain preferentially binds apo-, open Get3 (Kubota et al., 2012; Mariappan et al., 2011; Stefer et al., 2011), strongly suggesting that Get1 promotes the release of nucleotide and TA proteins from Get3 at the end of the targeting cycle.

Despite rich structural information, many key questions remain regarding how the Get3 ATPase cycle drives the efficient delivery of TA proteins. First, when, where and how ATP binding and hydrolysis occur in the GET pathway has been unclear. Second, ADP-bound Get3 has been solved in both open and closed structures (Mateja et al., 2009; Yamagata et al., 2010), raising questions as to the specificity of Get3 in recognizing nucleotides and generating

nucleotide-driven conformational changes. Third, the nucleotide states of Get3 required for interacting with Get4/5 or for Get4/5-mediated loading of TA proteins remain controversial (Chartron et al., 2010; Wang et al., 2010; 2011a). Most importantly, models based on a two-state open ⇔ closed transition are insufficient to explain the complex cascade of protein interactions that must be coordinated by Get3, which requires multiple functional states in this ATPase.

The requirement for the Sgt2•Get4/5 complex in the GET pathway raises additional questions. Why is Get3 unable to directly capture the TA substrate? How does the Get4/5 complex drive the transfer of TA proteins to Get3? Thus far, Get4/5 appears to be nothing more than a scaffold that brings Sgt2 and Get3 into close proximity. Whether Get4/5 can actively facilitate TA protein capture by Get3 is unclear.

Finally, while the predominant model for TA protein binding invokes a closed Get3 dimer (Mateja et al., 2009), there is also evidence for a tetrameric Get3 complex: recombinant Get3/TA complexes are predominantly tetramers in size exclusion chromatography, and several archaeal Get3 homologues form obligate tetramers (Bozkurt et al., 2009; Suloway et al., 2011). Whether and how a Get3 tetramer functions in TA protein targeting remain unclear.

To address these questions, here we establish a quantitative framework for the ATPase cycle of *Saccharomyces cerevisiae (Sc)* Get3. We demonstrate that Get4/5 and the TA protein substrate actively regulate this cycle to ensure the precise timing of ATP hydrolysis. These results provide an explicit model for

how Get3's ATPase cycle is coupled to conformational changes that drive TA protein targeting.

Results

Cooperative ATP binding to Get3. We began by establishing a quantitative framework for the Get3 ATPase cycle (Fig. 2.1). To probe for nucleotide-driven conformational changes, we compared Get3's activity under two conditions: (i) 'single-site' conditions, in which Get3 is in 10–1000 fold excess over the nucleotide so that, statistically the majority of nucleotide-bound Get3 dimers have a single ATPase site occupied; and (ii) 'multi-site' conditions, in which the nucleotide is in excess over Get3 so that both ATPase sites are occupied. Nucleotide binding to Get3 is measured using both ATPase assays (Fig. 2.2A and Supporting Information (SI): Fig. S2.1A) and direct measurements based on changes in anisotropy of the fluorescent ATP analogue 2'-/3'-O-(N'-methylanthraniloyl)-ATP (mantATP; Fig. 2.2B). Under single-site conditions, Get3 binds ATP weakly and displays no discrimination between ATP and ADP (Fig. 2.2A, B; Fig. 2.1 & SI: Table S2.1, K_1 & K_9). In contrast, under 'multi-site' conditions, Get3's ATPase reaction exhibited a cooperative dependence on ATP concentration, giving a Hill co-efficient of 2 and a ~10-fold higher affinity for binding of the second ATP (Fig. 2.2C; Fig. 2.1 & SI: Table S2.1, K_3).

To test the specificity of this cooperative effect, we directly measured the rates of nucleotide binding to and release from Get3 using: (i) environmentally

sensitive changes in mantATP under single-site conditions (SI: Fig. S2.1B); and (ii) FRET between a native tryptophan in Get3 and mantATP under multi-site conditions (SI: Fig. S2.1C; (Mariappan et al., 2011)). These measurements show that ATP binds two-fold faster and dissociates three-fold more slowly under multi-site conditions (Fig. 2.2D and SI: Fig. S2.2, black; Fig. 2.1 & SI: Table S2.1, k_1, k_{-1} vs. k_3, k_{-3}), providing independent support for cooperative ATP binding to Get3. This cooperativity is specific for ATP: compared to single-site conditions, the rate of mantADP binding was unchanged, and ADP release is over three-fold faster under multi-site conditions (Fig. 2.2D and SI: Fig. S2.2, gold; Fig. 2.1 & SI: Table S2.1, k_8, k_{-8} vs. k_9, k_{-9}), indicating that Get3 disfavors ADP occupancy at both active sites. Together, these results show that ATP specifically induces rearrangements in Get3 that lead to stronger binding of the second ATP molecule (Fig. 2.1, steps 1 & 3), whereas ADP does not.

Tetramerization of Get3 activates ATP hydrolysis and is required for TA protein targeting. Unexpectedly, the observed ATPase rate constant at saturating ATP concentrations, or k_{cat}, rises with increasing Get3 concentration (Figs. 2.2C & 2.3A). This phenomenon was observed even in the presence of BSA, an effective surfactant and crowding reagent, suggesting that it is unlikely to be caused by enzyme loss or inactivation at low concentrations. Instead, this result suggests that an oligomerization process stimulates Get3's ATPase activity. Quantitatively, these data are most consistent with a model in which dimeric Get3 is in dynamic equilibrium (K_d = 3.5 ± 1.9 μM) with tetrameric Get3,

which hydrolyzes ATP faster than dimeric Get3 (Fig. 2.1, steps 5–7; SI: Eq 2.9). Analysis of the data based on this model yielded a k_{cat} value for tetrameric Get3 of 1.3 ± 0.4 min^{-1} (Fig. 2.1 and Table S2.1, k_6), over 100-fold faster than dimeric Get3 (Fig. 2.3A and SI: Fig. S2.3A; Fig. 1 and Table S2.1, k_4). This phenomenon has previously escaped detection, likely because it is abolished in less physiological solution conditions (SI: Fig. S2.3B), whereas our ATPase measurements used the same buffer as for protein targeting/translocation reactions (Alberts, 2008). The transient nature of tetrameric Get3 could also render it susceptible to dissociation during size exclusion chromatography (Kiekebusch et al., 2012).

In a structure of the *Methanocaldococcus jannaschii* (*Mj*) Get3 tetramer, helix 8 plays a key role in stabilizing the tetramer interface. Mutations of conserved hydrophobic residues in this helix, F192D, M193D and M196D, destabilize the tetramer (Suloway et al., 2011). To independently test whether tetramerization of *Sc*Get3 is responsible for ATPase activation, we mutated homologous residues in *Sc*Get3 (P199D/M200D, M200D/L201D; Fig. 2.3B). Given their location, these mutations are unlikely to affect the TA binding groove of the dimer, but would specifically disfavor the formation or conformation of the tetramer. These mutations reduced activated ATP hydrolysis at high Get3 concentrations to almost the same extent as mutant Δ181-210, a negative control that lacks a large portion of the putative TA-binding groove (Fig. 2.3A, B) and completely abolishes TA protein capture and targeting (SI: Fig. S2.4D). In contrast, the k_{cat} values at low Get3 concentrations, where it is primarily a dimer,

were largely unchanged in these mutants (Fig. 2.3A). As additional controls, we mutated residues in the putative TA binding groove of Get3 in the dimer model (F190D or I193D; (Mateja et al., 2009)). In contrast to the mutants designed to disrupt the tetramer, F190D and I193D exhibit over 10-fold higher ATPase activity and tetramerize more favorably than wildtype Get3 (SI: Fig. S2.3C and Table S2.3). These results provide independent evidence that formation of a Get3 tetramer is required for activated ATP hydrolysis.

If tetramerization of Get3 and its associated ATPase activation were important, it would also be manifested in the targeting reaction. To test this hypothesis, we quantitatively measured the targeting and translocation of a TA substrate, Sbh1p, to ER microsomes (SI: Fig. S2.4A). An NXT glycosylation site was engineered into the C-terminus of Sbh1p, whose glycosylation reports on successful translocation across the membrane. Both the translation lysate and ER microsomes were derived from a Δ*get3* strain, so that Sbh1p targeting is dependent solely on exogenously added Get3. The efficiency of Sbh1p targeting and translocation exhibited a cooperative dependence on Get3 concentration with a Hill coefficient of 2 (Fig. 2.3C and SI: Fig. S2.4B), suggesting that efficient targeting requires two Get3 dimers to further associate to form a tetramer. Additionally, mutants P199D/M200D and M200D/L201D exhibit defects in targeting (Fig. 2.3D and SI: Fig. S2.4C) that quantitatively correlate with their defects in tetramerization-induced ATPase activation (Fig. 2.3D). Combined with previous observations that mutants M200D and L201D are deficient in TA substrate binding and supporting cell growth (Mateja et al., 2009), these results

provide strong evidence that transient formation of a Get3 tetramer is required for efficient TA protein targeting.

Get4/5 enhances ATP binding but inhibits ATP hydrolysis by Get3. We next asked how the Get4/5 complex, which acts as a scaffold to facilitate TA protein loading from Sgt2 onto Get3, regulates the Get3 ATPase. Intriguingly, Get4/5 stoichometrically inhibits the ATPase activity of Get3 (Fig. 2.4A & SI: Fig. S2.5A). Analysis of the ATP concentration dependence of the reaction showed that the average K_M value is lowered to 1.4 ± 0.3 μM with Get4/5 present, indicating that Get3 binds ATP more strongly when it is bound to Get4/5 (Fig. 2.4B & SI: Fig. S2.5B). In contrast, Get4/5 reduced the value of k_{cat}, indicating specific inhibition of ATP hydrolysis (Fig. 2.4B). Thus, Get4/5 induces Get3 into an alternative conformation in which ATP is bound more tightly but held in a catalytically compromised structure.

To provide independent evidence for this model, we tested how Get4/5 alters nucleotide binding of Get3 using the FRET assay. Get4/5 did not affect the rate of ATP binding to Get3 (Fig. 2.4C) but reduced the rate of ATP dissociation from Get3 at least 10-fold (Fig. 2.4D), providing direct evidence that Get3 binds ATP more tightly when it is bound to Get4/5. This effect is specific for ATP, as under the same conditions ADP release from Get3 remained fast and was largely unaffected by Get4/5 (SI: Fig. S2.5C).

If Get4/5 induces stronger ATP binding to Get3, then ATP-bound Get3 would also bind more strongly to Get4/5. To test this prediction, we measured

complex formation between Get3 and Get4/5 using gel filtration chromatography. With apo-Get3, complex assembly was not detected even at micromolar protein concentrations (SI: Fig. S2.5D). In contrast, with saturating ATP present almost all Get3 formed a complex with Get4/5 (SI: Fig. S2.5E). These results, though qualitative, are consistent with previous pull-down experiments in which a stable Get3-4/5 complex was enriched in the presence of nucleotides (Chartron et al., 2010; Wang et al., 2010; 2011a) Together, these results show that Get4/5 preferentially binds ATP-loaded Get3 and reciprocally, interaction with Get4/5 enables ATP to be more tightly bound to Get3.

As the Get3 ATPase activity is activated upon tetramerization, we asked whether Get4/5 inhibits this activation. Get4/5 also stoichiometrically inhibits the ATPase reaction at high Get3 concentrations, where it is predominantly a tetramer (SI: Fig. S2.5A). With saturating Get4/5 and ATP, the ATPase rate constant stayed constant at 0.16 ± 0.07 min^{-1} and was independent of Get3 concentration (Fig. 2.4E). Thus, Get4/5 inhibits formation of the Get3 tetramer or the ATPase activation induced by tetramerization.

Mutants F190D and I193D exhibit higher ATPase activities than wildtype Get3 in both the dimeric and tetrameric forms; both of these activities are substantially reduced in the presence of Get4/5 (Fig. 2.4F). Thus, these superactive mutant ATPases provide stronger evidence that the ATPase activity of dimeric Get3 is also inhibited by the Get4/5 complex.

TA protein induces rapid ATP hydrolysis and locks Get3 in the ADP-bound

state.

We next asked how the TA protein substrate regulates the Gte3 ATPase. To this end, we co-expressed Get3 with Sbh1p. The Get3/Sbh1 complex purified predominantly as a tetrameric complex (SI: Fig. S2.6A), consistent with previous observations (Bozkurt et al., 2009; Suloway et al., 2011).

To determine the ATP hydrolysis rate from this complex, we carried out pre-steady-state measurements using a high ATP concentration and Get3 active sites in 1:5 stoichiometry relative to ATP. Under these conditions, the ATPase reaction exhibited two distinct kinetic phases: (i) an initial burst whose magnitude increased with increasing Get3 concentration (Fig. 2.5A & SI: Fig. S2.6B), representing a rapid first round of ATP hydrolysis; and (ii) a slower linear phase representing subsequent rounds of ATP turnover at steady-state. The rate constant for the first round of ATP hydrolysis is 3.3 ± 1.1 min^{-1} (SI: Eq 2.10), over 100-fold faster than that of the Get3 dimer. The rate constant for steady-state ATP turnover is 0.055 ± 0.001 min^{-1}, 60-fold slower than the first turnover. Thus, loading of TA protein onto Get3 activates one round of ATP hydrolysis, but subsequent ATP turnover is inhibited. Further, ATPase activation in the Get3/TA complex was not observed under single-site conditions (Fig. 2.5B; cf. Fig. 2.2A), suggesting that it requires both Get3 active sites to be bound with ATP. Finally, the magnitude of the burst phase is stoichiometric with the concentration of Get3 active sites, suggesting that all four ATPs in the Get3 tetramer are hydrolyzed during the first turnover.

To test whether nucleotide binding or release could be rate-limiting for the

observed ATPase rates, we used the fluorescence assays to directly measure these events. MantATP binding to the Get3/Sbh1 complex was slow and concentration-independent at the lowest concentrations tested under both multi-site (Fig. 2.5C & SI: Fig. S2.6C) and single-site conditions (SI: Fig. S2.6D), suggesting that a slow conformational change of the Get3/Sbh1 complex becomes rate-limiting for ATP binding. The rate of the dominant, slow phase in ATP binding is similar to that of the burst phase in the ATPase reaction (5.0 vs. 3.3 min^{-1}), suggesting that the ATPase rate constant observed here may still be limited by a conformational change that precedes hydrolysis.

Remarkably, dissociation of ADP is at least 100-fold slower in the Get3/Sbh1 complex compared to free Get3 (Fig. 2.5D and SI: Table S2.2) and is indistinguishable from that of ATP or non-hydrolyzable ATP analogues (SI: Fig. S2.6E and Table S2.2), suggesting that the nucleotides are bound tightly and shielded from solvent in this complex. Nevertheless, ADP release from the Get3/TA complex is still 200-fold faster than the steady-state ATPase rate and is unaffected by up to 10 mM inorganic phosphate (SI: Fig. S2.6E and Table S2.2). This indicates that an additional conformational step, rather than product release, is rate-limiting for steady-state ATP turnover. Together, these data argue that only one round of ATP hydrolysis occurs in the GET pathway, after which the Get3/TA complex is locked in a catalytically inactive state loaded with ADP, and disassembly of this complex would be needed to reset its ATPase cycle.

Discussion

Efficient and accurate delivery of membrane proteins often requires energy input from nucleotide triphosphates, which in the GET pathway is harnessed and utilized by the Get3 ATPase (Chartron et al., 2012b; Saraogi et al., 2011a). When, where, and how ATP binding and hydrolysis occur in the GET pathway remain open questions. Little is known about how Get3's nucleotide state, conformation and activity are regulated during TA protein targeting. Here, quantitative mechanistic analyses define a precise framework for Get3's ATPase cycle and elucidate how it is used to drive this fundamental cellular process.

Previous work showed that Get3's ATPase domain acts as a fulcrum at the dimer interface to generate a variety of structures (Chartron et al., 2012b). The cooperative ATP binding observed here supports a model in which Get3 changes from a largely open conformation in apo-Get3 to increasingly closed conformations upon successive ATP binding (Fig. 2.1, steps 1 & 3). Importantly, this cooperativity is specific to ATP but not ADP. Thus, an ADP-bound Get3 dimer remains in a largely open conformation (Suloway et al., 2009; Yamagata et al., 2010), despite the occasional observation of 'closed', ADP-bound Get3 structures (Bozkurt et al., 2009). Nevertheless, the cooperativity induced by ATP is fairly modest, ~10-fold. Together with previous work (Wereszczynski and McCammon, 2012), we speculate that Get3 exists in an ensemble of conformations that are in close equilibrium with one another, and each ATP binding event induces a modest shift in the conformational landscape. Thus,

even the Get3 dimer bound with both ATPs is not completely 'closed', and is termed *semi-closed* here (Fig. 2.1).

Intriguingly, Get3 is catalytically activated through tetramerization (Fig. 2.1, steps 5, 6). This phenomenon was previously suggested by the structure of an *Mj*Get3 tetramer and by the formation of tetrameric Get3/TA complexes (Suloway et al., 2011). Our findings, for the first time, provide a function for tetrameric Get3, showing that it is the active species for ATP hydrolysis and for efficient TA protein targeting. In further support of this model, hydrophobic residues in helix 8 that stabilize the tetramer interface are conserved (Suloway et al., 2009; 2011); their mutations disrupt ATPase activation and protein targeting by Get3 (this work) and lead to defects in cell viability and TA binding (Mateja et al., 2009; Suloway et al., 2011). Given the location of these residues, these phenotypes are difficult to reconcile with a dimeric model for Get3. Although each of these observations can be explained by alternative models, activation of Get3 via tetramerization provides a cohesive, unifying model that explains this diverse collection of data.

In vivo, tetramerization of Get3 by itself should be disfavored to minimize futile ATPase cycles. This could be achieved in part by the low *in vivo* concentration of Get3, ~1 μM (Ghaemmaghami et al., 2003), which is below the K_d value for tetramerization (3.5 μM). The results here further show that futile ATPase cycles of Get3 are minimized by the Get4/5 complex, which mediates the loading of TA proteins from Sgt2 onto Get3 (Wang et al., 2010; 2011a). Despite previous reports of Get4/5 binding to apo-Get3 (Chang et al., 2012), our

results demonstrate that Get4/5 preferentially binds ATP-loaded Get3 and locks it in the ATP-bound state (Fig. 2.6, step 2). This is achieved by tightening Get3's ATP binding but inhibiting its hydrolytic activity, particularly the tetramerization-induced activation of ATP hydrolysis. Get4/5 could exert these effects by inducing Get3 into a distinct, 'occluded' conformation in which its ATPase site is more closed but incompetent for hydrolysis (Fig. 2.1). In addition, Get4/5 could prevent Get3's tetramerization. The latter model is particularly attractive as it explains why Get5 is a stable dimer (Chartron et al., 2012a): a complete Get4/5 complex could hold two closed Get3 dimers in the ATP-bound state, priming them for subsequent tetramer formation once the TA protein is loaded onto Get3 (Fig. 2.6, step 3). Regardless of the model, our data show that Get4/5 is not a passive scaffold that simply brings Sgt2 and Get3 into close proximity. Rather, Get4/5 actively promotes TA protein loading onto Get3 by locking it in the correct nucleotide state and priming its conformation for TA substrate capture (Mariappan et al., 2010; Wang et al., 2010).

In contrast to Get4/5, multiple evidence strongly suggest that the TA protein induces the tetramerization and activation of Get3's ATPase activity (Fig. 2.6, step 3): (i) co-expression of TA protein with Get3 results in a stable Get3 tetramer (this work; (Bozkurt et al., 2009; Suloway et al., 2011)); (ii) Rapid ATP hydrolysis was observed with the Get3/TA complex, as would be expected for an activated Get3 tetramer. Several important lessons are learned from analysis of the Get3/TA complex. First, after the first round of ATP hydrolysis, subsequent ATP turnover is 60-fold slower and incompatible with the timescale

of protein targeting *in vivo*, arguing that only one round of ATP hydrolysis occurs in the GET pathway. Second, following ATP hydrolysis, Get3 is locked in a catalytically inactive state. Together with observations with the Get3•Get4/5 complex, these results demonstrate that the open-to-closed rearrangement of Get3 can be conceptually and experimentally uncoupled: even when Get3 is globally 'closed' and nucleotide release is slow, additional active site adjustments specifically regulate catalytic activity. We speculate that this relates to local rearrangements of the switch II loops (Chartron et al., 2012b), which provide multiple essential catalytic residues. The ADP-bound *Mj*Get3 tetramer structure possibly provides a view of a closed but catalytically inactive Get3 tetramer, in which the switch II loop is pulled away and incompatible for hydrolysis (Suloway et al., 2011). Finally, ADP release is substantially slowed in the Get3/TA complex and becomes indistinguishable from that of ATP, suggesting that the TA protein is dominant in inducing a closed Get3 tetramer.

In the context of the targeting cycle, TA-induced Get3 tetramer formation would be beneficial as the hydrophobic TM of the TA substrate can be completely protected in a cage at the tetrameric interface (Suloway et al., 2011), minimizing its potential aggregation (Fig. 2.6). Our results also suggest that following hydrolysis, ADP release from the Get3/TA complex may be delayed until Get3 finds the Get1/2 membrane receptor. Tetramer disassembly by this receptor would be needed to release the TA protein. As ATP- and Get1-binding to Get3 are strongly antagonistic to one another (Mariappan et al., 2011; Stefer

et al., 2011; Wang et al., 2011a), ATP hydrolysis in the Get3/TA complex likely primes it for disassembly at the membrane.

Collectively, our results lead to a new model for how the Get3 ATPase cycle is used to drive TA protein targeting (Fig. 2.6). Under cellular conditions, the majority of Get3 cooperatively binds ATP at both active sites, which induces it into a semi-closed conformation (step 1). ATP-loaded Get3 is preferentially captured by Get4/5, which brings Get3 into the vicinity of Sgt2 and induces the Get3 dimer into an 'occluded' conformation in which it is further closed but ATP hydrolysis is delayed (step 2). In this configuration, Get3 is primed to capture the TA substrate from Sgt2 (step 2). Loading of TA protein induces tetramerization of Get3 (step 3), which might also drive dissociation of Get3 from Get4/5. The tetrameric Get3/TA complex undergoes a rapid round of ATP hydrolysis, giving a stable ADP-loaded complex that binds its receptor, Get1/2, at the ER membrane (step 4). Tetramer disassembly, ADP dissociation, and TA protein release into the membrane are likely coupled, resulting in Get1 bound to apo-Get3 in the open conformation (step 5). ATP binding then releases Get3 from Get1 (Mariappan et al., 2011; Stefer et al., 2011; Wang et al., 2011a) to re-initiate the cycle.

Get3 is the only eukaryotic ATPase in the SIMIBI (for SRP, MinD, and BioD) family of deviant P-loop NTPases, including the SRP and SRP receptor (SR) that mediate co-translational protein targeting (Leipe et al., 2002). Although the details of each system differ, the results here reveal many similarities in the regulatory principles between Get3 and SRP/SR. Both exhibit low nucleotide

affinity and forego the need of external exchange factors and activating proteins as regulatory elements (Shan et al., 2009). Instead, both use dimeric complexes as the functional unit. As dimers, both undergo conformational changes on the global (open → closed transitions) and local (catalytic loop adjustments) scale to generate multiple functional states during an NTPase cycle. For both, these rearrangements provide key regulatory points to sense and respond to upstream and downstream components and effect the precise timing of nucleotide hydrolysis in the pathway: GTP hydrolysis in the SRP/SR complex is stalled by the translation ribosome and re-activated by the SecYEG machinery (Zhang et al., 2009) (Akopian et al., 2013a), whereas ATP hydrolysis in Get3 is stalled by Get4/5 and activated by the TA substrate. Based on regulatory principles, Get3 could be placed in the class of NTPases regulated by dimerization (Gasper et al., 2009) whose members, aside from SRP and SR, also include the human GBP1, the septins, HypB, MnmE, and the dynamin family of GTPases (Chappie et al., 2010; Gasper et al., 2009). Investigation of Get3 undoubtedly enhances our understanding of the mechanism, regulation, and evolution of this novel class of regulators.

Materials and Methods

***Protein expression and purification*.** Mutant Get3s were generated using Quikchange Mutagenesis protocol (Stratagene). Wildtype and mutant Get3s

were expressed and purified as described (Chartron et al., 2010; Suloway et al., 2009). Purification of the Get4/5 and Get3/Sbh1 complexes is described in SI.

***Fluorescence measurements*.** All fluorescent nucleotides were from Jena Biosciences. All measurements were carried out at 25 °C in Get3 assay buffer (50mM HEPES pH 7.4, 150mM potassium acetate, 5mM magnesium acetate, 1mM DTT and 10% glycerol) using a Fluorolog-3-22 spectrofluorometer (Jobin Yvon) or a Kintek stopped-flow apparatus. Determination of individual rate and equilibrium constants is described in SI.

ATPase assays. All reactions were performed in Get3 assay buffer at 25 °C with [γ-^{32}P]-ATP (MP Biomedicals). Reactions at Get3 concentrations below 0.5 μM also included 0.2 mg/mL BSA. Reactions were quenched in 0.75 M potassium phosphate (pH 3.3), analyzed by PEI cellulose thin layer chromatography (TLC) in 1 M formic acid/ 0.5 M LiCl, and quantified by autoradiography. Observed rate constants were obtained as described (Peluso et al., 2001). Determination of individual rate and equilibrium constants is described in SI.

***TA protein targeting and translocation*.** Yeast translation extracts were prepared as described (Suloway et al., 2011; Wu et al., 2007), except that an additional centrifugation step (SW55Ti, 30 min at 49,000 rpm) was included prior to chromatography on the G25 column. Yeast microsomes were prepared as described (Rothblatt and Meyer, 1986; Schuldiner et al., 2008). Translation and translocation of TA protein is detailed in SI.

Supplementary Materials and Methods

***Protein expression and purification*.** Get4/5 and the Get3/Sbh1 complexes were expressed and purified according to previously published protocols with slight modifications (Chartron et al., 2010; Suloway et al., 2011). For Get4/5, the tetrameric fractions from MonoQ and size-exclusion chromatography were collected and used for all assays. For Get3/Sbh1, N-terminally tagged MBP-thrombin-Get3 and His_6-tagged Sbh1 were purified by affinity chromatography using Ni-NTA, followed by the amylose resin (NEB). Proteins eluted from amylose resin were treated with thrombin overnight at room temperature. The resulting thrombin digest was separated by size exclusion chromatography (Superdex 200, GE Healthcare) and the tetrameric Get3/Sbh1 fractions were collected and pooled. All proteins were exchanged into Get3 assay buffer in the gel filtration step.

Fluorescence measurements.

Equilibrium nucleotide binding under single-site conditions. Measurements were based on a fluorescence anisotropy readout with identical numerical processing as described previously (Zhang et al., 2010). Samples were excited at 355 nm and fluorescence emission at 448 nm was monitored. For all titrations, mantATP/ADP was held constant at 0.3 μM and Get3 was varied as indicated. Incubation time was calculated based on the nucleotide binding rate under the same conditions, and varied from 5 to 10 minutes

depending on Get3 concentration. Observed anisotropy values (A_{obsd}) were plotted as a function of Get3 concentration and fit to Eq 2.1,

$$A_{obsd} = A_0 + (A_1 - A_0) \times \frac{[\text{Get3}]}{[\text{Get3}] + K_d}, \qquad (2.1)$$

in which A_0 is the anisotropy value of free mantATP/ADP, A_1 is the anisotropy when mant-ATP/ADP is bound to Get3, and K_d is the equilibrium dissociation constant of Get3 for mantATP/ADP.

Competition of ATP with mantATP. To test whether the mant group perturbs the binding affinity of ATP to Get3, 1.5 μM Get3 and either 8 or 11 μM mantATP were pre-incubated for 10 minutes and titrated with ATP. The observed fluorescence (F_{obsd}) were fit to Eq 2.2,

$$F_{obsd} = F_0 \times \frac{K_{i,app}}{[\text{ATP}] + K_{i,app}} + F_1 \times \frac{[\text{ATP}]}{[\text{ATP}] + K_{i,app}}, \qquad (2.2)$$

in which F_0 is the fluorescence in the absence of the competitor, F_1 is the fluorescence in the presence of saturating competitor, and $K_{i,app}$ is the apparent inhibition constant of ATP at the specified mantATP concentration, determined to be 14.2 μM at 8 μM mantATP and 18.5 μM at 11 μM mantATP. These $K_{i,app}$ values are related to the true inhibition constant of ATP, K_i, by Eq 2.3,

$$K_{i,app} = K_i \times (1 + \frac{[\text{mantATP}]}{K_d}), \qquad (2.3)$$

in which K_d is the equilibrium dissociation constant of mantATP. The value of K_i determined from these experiments is 4.6 ± 0.1 μM, the same, within error, as the K_d value determined for mantATP, indicating that the mant group does not perturb the binding of ATP to Get3.

Nucleotide association and dissociation kinetics. All rate measurements were performed on a Kintek stopped-flow apparatus. Under single-site conditions, the environmental sensitivity of mantATP/ADP was used as a readout. Samples were excited at 355 nm and fluorescence emissions were collected at 445 nm. MantATP/ADP concentration was held constant at 0.3 μM and Get3 concentration was varied as indicated. Observed rate constants (k_{obsd}) were plotted as a function of Get3 concentration and fit to Eq 2.4,

$$k_{obsd} = k_{on}[\text{Get3}] + k_{off}, \qquad (2.4)$$

in which k_{on} is the association rate constant, and k_{off} is the dissociation rate constant.

Under multi-site conditions, FRET between a native tryptophan in Get3 and mantATP/ADP was used. Samples were excited at 280 nm and fluorescence emission was collected at 445 nm. For association rate measurements, Get3 was held constant at 1.5 μM and mant-ATP/ADP concentration was varied as indicated. The data were fit to Eq 2.4 above, except that the concentration of Get3 was replaced with that of mantATP/ADP. For dissociation rate measurements, a pulse-chase setup was used. A complex between Get3 and mantATP/ADP (at 30 μM) was preformed by incubation for 10 minutes, followed by addition of unlabeled ATP•Mg^{2+} or ADP•Mg^{2+} at 2-4 mM as the chase to initiate mantATP/ADP dissociation. The time course for change in acceptor fluorescence (F_{obsd}) was fit to either a single (Eq. 2.5) or double (Eq. 2.6) exponential function, in which F_e is the fluorescence when reaction reaches equilibrium, DF_1 and k_{fast} are the magnitude and rate constant of the

fluorescence change in the fast phase, and DF_2 and k_{slow} are the magnitude and rate constant of the fluorescence change in the slow phase,

$$F_{obsd} = F_e + \Delta F_1 \times e^{-k_{fast}t} \quad , \qquad (2.5)$$

$$F_{obsd} = F_e + \Delta F_1 \times e^{-k_{fast}t} + \Delta F_2 \times e^{-k_{slow}t} \; . \qquad (2.6)$$

Eq 2.6 was often needed to fit kinetic data, because the time courses for mantATP/ADP binding or dissociation were biphasic in most cases (Figure S2.7). We cannot rule out the possibility of enzyme conformational changes or heterogeneity that might in part give rise to the biphasic behavior. Nevertheless, the following strongly suggests that this behavior is primarily caused by heterogeneity in the mant nucleotides (where the mant group isomerizes between the 2'- and 3'-position). (i) The relative magnitude of the two kinetic phases, in the absence of perturbation by enzyme, is ~35%:65%, comparable to the equilibrium distribution of the two isomers (Cremo et al., 1990). (ii) In single-site binding measurements, while the observed rate constants from the fast phase showed a linear concentration dependence expected for bi-molecular association, the rate constants for the slow phase are concentration independent and occur at a time scale (k_{slow} ~ 0.005 s^{-1}) consistent with the time scale for conversion of one mant isomer to the other (Eccleston et al., 2006). (iii) The relative magnitudes of the two kinetic phases in binding measurements are unchanged by varying Get3 concentration, but the magnitude of the fast phase increases with increasing concentration of ATP or mantATP. This is inconsistent with enzyme heterogeneity giving rise to the biphasic behavior (as the faster

binding enzyme population would sequester most of the ATP and dominate the signal if this were the case). Instead, these observations are expected if the faster-binding mant-isomer sequesters most of the enzyme and dominates the signal at higher concentrations. Further, unlabeled ATP also increases the magnitude of the fast phase, suggesting that the faster-binding isomer favors the same binding mode as that for ATP. For these reasons, and because the kinetics and equilibrium derived from the fast phase were in excellent agreement with those from direct ATPase assays, the faster-binding isomer faithfully reports on the nucleotide binding and release kinetics of Get3 and were used for determination of binding constants in this work (Figure 2.1 and Table S2.1).

Although it is theoretically possible to remove one of the mant isomers by substituting 3'-OH with 3'-H, we found that this substitution itself significantly weakens nucleotide binding to Get3 and hence could not be used to obtain the correct rate and equilibrium constants.

ATPase measurements.

Single-site, single turnover ATPase rate (k_2). Get3 was in excess over a trace amount of ATP* (<0.1nM) and titrated at indicated concentrations. The data were fit to Eq 2.7:

$$k_{obsd} = k_{cat} \times \frac{[\text{Get3}]}{[\text{Get3}] + K_M} . \qquad (2.7)$$

Here, k_{cat} is the rate constant at saturating Get3 concentration, and K_M is the concentration of Get3 required to reach half saturation.

Multi-site, multiple turnover Get3 ATP hydrolysis rate. In this assay, a fixed amount of Get3 was titrated with excess ATP as indicated. The data were fit to an allosteric sigmoidal curve with a Hill coefficient of two (Eq 2.8):

$$k_{obsd} = \frac{k_{cat} \times [\mathrm{ATP}]^2}{K_M^2 + [\mathrm{ATP}]^2}. \qquad (2.8)$$

Here, k_{cat} is the rate constant at saturating Get3 concentrations, and K_M^2 is the product of ATP binding affinities for the first and second active site, i.e., $K_{\mathrm{M}}^2 = K_1 \times K_3$.

ATPase activation through tetramerization of Get3. Observed k_{cat} values were determined under multi-site conditions as above, at a series of Get3 concentrations. The plot of observed k_{cat} as a function of Get3 concentration was fit to Eq 2.9,

$$observed\ k_{cat} = k_6 + (k_4 - k_6) \times \frac{\left(-K_5 + \sqrt{K_5^2 + 4K_5[\mathrm{Get3}]}\right)}{2[\mathrm{Get3}]}, \qquad (2.9)$$

where k_4, k_6, and K_5 are defined in Figure 2.1.

ATPase rate constants in the Get3/Sbh1 complex. Pre-steady-state measurements were carried out with Get3 active sites in 1:2.5 – 1:10 stoichiometry relative to saturating ATP (1 mM), so that both the first and subsequent ATP turnovers can be visualized. The reaction time course is bi-phasic, as explained in the text, and was fit to Eq 2.10,

$$Fraction(\mathrm{ATP}) = (a - b)e^{-k_{burst}t} - k_{linear}t + b, \qquad (2.10)$$

where *a* is the fraction of ATP before initiation of the reaction, *b* is the reaction end point, k_{burst} is the rate constant associated with the burst phase and k_{linear} is the rate associated with the slower, linear phase.

TA protein targeting and translocation. For translation, a model substrate (N-Sbh1p) was used, which contains an N-terminal flag tag, a fragment of MBP (to facilitate separation on SDS-PAGE) fused to yeast Sbh1p, a C-terminal bovine opsin tag for glycosylation, and optimized methionine content to increase signal: MDYKDDDDKMENAQKGEIMPNIPQMSAFWYAVRTAVINAASGRQTVDEAL KDAQTNSSSNNNNNNNNNNLGLVPRGSISEFGSSSPTPPGGQRTLQKRKQ GSSQKVAASAPKKNTNSNNSILKIYSDEATGLRVDPLVVLFLAVGFIFSV VALHVISKVAGKLFRMNGTEGPNMYMPMSNKTVD.

The coding sequence for this protein was cloned into a transcription plasmid (Zhang et al., 2008) under control of an SP6 promoter. mRNAs were transcribed using the SP6 Megascript kit (Ambion). All translation and translocation assays were carried out as described in (Suloway et al., 2011). ^{35}S-methionine labeled pre- and glycosylated proteins were separated by 15% SDS-PAGE and quantified by autoradiography using a Typhoon (GE Healthcare) phosphoimager and Image QuantTL (GE Healthcare). Translocation efficiency (%glycosylated protein) was plotted as a function of Get3 concentration and fit to Eq 2.11,

$$T_{obsd} = T_o + T_{\max} \times \frac{[\mathrm{Get3}]^h}{[\mathrm{Get3}]^h + {K_d}^h} \quad , \tag{2.11}$$

in which T_0 is the fraction of translocation in the absence of Get3, T_{max} is the maximal amount of translocation with saturating Get3, K_d is the concentration of Get3 at half saturation, and h is the Hill co-efficient.

TA protein capture by Get3 in translation extract. A Get3 pull-down assay in translation extract was performed. A 50 µl translation reaction in Δ*get3* lysate was initiated for 1 minute at 26 °C, at which time His_6-tagged Get3 was added. After 40 min, the reaction mixture was adjusted with 20 mM imidazole and 1 mM cyclohexamide (final concentrations), followed by the addition of 10 µl Ni-NTA beads. After incubation on a rotating wheel at room 25 °C for 40 minutes, the beads were washed three times for five minutes in Get3 assay buffer with 30 mM imidazole and 0.5 mM ATP, and eluted with SDS-PAGE buffer containing 200 mM DTT and 300 mM imidazole.

Complex formation by gel filtration: Complex formation between Get3 and Get4/5 was assayed using size exclusion chromatography (Superdex 200, GE Healthcare). To generate the complex, 13.3 µM of Get3 was incubated with 13.3 µM of Get4/5 in Get3 assay buffer for 30 min at room temperature, with or without 200 µM ATP. Complex formation was assayed by following the depletion of the Get3 peak at ~14.8 ml.

Figures

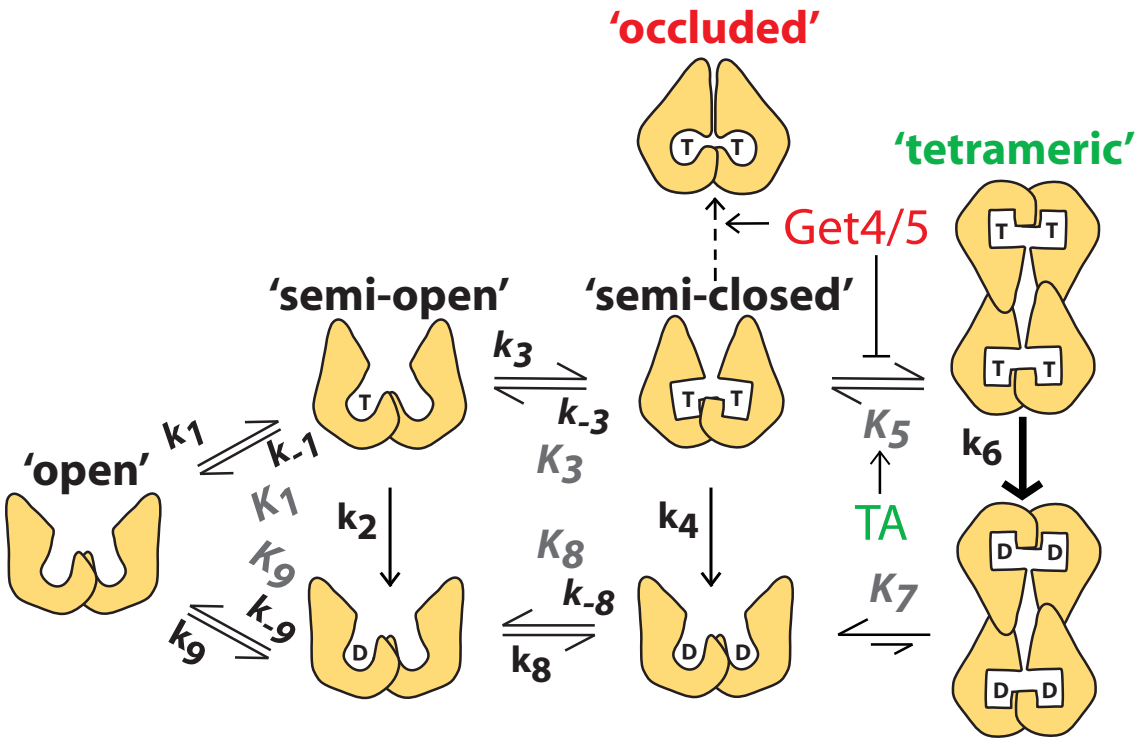

Figure 2.1

Model for the ATPase cycle of Get3. T denotes ATP, D denotes ADP. The shapes depict various Get3 conformations. Steps 1–2, ATP binding and hydrolysis by a single active site in Get3. Step 3, ATP binding to a second active site of Get3. Step 4, ATP hydrolysis from dimeric Get3. Step 5, formation of the Get3 tetramer. Steps 6–7, ATP hydrolysis and ADP release from tetrameric Get3. Steps 8–9, release of ADP from the two active sites of Get3. The individual rate and equilibrium constants are listed in SI: Table S2.1.

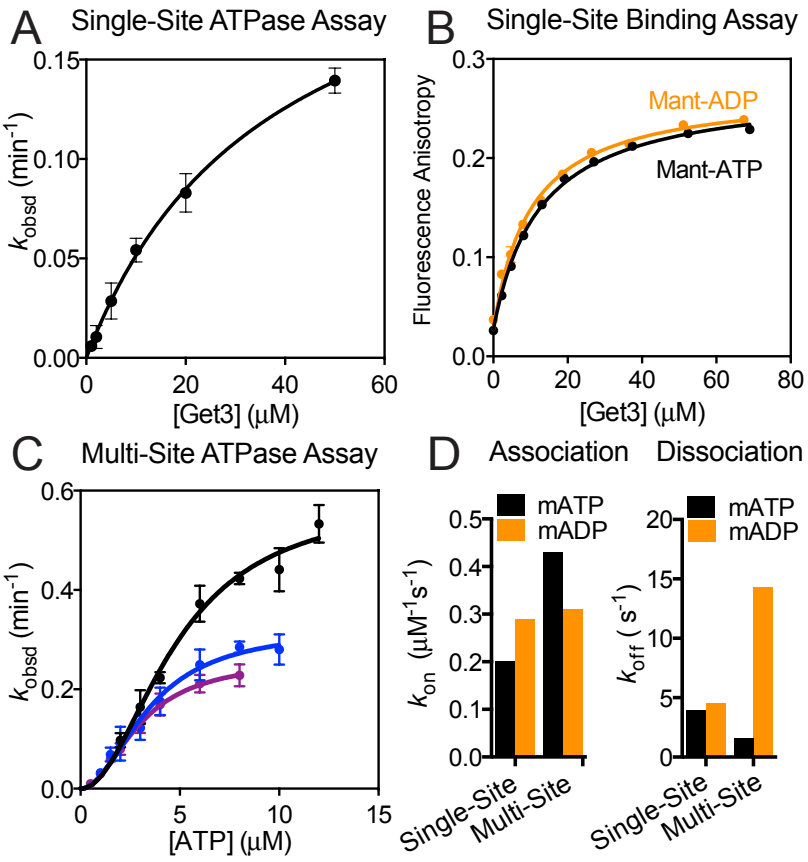

Figure 2.2

Cooperative ATP binding to Get3. (**A**) Single-site ATP hydrolysis by Get3. The data were fit to SI: Eq 2.7 and gave a K_M of 37 ± 6.7 μM. (**B**) Equilibrium titration of mantATP (0.3 μM, black) and mantADP (0.3 μM, gold) binding to Get3 under single site conditions. The data were fit to SI: Eq 2.1. (**C**) ATP hydrolysis by Get3 under multi-site conditions. The data were fit to SI: Eq 2.8 and gave a Hill coefficient of 2, average K_M values of 3.0 ± 0.2, 3.6 ± 1.0 and 4.8 ± 0.2 μM, and observed k_{cat} values of 0.26 ± 0.02, 0.33 ± 0.03 and 0.58 ± 0.03 min^{-1}, respectively, for reactions with 0.2 (purple), 0.5 (blue), or 1.0 (black) μM Get3. (**E**) Summary of nucleotide binding and release kinetics. See also SI: Table S2.1.

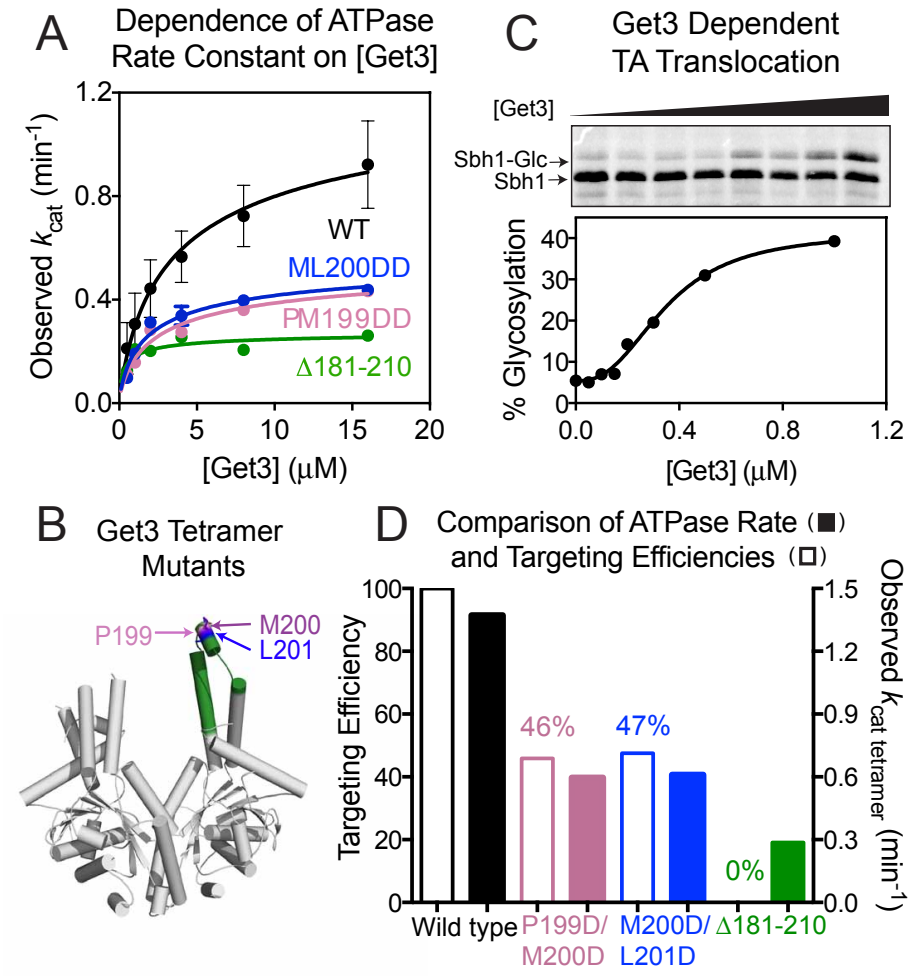

Figure 2.3

Tetramerization stimulates Get3's ATPase activity and is required for TA protein targeting. (**A**) Observed k_{cat} values as a function of Get3 concentration, for wildtype Get3 (black) and mutants Δ181-210 (green), P199D/M200D (pink), and M200D/L201D (blue). The data were fit to SI: Eq 2.9 and summarized in (D). (**B**) Structure of *Sc*Get3 (PDB: 3A36) highlighting the residues mutated. The remainder of residues 181-210 is in green. (**C**) Targeting and insertion of Sbh1p by wildtype Get3. The data were fit to SI: Eq 2.11 and gave a Hill coefficient of 2. (**D**) Comparison of TA targeting efficiencies (open) and tetramer ATPase rate

constants (filled) for wildtype Get3 (black) and mutants P199D/M200D (pink), M200D/L201D (blue), and Δ181-210 (green). %translocation was normalized to wildtype Get3.

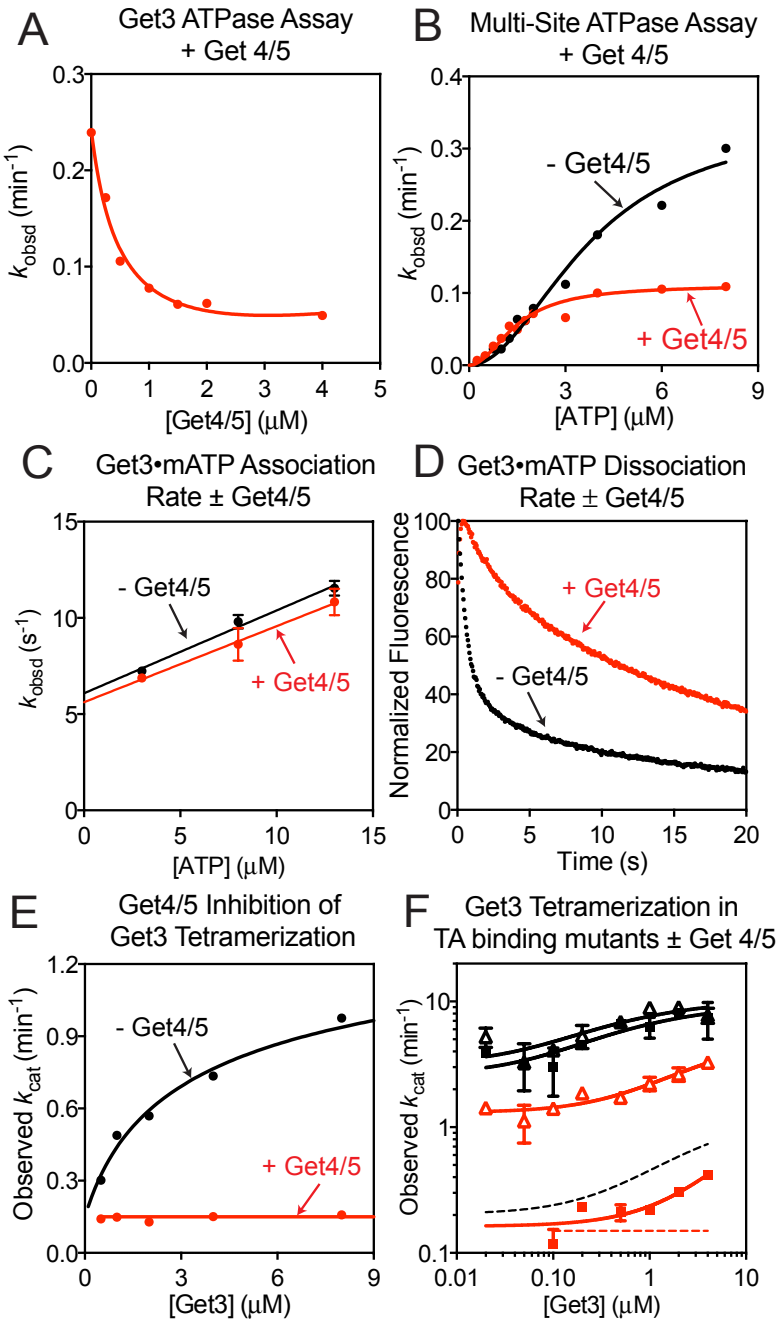

Figure 2.4

Get4/5 tightens ATP binding to Get3 and inhibits ATPase activity. (**A**) Get4/5 stoichiometrically inhibits Get3's ATPase activity. Reaction contained 0.5 μM Get3 and 10 μM ATP. (**B**) ATP concentration dependence of ATPase activity at 0.5 μM Get3, with (red) or without (black) 5 μM Get4/5 present. The data were fit

to SI: Eq 2.8 and gave average K_M values of 3.7±0.2 and 1.4 ± 0.3 μM with and without Get4/5, respectively. (**C**) Kinetics of mantATP binding to Get3 with (red) and without (black) 3.0 μM Get4/5 present. The data were fit to SI: Eq 2.4. (**D**) Dissociation of mantATP from Get3 was slowed in the presence (red) of 3.0 μM Get4/5. (**E**) Observed k_{cat} values as a function of Get3 concentration with (red) or without (black) 50 μM Get4/5 present. The data with Get3 were analyzed as in 3(A), and the data with the Get3•Get4/5 complex were fit to a linear function. (**F**) Same as (**E**) but with Get3 mutants F190D (triangles) and I193D (squares) with (red) or without (black) Get4/5 present. Dotted lines are fits for wildtype Get3 in (**E**) and shown for comparison. All rate constants are reported in Tables S2.2 & S2.3.

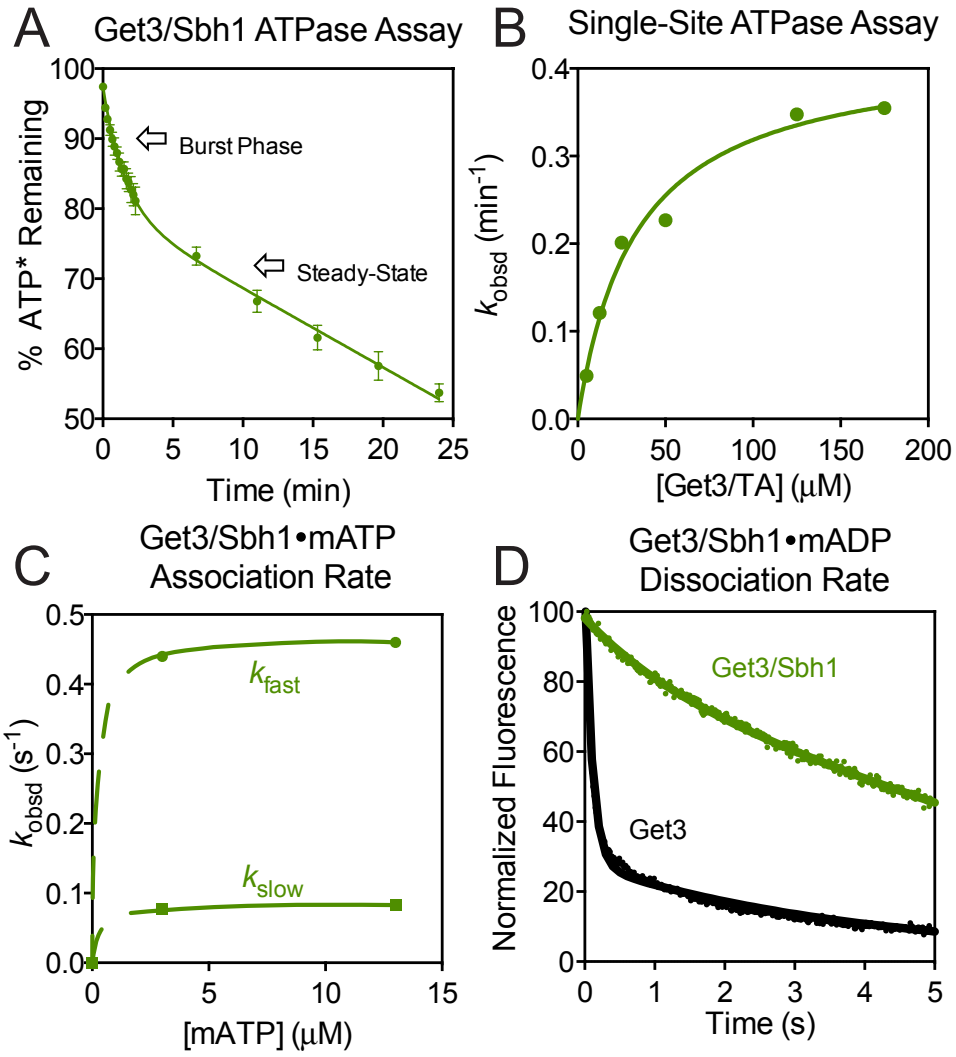

Figure 2.5

TA substrate induces rapid ATP hydrolysis. (**A**) Pre-steady-state ATPase reaction at a 1:5 ratio of Get3/TA:ATP. The data were fit to SI: Eq 2.10. (**B**) ATP hydrolysis from the Get3/TA complex under single-turnover conditions. The data were fit to SI: Eq 2.7 and gave a k_{cat} value of 0.42 min^{-1} and a K_M value of 33 μM. (**C**) Kinetics of mantATP binding to the Get3/TA complex. Two phases were observed. The dashed part of the curve depicts theoretical increases in binding

rates at lower ATP concentrations where bi-molecular association is rate-limiting, but which was inaccessible in our experiments. (**D**) MantADP dissociation from the Get3/TA complex. The data with Get3 (black) were from Figure S2.2F (black) and shown for comparison. All rate constants are reported in Table S2.2.

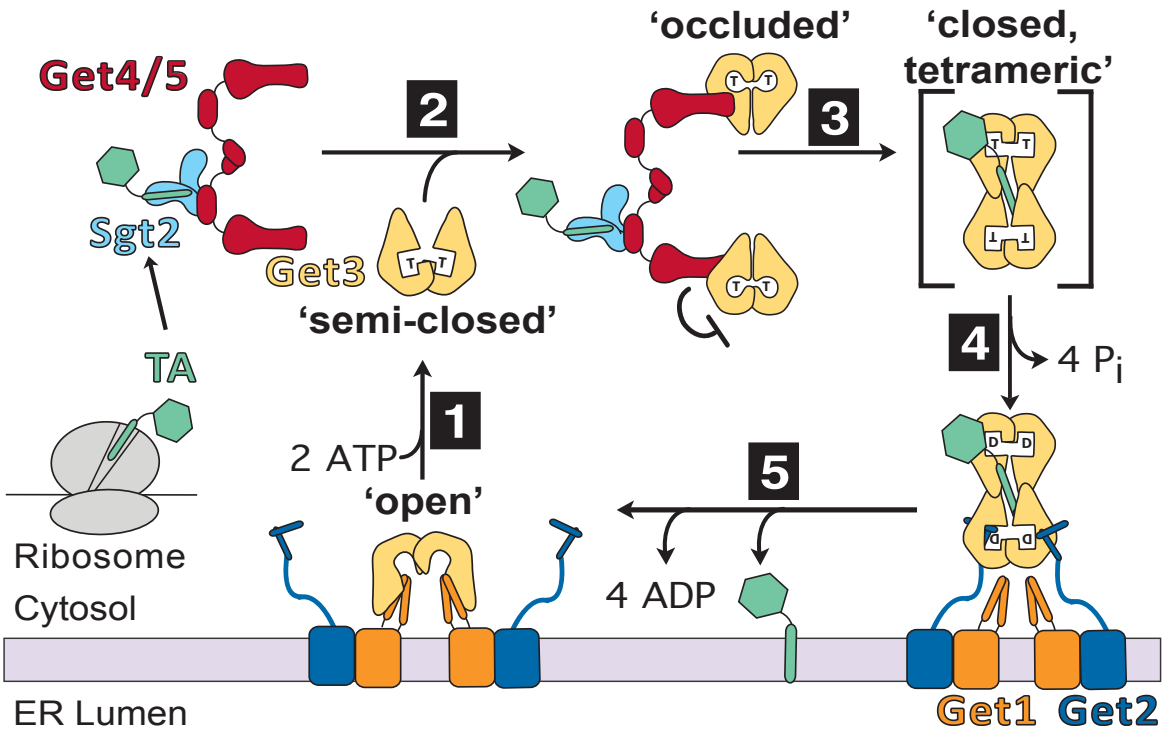

Figure 2.6

Model for TA protein targeting driven by the ATPase cycle of Get3, as described in the text.

Supplementary Figures

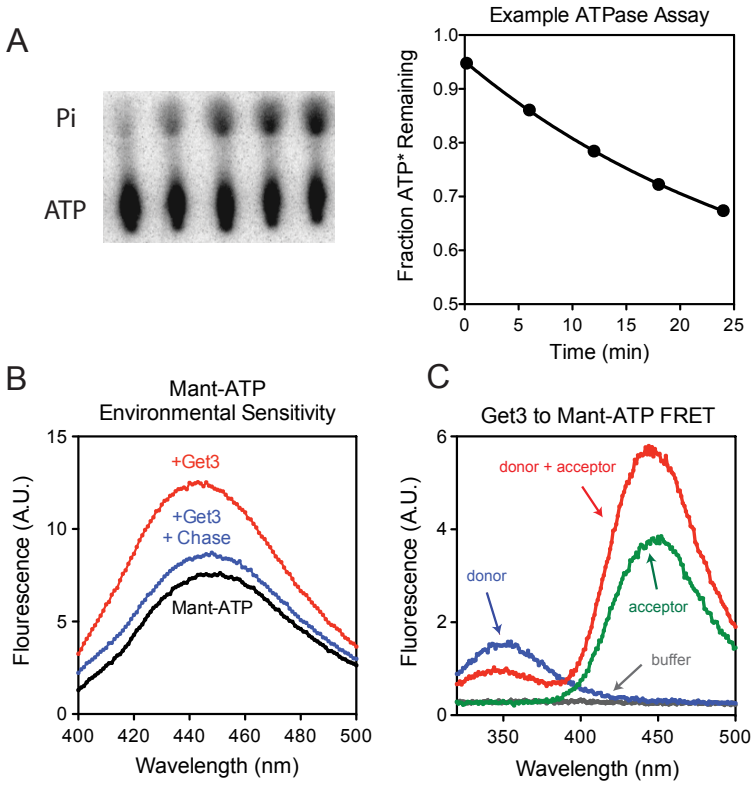

Figure S 2.1

Assays for ATP binding and hydrolysis by Get3, related to Figure 2.1 and Figure 2.2. (**A**) Representative thin layer chromatography (TLC) analysis for monitoring the progress of a Get3 ATPase reaction (see Methods). Right panel shows quantification of the TLC data, which were fit to a single exponential function to obtain observed rate constants (k_{obsd}). (**B**) Fluorescence emission spectra of 0.4 μM mantATP with (red) or without (black) 35.8 μM Get3, and for the Get3-mantATP complex chased with 2 mM ATP (blue). (**C**) Fluorescence emission spectra for 1.2 μM Get3 (donor, blue), 60 μM mantATP (acceptor, green), 1.2 μM Get3 incubated with 60 μM mantATP (donor + acceptor, red), or buffer (gray).

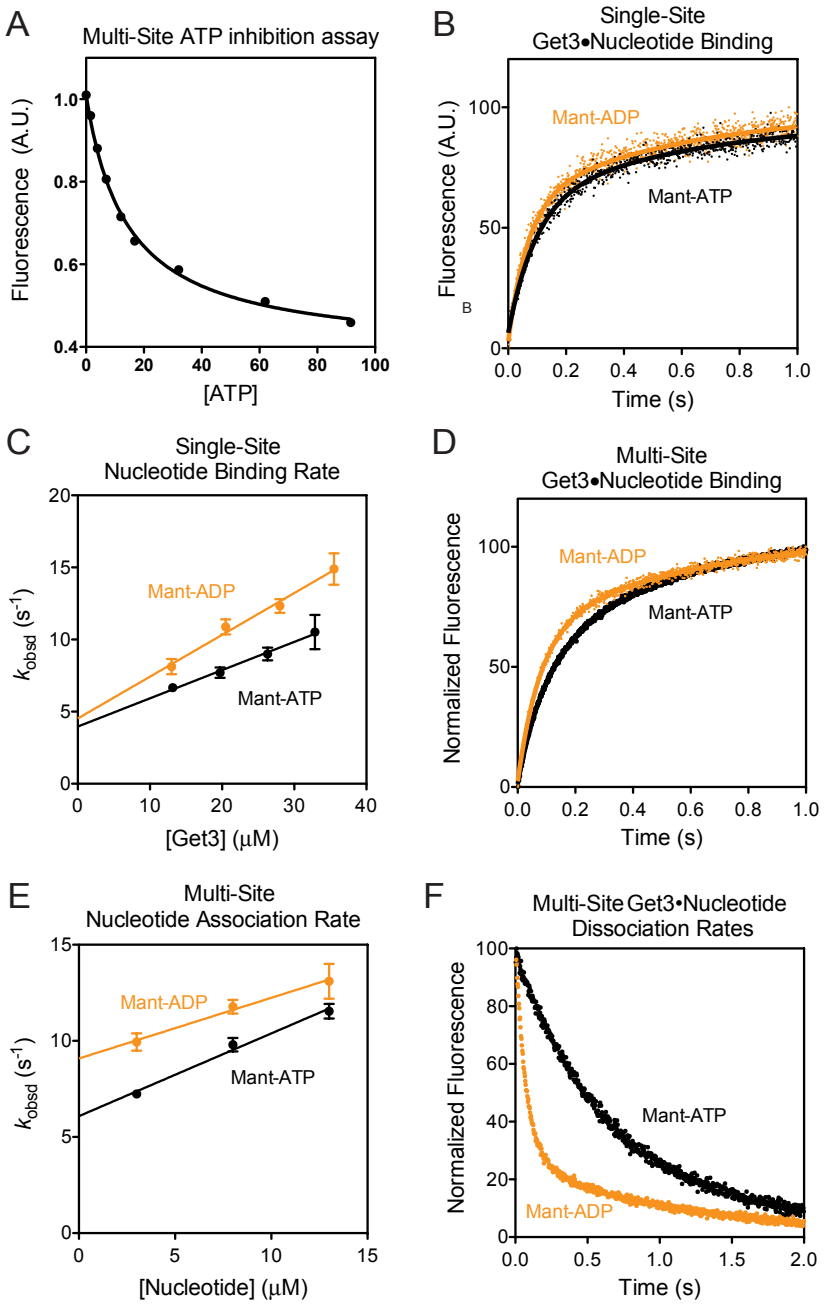

Figure S 2.2

Mant-ATP and mant-ADP binding and dissociation to Get3 related to Figure 2.1 and Figure 2.2. (**A**) Competition of mantATP binding to Get3 by ATP, performed with 1.5 μM Get3, 8 μM mantATP, and varying concentrations of ATP as indicated. The data were fit to Eq 2.2 in Methods, which gave a $K_{i,app}$ value of 4.5

μM. (**B**) Single-site time courses for mantATP (black) or mantADP (gold) binding to 37 μM Get3. (**C**) Single-site observed association rate constants were plotted as a function of Get3 concentration. Linear fits of the data (Eq 2.4) gave k_{on} values of 0.20 ± 0.01 and 0.29 ± 0.02 $\mu M^{-1}s^{-1}$ for ATP (black) and ADP (gold), respectively. The values reported are the mean ± SD, with n = 3. (**D**) Multi-site time courses for binding of 13 μM mantATP (black) or mantADP (gold) to 1.5 μM Get3 using the FRET assay. (**E**) Multi-site observed nucleotide binding rate constants were plotted as a function of Get3 concentration. Linear fits of the data gave k_{on} values of 0.43 ± 0.04 $\mu M^{-1}\, s^{-1}$ for ATP (black) and 0.31 ± 0.03 μM^{-1} s^{-1} for ADP (gold). (**F**) Time courses for mantATP (black) or mantADP (gold) dissociation from Get3 under multi-site conditions. The data were fit to double exponential functions. Rate constants derived from the fast phase are reported in the text and table S2.1.

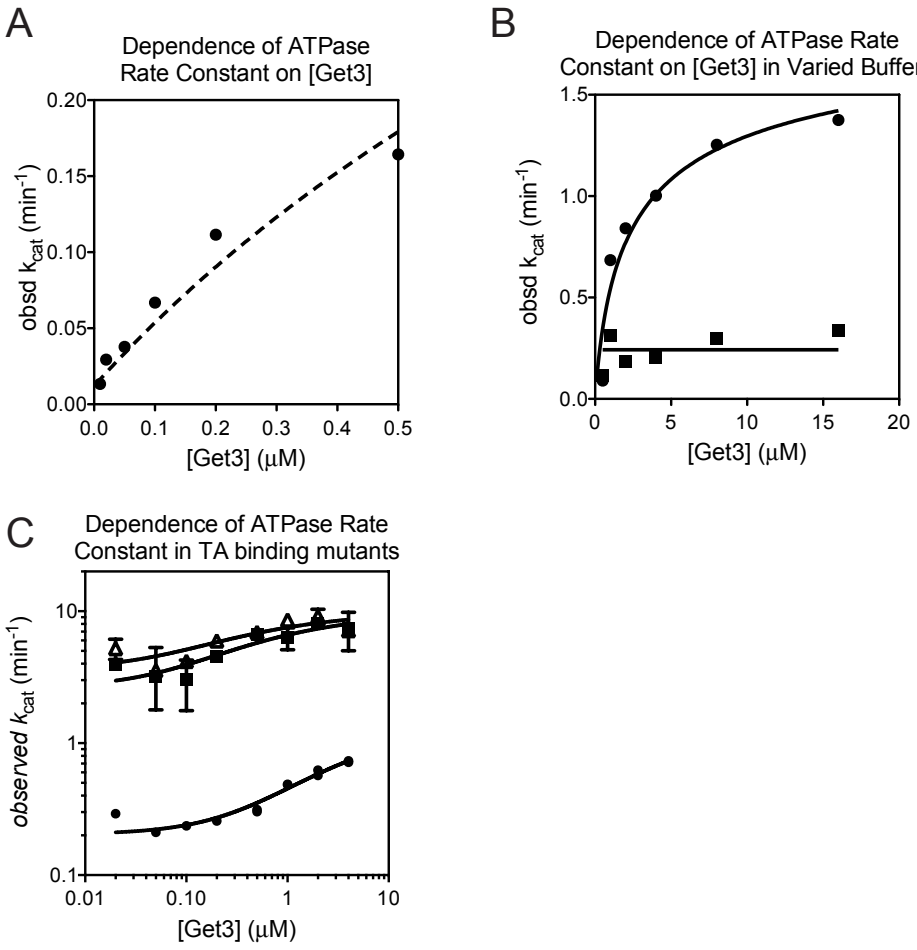

Figure S 2.3

Controls for Get3 concentration-dependent ATPase stimulation, related to Figure 2.3. (**A**) Zoom-in of the dependence of observed k_{cat} values at low Get3 concentrations. Reactions were performed as in Figure 2.3A in the presence of 1 mg/mL BSA (see methods). (**B**) Dependence of observed k_{cat} of Get3 in assay buffer (circles, 50mM HEPES pH 7.4, 150mM potassium acetate, 5mM magnesium acetate, 1mM DTT and 10% glycerol) or purification buffer (squares; 10 mM Tris, pH 7.5, 150 mM NaCl, 1 mM $MgCl_2$). (**C**) Observed k_{cat} values were determined as a function of Get3 concentration. The data with Get3 were analyzed as in (Fig. 2.3A) using Get3 mutants F190D (open triangles) and I193D

(closed squares).

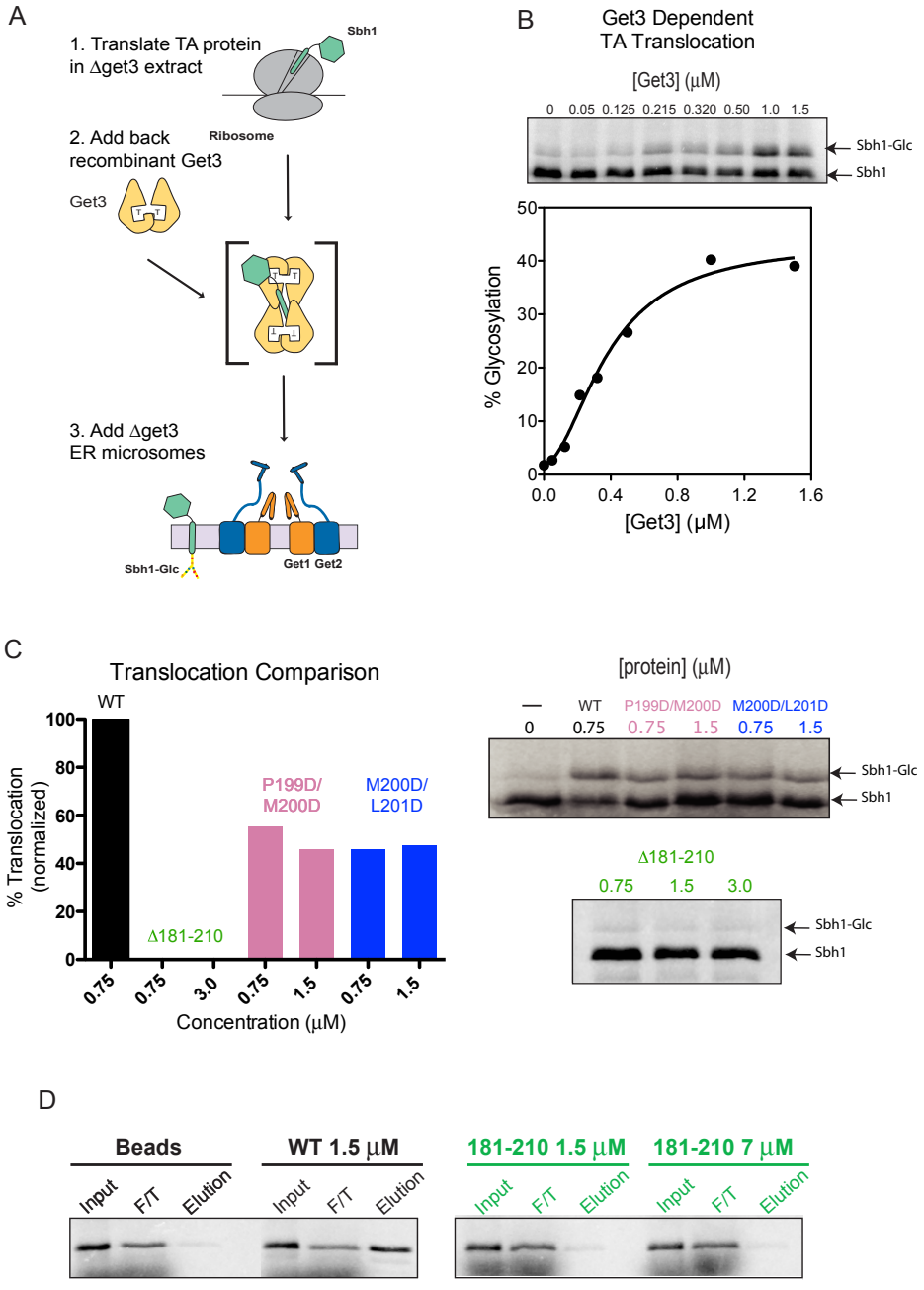

Figure S 2.4

Targeting and translocation of TA protein by wildtype and mutant Get3, related to Figure 2.3. (**A**) Cartoon diagram of the Get3 dependent TA targeting and translocation assay, as described in the Experimental Procedures and text. (**B**)

Get3-dependent targeting and translocation of Sbh1p, performed under identical conditions to Figure 2.3C, but in an independent experiment on a separate day using different Get3 concentrations. The data were analyzed as in Figure 2.3C and gave a Hill coefficient of 2. (**C**) Sbh1p targeting and translocation by wildtype and mutants P199D/M200D, M200D/L201D, and Δ181-210 at high Get3 concentrations. Gels for the data are on the right panel. (**D**) Capture of Sbh1p by wildtype Get3 (left) and mutant (Δ181-210) (right), using pulldown of His_6-tagged Get3 by Ni-NTA beads as described in the Experimental Procedures.

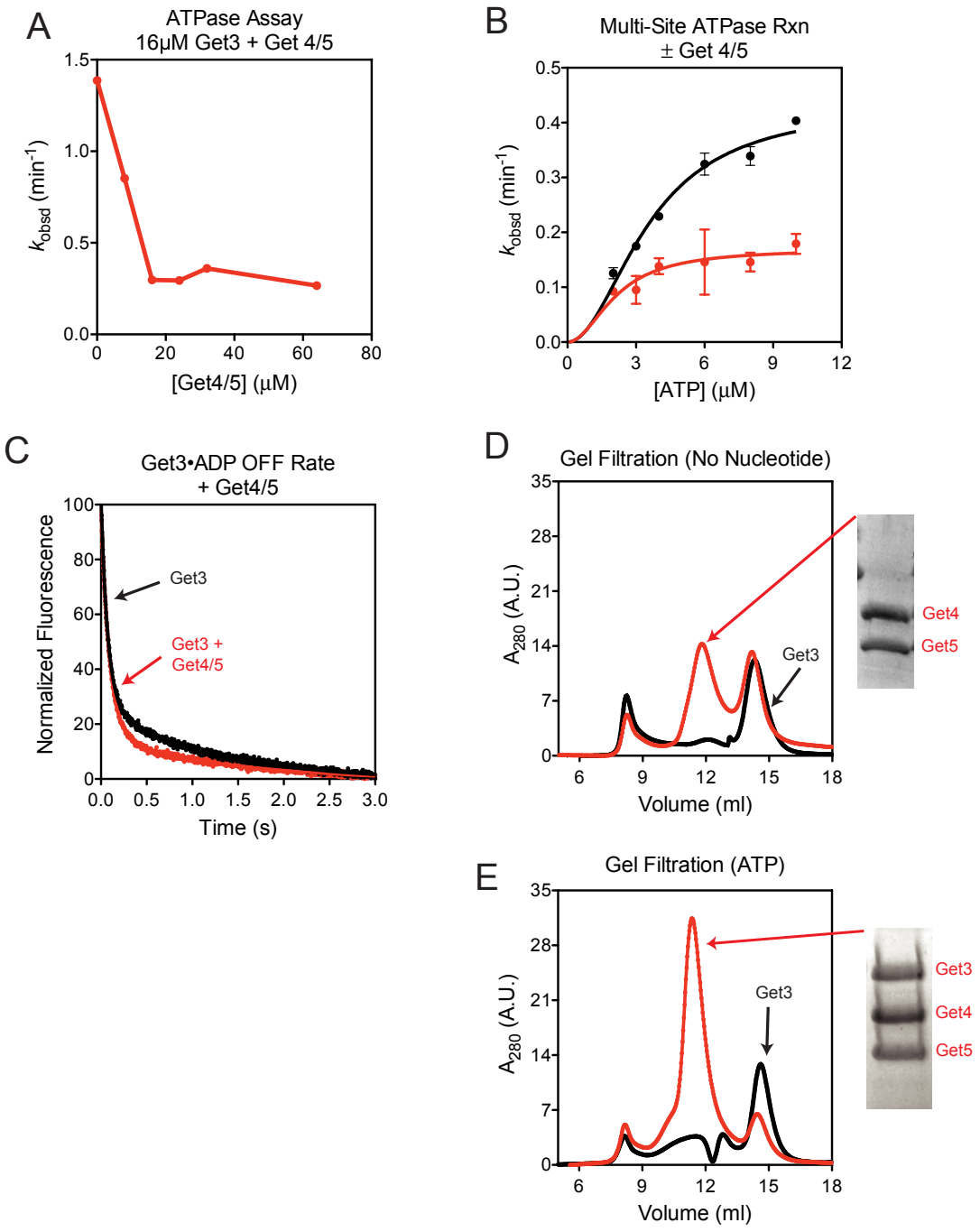

Figure S 2.5

Get4/5 increases Get3's affinity for ATP, and vice versa. Related to Figure 2.4. (**A**) Get4/5 stoichiometrically inhibits the ATPase activity of Get3. Reaction contained 16 μM Get3 and 320 μM ATP. (**B**) ATP concentration dependence of

observed ATPase activity at 1 μM Get3, in the absence (black) and presence (red) of 5 μM Get4/5. The data were fit to Eq 2.8 in the Extended Experimental Procedures, and gave average K_M values of 3.6 ± 0.01 and 2.2 ± 1.0 μM, and k_{cat} values of 0.43±0.003 and 0.18±0.04 min^{-1} with and without Get4/5, respectively. (**C**) Get3•mantATP dissociation kinetics, determined in the presence (red) or absence (black) of 3.0 μM Get4/5. Exponential fits of data gave dissociation rate constants of 14.4 s^{-1} and 11.3 s^{-1} with and without Get4/5, respectively. (**D**) Gel filtration chromatogram of apo-Get3 without (black) or with (red) Get4/5. Shown is a gel image for the fractions collected at ~11 ml. (**E**) Same as (**D**) but in the presence of saturating ATP.

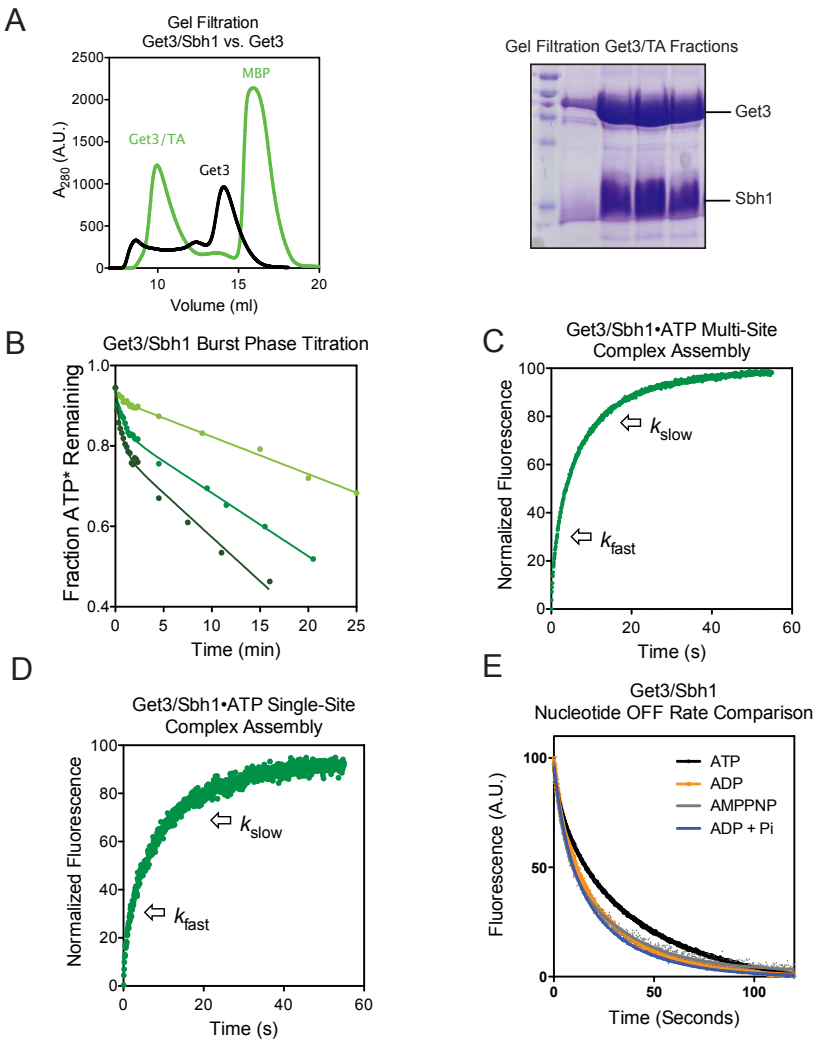

Figure S 2.6

Purification and activity of the Get3/TA complex, related to Figure 2.5. (**A**) Purification of the recombinant Get3/TA complex over Superdex 200 (green). Maltose binding protein (MBP) was a cleavage product from MBP-tagged Get3 during the purification, as described in the Methods. Chromatogram for dimeric Get3 is shown in black. Right panel shows SDS-PAGE analysis of the elution peak at ~10 ml, which contain both Get3 and Sbh1p. (**B**) Pre-steady-state ATPase reaction from the Get3/TA complex, performed as in Figure 2.6A but

with different ratios of Get3/TA complex relative to ATP: 1:10 (light green), 1:5 (green), 1:2.5 (dark green). Data were analyzed as in Figure 2.5A. (**C, D**) Representative time course for mantATP binding to the Get3/TA complex under multi-site (C) and single-site (D) conditions. Reaction in (C) used 2 μM Get3/TA complex and 13 μM mantATP and the obtained rate constants are plotted in Figure 2.6C. Reaction in (D) used 12.5 μM Get3/TA complex and 0.4 μM mantATP, and double exponential fit of the data gave rate constants of 0.4 s^{-1} and 0.073 s^{-1}. (**E**) Dissociation rate measurements for the Get3/TA complex in various nucleotide states. 2 μM Get3/TA was preincubated with 20 μM of the following: mantATP (black), mantADP (gold), mantAMPPNP (grey), and ADP + 10 mM P_i (blue). Dissociation rate constants are reported in Table S2.2.

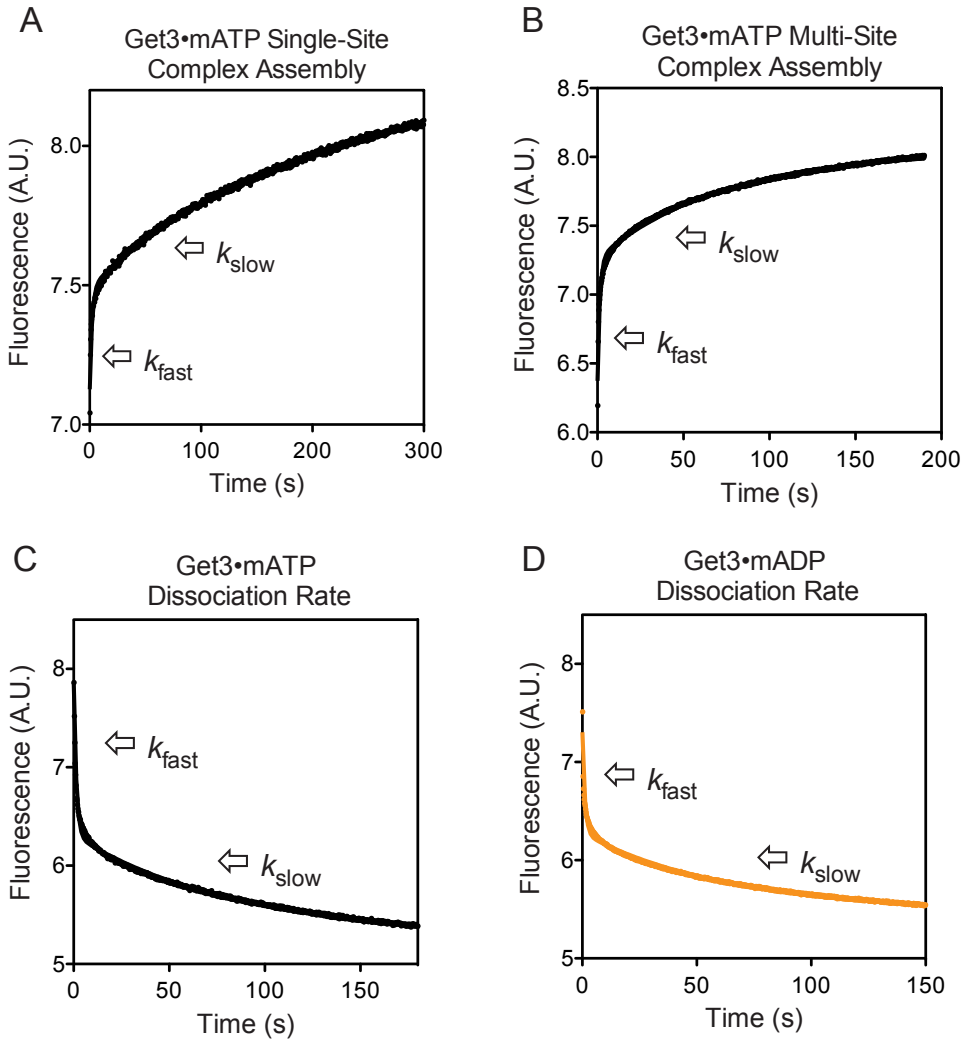

Figure S 2.7

MantATP binding to Get3 is biphasic, related to Figure 2.2, and described in Extended Experimental Procedures. (**A, B**) Time course for mantATP binding to Get3 under single-site (A) and multi-site (B) conditions. The data were fit to double exponential functions. Rate constants derived from the fast phase are reported in the text. (**C, D**) Time courses for mantATP (C) or mantADP (D) dissociation from Get3 under multi-site conditions. The data were fit to double exponential functions. Rate constants derived from the fast phase are reported, as explained in the Methods.

Table S 2.1

Summary of the rate and equilibrium constants during Get3's ATPase cycle, related to Figures 2.1–3. The individual constants are defined in Figure 2.1. The values reported are the mean ± SD, with n = 3.

Rate or equilibrium constants	
K_1	12.4 ± 0.1 μM
k_1	(2.0 ± 0.1) × 10^5 M^{-1} s^{-1}
k_{-1}	4.0 ± 0.3 s^{-1}
k_2	Not determined
K_3	1.3 μM
k_3	≥ (4.3 ± 0.4) × 10^5 M^{-1} s^{-1}
k_{-3}	1.6 ± 0.1 s^{-1}
k_4	≥ 0.012 min^{-1}
K_5	3.5 ± 1.9 μM
k_6	1.3 ± 0.4 min^{-1}
k_8	(3.1 ± 0.3) × 10^5 M^{-1} s^{-1}
k_{-8}	14.4 ± 0.9 s^{-1}
K_9	11.7 ± 1.3 μM
k_9	(2.9 ± 0.2) × 10^5 M^{-1} s^{-1}
k_{-9}	4.5 ± 0.6 s^{-1}

Table S 2.2

Summary of nucleotide dissociation rate constants from Get3 with and without effector proteins, related to Figures 2.4 and 2.5. The values reported are the mean ± SD, with n = 3.

Nucleotide	Effector	1st Phase		2st Phase	
		rate constant (s^{-1})	amplitude (%)	rate constant (s^{-1})	Amplitude (%)
ATP (k_{-3})	–	1.6	60	0.012	40
ADP (k_{-8})	–	14.4	56	0.015	44
ATP	+ Get4/5	0.15	40	0.0086	60
ADP	+ Get4/5	11.3	38	0.012	62
ATP	+ Sbh1	0.18	24.5	0.022	75.5
ADP	+ Sbh1	0.15	34.5	0.033	65.5
ADP + P_i	+ Sbh1	0.14	39	0.036	61
AMPPNP	+ Sbh1	0.214	40	0.032	60

Table S 2.3

Summary of ATPase rate constants from Get3 and Get3 TA binding mutants. related to Figure 2.3. The values reported are the mean ± SD, with n = 3.

	F190D	I193D
$k_{tetramer}$ (min^{-1})	10.0 ± 1.5	10.1±1.6
k_{dimer}(min^{-1})	2.7±0.9	3.6±1.2
K_d(μM)	0.37±0.4	0.26±0.4

Acknowledgements. We thank J. Chartron, H. Gristick and C.J.M. Suloway for expression constructs, purification protocols, and critical discussions, M. Sachs and C. Wu for help with yeast translation extracts, R. Schekman for help with yeast microsomes, and D.C. Rees and members of the Shan and Clemons groups for helpful comments. This work was supported by career awards from the David and Lucile Packard foundation and the Henry Dreyfus foundation to S.S., NSF graduate research fellowship DGE-1144469 to M.E.R, NIH training grant 5T32GM007616-33 to M.R., and NIH grant R01 GM097572 to W.M.C.

Chapter 3 : Multiple Selection Filters Ensure Accurate Tail-Anchored Membrane Protein Targeting

A version of this chapter was first published as Meera Rao, Voytek Okreglak, Un Seng Chio, Hyunju Cho, Peter Walter, Shu-ou Shan. Multiple selection filters ensure accurate tail-anchored membrane protein targeting. *In Preparation*

Abstract

Accurate protein localization is crucial to generate and maintain organization in all cells. Achieving accuracy is challenging, as the molecular signals that dictate a protein's cellular destination are often promiscuous. A salient example is the targeting of an essential class of tail-anchored (TA) proteins, whose sole defining feature is a transmembrane domain near their C-terminus. Here we address how the Guided Entry of Tail-anchored proteins (GET) pathway selects TA proteins destined to the endoplasmic reticulum. Quantitative analyses define multiple physicochemical features that distinguish TA proteins destined to different organelles. Further, the GET pathway selects for these features at distinct stages using a variety of mechanisms including differential binding, induced fit, and kinetic proofreading after ATP hydrolysis by Get3. Our results also reveal new roles for the cochaperone Sgt2 in providing key selection filters, and provide a biological logic for the complex cascade of substrate relay events during post-translational membrane protein targeting.

Introduction

Efficient and accurate localization of proteins is a prerequisite for the generation and maintenance of compartmentalization in all cells. Understanding how protein-targeting pathways achieve highly accurate membrane protein localization has been challenging for multiple reasons. First, topogenic signals that define a protein's final destination tend to be degenerate and lack consensus motifs (Heijne, 1985; Zheng and Gierasch, 1996); this demands targeting machineries to be highly adaptable and able to recognize a diverse set of signals. Second, only minor differences in signal sequences distinguish proteins that belong to alternative pathways or organelles (Emanuelsson and Heijne, 2001; Zhang and Shan, 2014; Zheng and Gierasch, 1996). Thus, protein-targeting machineries must also evolve robust selection mechanisms that can detect these minor differences. Furthermore, hydrophobic transmembrane domains (TMDs) on membrane protein substrates are prone to irreversible aggregation that can lead to mislocalization and proteostasic stress, requiring targeting machineries to also effectively shield the TMDs during targeting (Shao and Hegde, 2011). With a few exceptions (see (Randall and Hardy, 1995; Zhang and Shan, 2014)), the molecular mechanisms by which protein targeting machineries overcome these challenges are not well understood for most pathways.

A salient example of these challenges is provided by an essential class of tail-anchored (TA) membrane proteins, defined solely by a single TMD near the

C-terminus. TA proteins comprise 3-5% of the eukaryotic membrane proteome and play essential roles in numerous processes including membrane fusion/fission, vesicular trafficking, protein translocation, quality control, and apoptosis (Beilharz, 2003; Hegde and Keenan, 2011; Kalbfleisch et al., 2007). TA proteins are found in nearly all membranes in eukaryotic cells including the endoplasmic reticulum (ER), the mitochondrial outer membrane (OMM), and peroxisomes (Kutay et al., 1993). To a first approximation, the C-terminus of TA proteins (including the TMD) is necessary and sufficient to ensure their proper localization (Beilharz, 2003; Whitley et al., 1996), but the molecular information that directs TA proteins to diverse organelles is poorly understood. Previous work has noted that modulation of the hydrophobicity of TMDs and basic residues at the extreme C-termini alter the localization of TA proteins to the ER versus mitochondria (Beilharz, 2003; Borgese et al., 2003; 2007; Rapaport, 2003). Nevertheless, whether and how these features are distinguished by protein targeting machineries remain poorly understood.

Recent advances in understanding TA protein targeting pathways provide an opportunity to address this question. Biochemical and genetic analyses have identified the Guided Entry of Tail-anchored protein (GET) pathway, which targets TA proteins destined to the ER through an elaborate series of substrate handoff events. A co-chaperone, Sgt2, initially associates with the TMDs of TA proteins (Wang et al., 2010). A scaffolding complex, comprised of Get4 and Get5 (Get4/5), bridges Sgt2 and the central targeting factor, the Get3 ATPase (Chartron et al., 2010; 2012c; Wang et al., 2010). Get4/5 also preorganizes Get3

into the optimal conformation for TA binding (Gristick et al., 2014; Mateja et al., 2015) and thus facilitates the transfer of TA substrates from Sgt2 to Get3 (Wang et al., 2010). TA loading drives the dissociation of Get3 from Get4/5 and activates its ATP hydrolysis (Rome et al., 2014; 2013). After ATP hydrolysis, the Get3•TA complex associates with a receptor complex on the ER membrane, comprised of Get1 and Get2, via which the TA protein is released from Get3 and inserted into the membrane (Schuldiner et al., 2008; Wang et al., 2014).

While it has been established that the C-terminal TMD of a TA protein is sufficient for its association with both Sgt2 and Get3 (Hegde and Keenan, 2011; Wang et al., 2010), it is unclear how the GET pathway distinguishes TAs destined to different organelles and accurately selects the correct set of substrates. We addressed these questions by systematically varying particular physicochemical properties of a TA protein, and quantitatively analyzing how each step in the GET pathway senses and responds to these variations through a combination of biochemical, biophysical, and cell biological studies. Our results rigorously define at least two properties that distinguish TA proteins destined to different organelles, decipher multiple mechanisms by which these properties are selected by the GET pathway, and reveal new roles of Sgt2 in determining the specificity of TA selection.

Results

TAs are targeted to the ER based on TMD hydrophobicity and C-terminal charges.

Previous work suggests that a highly hydrophobic transmembrane domain (TMD) directs TA proteins to the ER (Burri and Lithgow, 2004; Kalbfleisch et al., 2007). A comprehensive analysis of the hydrophobicity score (Grand Average of Hydropathy (GRAVY) Calculator (http://www.gravy-calculator.de/)(Kyte and Doolittle, 1982) of TAs shows that: (i) the TMD of TAs span a wide range of hydrophobicity (Figure 3.1A); (ii) among these, well characterized GET substrates (Mateja et al., 2015; Schuldiner et al., 2008) (Figure 3.1A, highlighted) are enriched in the range of higher hydrophobicity; (iii) mitochondrial TAs tend to span a range of lower hydrophobicity, but exhibit significant overlap with that of GET substrates (Figure 3.1B; cf OMP25, MAVS, Fis1 versus Sec22, Ysy6 and Nyv1). These observations suggest that features in addition to TMD hydrophobicity also dictate the localization of TAs. A potential distinguishing feature is the enrichment of basic residues C-terminal to the TMD, which has been shown to direct proteins to OMM in *Arabidopsis* and mammalian cells (Marty et al., 2014; Yabal et al., 2003).

To mechanistically understand how TA substrates are selectively targeted to the ER, we established a set of model TAs in which we systematically varied the hydrophobicity TMD and the positive charge in the C-terminal element (CTE). As model substrates destined to the ER and mitochondria, we focused on

the TMD and CTE of Bos1p (residues 207-244) and Fis1p, respectively (Figure 3.2A). A non-cleavable, N-terminal 3xStrep-SUMO motif was fused to this sequence to enable purification and improve solubility of the substrate (Figure 3.2A; see also (Wang et al., 2010; 2011a)). We replaced increasing numbers of hydrophobic residues in the Bos1 TMD with Ala and Gly, creating a set of substrates that span the overlapping range of hydrophobicity between mitochondrial and ER-destined TAs (Figure 3.2A and 3.1C). In addition, we swapped the TMDs and CTEs of Bos1p and Fis1p (Figure 3.2A, Fis1-FisC) and systematically varied the number of basic residues in the CTE to isolate the contribution of C-terminal charges (Figure 3.2A).

To test if the GET pathway can select substrates based on these features and whether this selection can be recapitulated *in vitro*, we measured the ability of purified Get3 to target and translocate TA substrates into ER microsomes in a *Δget3* yeast lysate (Rome et al., 2013; Wang et al., 2010) (Figures 3.2B-E). Successful translocation into ER enables glycosylation of an opsin tag fused to the C-terminus of substrates (Figure 3.2A), providing a semi-quantitative measure for targeting and translocation efficiency (Rome et al., 2013). Of the TAs that had altered TMDs, 2AG was translocated as efficiently as Bos1; 3AG, 4AG, and 5AG underwent Get3-dependent insertion but exhibited increasing defects; and 6AG abolished Get3-dependent translocation (Figures 3.2B-C). Replacement of the CTE of Bos1 with an increasing number of Arg residues (Bos-RR and Bos-RRRR) or with the charged Fis1-CTE (Bos1-FisC) also substantially reduced Get3-dependent translocation (Figure 3.2D). Reciprocally,

reducing the charges in the CTE of Fis1-FisC by replacing it with the Bos1 CTE or with two Args enhances TA insertion into ER, whereas replacing the CTE with four Args retained the low level of ER insertion of the TA substrate (Figure 3.2E). Thus, efficient TA targeting to the ER depends on both the TMD and positive charges in the CTE, and these dependences can be recapitulated in the GET pathway using this set of model substrates.

Several additional observations can be made from these data. First, the translocation defects of 3AG, 4AG, and 5AG are more pronounced at low Get3 concentrations but can be rescued by higher amounts of Get3 to levels comparable to that of Bos1 (Figure 3.2C). In contrast, the translocation of Bos1-CTE mutants saturated at ≤ 0.5 μM Get3 and was not further improved by higher Get3 concentration (Figure 3.2D). This suggests that distinct mechanisms are used to reject a suboptimal TMD versus CTE of TA substrates; this hypothesis is further supported by in-depth analyses below. Second, substrates containing a Fis1 TMD exhibited Get3-independent insertion into ER microsomes, and insertion was abolished by a highly charged CTE (Fis1-FisC or Fis1-RRRR) (Figure 3.2E). This suggests the presence of additional pathways that could target TA proteins with suboptimal TMDs to the ER, and more importantly, that a positively charged CTE serves as a general feature to reject TA proteins from the ER in both GET-dependent and GET-independent pathways.

Sgt2 discriminates TAs based on TMD hydrophobicity

To understand how substrates are selected by the GET pathway, we dissected the individual molecular steps in this pathway. To this end, we adapted an *E. coli in vitro* translation system (Goerke and Swartz, 2009; Jewett and Swartz, 2004). Highly efficient translation in this lysate provides a robust source of TA proteins. Further, the lack of GET homologues in bacteria makes this lysate a bio-orthogonal system in which all the molecular steps in the GET pathway can be reconstituted using purified components.

The first known step in the GET pathway is the capture of TA substrates by the co-chaperone Sgt2. To understand whether and how TA substrates are distinguished during this step, we translated TA proteins in *E. coli* lysate in the presence of ^{35}S-methionine and His_6-tagged Sgt2, and analyzed the amount of TA substrate associated with Sgt2 after affinity-capture with Ni-NTA (Figure 3.3A). To provide better quantification and reduce variability, each substrate was translated and captured together with a smaller Bos1 construct lacking the 3xStrep tag (Ctrl). Both the substrate and Ctrl can be visualized on SDS-PAGE and autoradiography (Figure 3.3B), and the capture efficiencies of the substrates of interest were directly normalized against Ctrl. The only exception was the experiment with Fis1-FisC, in which the 3xStrep tag was placed on the control (Ctrl+3xStrep) rather than Fis1-FisC (Fis1-FisCΔ). This change was necessary to enhance the translation of Fis1-FisC, but otherwise did not affect the outcome or interpretation of the experiment.

The results showed that, compared to Bos1, 2AG and 3AG were captured by Sgt2 with comparable efficiency and 4AG, 5AG and Fis1-FisC

exhibited statistically significant defects, whereas 6AG was poorly captured by Sgt2 (Figures 3.3B and C). There is a good agreement between the GRAVY scores of these TMD variants and their efficiencies of capture by Sgt2 (Figure 3.1C versus 3C). On the other hand, Bos1-FisC was captured by Sgt2 as efficiently as Bos1, indicating that a positively charged CTE does not affect TA binding to Sgt2. Thus, the efficiency of TA capture by Sgt2 is highly sensitive to the hydrophobicity of the TMD, but not to basic residues at the extreme CTE.

Fis1 is rejected during TA transfer from Sgt2 to Get3

In the next step of the pathway, TA substrates are transferred from Sgt2 to Get3 with the help of the Get4/5 complex. To quantitatively understand this substrate handover event, we developed an assay based on Förster Resonance Energy Transfer (FRET). Using an *E. coli* translation lysate that harbors a pair of engineered amber suppressor tRNA and tRNA synthetase, a fluorescent unnatural amino acid, 7-hydroxycoumaryl ethylglycine (Cm), was efficiently and site-specifically incorporated into the TA substrate during translation (Figures 3.4A, 3.4B and 3.5B) (Charbon et al., 2011; Saraogi et al., 2011a). Cm was incorporated four residues upstream of the TMD of TA substrates and served as the FRET donor (denoted as TA^{Cm}). As the FRET acceptor, CoA-BODIPY-FL was enzymatically conjugated to ybbR-tagged Get3 via the Sfp phosphopantetheinyl transferase enzyme and CoA chemistry (Figure 3.4E-G; (Yin et al., 2006)). BODIPY-FL-labeled Get3 (denoted as $Get3^{BDP}$) exhibits

translocation and ATPase activities comparable to those of wildtype Get3 (Figures 3.4H-I).

To reconstitute TA transfer from Sgt2 to Get3, we generated and affinity purified Sgt2•TA^{Cm} complexes (Figure 3.4C-D) and incubated the complex with Get4/5, ATP, and Get3 to allow TA transfer (Figure 3.5A). We observed a 52% reduction in Cm fluorescence when the transfer reaction was carried out with Get3^{BDP} but not with unlabeled Get3 (Figure 3.5B), indicating a high efficiency of both TA transfer and FRET between TA^{Cm} and Get3^{BDP}.

Using this FRET assay, we asked whether the transfer of substrates from Sgt2 to Get3 is specific for ER-destined TA proteins. First, we measured FRET when the transfer reaction was allowed to reach equilibrium at varying concentrations of Get3^{BDP} (Figure 3.5C). These titrations showed that the equilibrium of TA transfer between Sgt2 and Get3, quantified empirically by the concentration of Get3 required for 50% transfer (denoted as $K_{1/2}$), varied modestly (< 3-fold) among all the substrates tested (Figure 3.5D and Table 3.2). Thus at equilibrium, the preference of Get3 for these TA variants closely parallels that of Sgt2, such that the transfer of TA from Sgt2 to Get3 is largely isoenergetic for this set of TA variants.

Real-time measurement of TA transfer from Sgt2 to Get3 showed that the Get4/5 complex significantly accelerated the substrate transfer process (Figure 3.5E), and revealed two kinetic phases during this transfer. For Bos1, the rate constants of the fast and slow phases are 0.0094 s^{-1} and 0.003 s^{-1}, respectively, in the absence of Get4/5, and increased to 0.047 s^{-1} and 0.011 s^{-1}, respectively,

in the presence of Get4/5 (Figures 3.5E and Table 3.2). As no kinetic phases characteristic of the Get4/5-independent reaction were observed during Get4/5-dependent TA transfer, this ruled out the possibility that the slow phase observed during the latter reaction arose from TAs that underwent Get4/5-independent transfer. Finally, highly efficient TA transfer was observed even when the reaction was carried out in the presence of ribosome-depleted D*get3* lysate (Figure3. 5H), strongly suggesting that Get4/5-dependent TA transfer is robust and can withstand competition from other cellular factors.

The set of TA variants, in which the hydrophobicity of the TMD is systematically altered (Bos1 – 5AG), varied modestly in their kinetics of Get4/5-dependent transfer to Get3. The rate constants of both the fast and slow phases varied approximately 4-fold among these substrates, with TAs containing less hydrophobic TMDs exhibiting higher rate constants in each phase (Figure 3.5F). These effects were offset, however, by the larger contribution of the fast phase to the transfer reaction of the more hydrophobic substrates (Figure 3.5G and Table 3.2). Surprisingly, the TA transfer reaction was completely abolished for Fis1-FisC (Figure 3.5E), consistent with the Get3-independence of the TA insertion reactions for substrates containing the Fis1-TMD (Figure 3.2E). In contrast, Bos1-FisC exhibited transfer kinetics comparable to that of Bos1 (Figure 3.5F-G), indicating that the Fis1-TMD, rather than its charged CTE, is responsible for the observed rejection of Fis1-FisC during TA transfer. Together, these results showed that a less hydrophobic TMD poses a modest barrier for TA handover from Sgt2 to Get3 and the Fis1-TMD

are strongly discriminated during this transfer reaction, whereas the C-terminal positive charges are not recognized by the GET pathway at this stage.

C-terminal basic residues slow TA insertion into ER.

In the last stage of the GET pathway, the Get3•TA complex is targeted to the Get1/2 receptors on the ER and the TA substrate is inserted into the membrane. To reconstitute this step, we generated ^{35}S-methionine labeled TAs during *in vitro* translation in the presence of Sgt2, Get4/5 and His_6-tagged Get3 and affinity purified Get3•TA complexes using Ni-NTA. Purified complexes were presented to ER microsomes derived from *Δget3* yeast, and the efficiency of targeting and insertion was assessed by glycosylation (Figures 3.6A-C). Real time measurement of the insertion reaction showed that 2AG, 3AG, 4AG, and 5AG were targeted and inserted with similar kinetics and efficiency as Bos1 (Figures 3.6B-C). 6AG showed a marked reduction in insertion efficiency at steady state but not in the rate to reach the steady state (Figure 3.6D). In contrast, Bos1-FisC, Bos1-RR, and Bos1-RRRR showed significant reductions in both the level of translocation at steady state and the rate to reach steady state compared to Bos1, mirroring their translocation defects observed in the complete yeast lysate. Bos1-RR showed a reduction in the rate to reach steady state compared to Bos1 (see Figure 3.3).

Further analyses of the kinetics of TA insertion strongly suggest that the observed translocation defects of 6AG and Bos1-FisC arise from different mechanisms. During the observed insertion reaction, the productive targeting

and insertion processes (Figure 3.6F, k_{insert}) must compete with nonproductive events ($k_{nonproductive}$) including the reversal of this reaction or more likely, disassembly of the Get3•TA complex (k_{dis}) which could lead to aggregation of the TA substrate (k_{agg}). The observed rate constant of the insertion reaction (k_{obsd}) is the sum of the rate constants for insertion from the Get3/TA complex and competing nonproductive reactions. The level of insertion at steady state reflects how fast the insertion reaction is compared to the nonproductive reactions (see Methods). Dissection of the observed reaction kinetics into these components showed that the observed translocation defect of 6AG arises primarily from a much faster rate of nonproductive reactions (Figure 3.6G, open bar). In contrast, the observed defects of Bos1-RR, Bos1-FisC, and Bos1-RRRR arise primarily from a much slower rate of insertion into the ER (Figure 3.6 G-H, solid bars). Thus, the TA insertion step provides the main selection mechanism by which substrates with charged CTE are rejected from the ER.

A likely source of the nonproductive reactions is the disassembly of the Get3•TA complex, which can lead to TA aggregation and/or misfolding. To test whether this was the case, we directly measured the kinetic stability of the Get3•TA complex. We generated and purified Get3•TA complexes as for the insertion reaction, except that TA and Get3 were labeled with Cm and BODIPY-FL, respectively. The rate constant for disassembly of the Get3•TA complex was measured using pulse-chase experiments and monitored by loss of FRET between TA^{Cm} and $Get3^{BDP}$. The results showed that, with the exception of 6AG, dissociation of the Get3•TA complexes are extremely slow, at a rate constant of

~3 x 10^{-4} s^{-1} (or half time of ~ 40 min), for most of the substrates tested (Figure 3.6I). In contrast, 6AG dissociates from Get3 with a rate constant of 3x10^{-3} s^{-1} (or half time of ~ 4 min), in close agreement with the rate of nonproductive reactions calculated from the translocation data (Figure 3.6G and Table 3.3). Thus, Get3 binds tightly to most TA substrates with TMDs above a modest degree of hydrophobicity, such that dissociation of the Get3•TA complex is much slower than its subsequent targeting and insertion. Only less hydrophobic substrates such as 6AG exhibit significantly faster dissociation from Get3, which competes effectively with the insertion of TA protein into the ER.

Sgt2 enhances specificity of the GET pathway.

The analyses above strongly suggest that Sgt2 plays important roles in discriminating against TAs with suboptimal TMDs before they are loaded onto Get3. To more directly test this idea, we prepared yeast lysate using the *SGT2FLAG/Δget3* strain and immuno-depleted Sgt2-Flag using anti-FLAG resin (Figure 3.7A). We tested the overall targeting and insertion of Bos1 and 5AG in the Sgt2-depleted lysate. A mock-depleted *Δget3* lysate was also tested as a positive control. The results showed that in the mock-depleted lysate, Bos1 was targeted and inserted 2.5-fold more efficiently than 5AG (Figure 3.7B-C), whereas this difference was significantly smaller in the Sgt2-depleted lysate (Figure 3.7B-D). These results provide independent evidence for selection mechanisms upstream of TA loading on Get3 that help reject 5AG from the GET

pathway. Thus, Sgt2 plays a critical role in enhancing discrimination against suboptimal substrates.

The charge at the CTE significantly alters organellar localization of Fis1

While the role of TMD in directing proteins to ER versus mitochondria has been extensively studied *in vivo* (Borgese et al., 2001; 2003; 2007; Marty et al., 2014; Pedrazzini, 2009), the role of the CTE in distinguishing mitochondria and ER-destined TAs is far less well characterized. To more systematically understand the importance of the basic CTE, we examined the *in vivo* localization of CTE variants of a Fis1 fused to GFP. As previously reported (Habib et al., 2003), the TMD and the basic CTE of Fis1 (Figure 3.8, Fis1-TMD-CTE) are sufficient to direct GFP to the OMM and peroxisomes and exclude its accumulation in the ER. Deletion of the CTE leads to a loss of specific mitochondrial targeting and the accumulation of Fis1-TMD in the ER, as shown by the co-localization of GFP with the ER marker Sec63 tagged with tdTomato (Figure 3.8, Fis1-TMD). We next probed the minimal charge requirement of the CTE that provides mitochondrial specificity and excludes Fis1-TMD from the ER. To this end, we created variants of Fis1-CTE with increasing numbers of arginine residues (Figure 3.8, Fis1-TMD-R^n) and quantified their co-localization with Sec63-tdTomato and mitochondrially targeted TagBFP (mito-TagBFP). These data show that when the net positive charge on the CTE reached +4 (Figure 3.8, Fis1-TMD-RRRR), equivalent to that of the native CTE, specific mitochondrial localization was fully restored. Thus, the net charge of the CTE

plays an important role in providing a selectivity filter to exclude mitochondria-destined TA proteins from the ER.

Discussion

Accurate protein localization is essential for cells to establish and maintain compartmentalization. TA proteins, with a C-terminal TMD as their only defining feature, pose special challenges for protein targeting pathways that need to sort these proteins to the correct cellular membranes. In this work, systematic analyses corroborate previous observations (Borgese et al., 2007; Marty et al., 2014; Whitley et al., 1996) and rigorously define at least two physicochemical properties, the hydrophobicity of the TMD and basic residues at the extreme C-termini, which distinguish TA proteins destined to different organelles. For the first time, we define multiple, distinct mechanisms that allow the GET pathway to recognize these properties and select for the correct substrates. These findings also reveal new roles of the co-chaperone Sgt2 and rationalize, in part, the chemical and biological logic for the complex series of substrate handover events in this targeting pathway.

In the initial entry into the GET pathway, capture of TA proteins by Sgt2 provides the first selection filter that discriminates substrates based on hydrophobicity (Figure 3.9A, Step 1). TA substrates with increasing number of Ala/Gly replacements in the TMDs form decreasingly stable complexes with Sgt2 (this work, (Wang et al., 2010)). The good agreement between the TA capture efficiency by Sgt2 and the GRAVY scores of the TMD variants tested here strongly suggests that overall hydrophobicity is the dominant feature recognized by Sgt2. On average, the TMDs of TA proteins destined to the OMM

have hydrophobicity comparable to or lower than those of the 4AG substrate examined here, and many could be partially or completely rejected from the GET pathway at this step. Nevertheless, Sgt2 is insensitive to enrichment of basic residues at the extreme C-terminus that characterizes some mitochondrial TAs, suggesting that this property must be detected by other mechanisms.

The handover of TA proteins from Sgt2 to the central targeting factor, Get3, provides a second selection filter in the pathway (Figure 3.9A, Step 2). Intriguingly, substrate discrimination based on hydrophobicity of the TMD or charges in the CTE is fairly modest during this transfer. In contrast, the TMD of Fis1p is completely rejected during the transfer of TAs from Sgt2 to Get3. This rejection, combined with the suboptimal capture of this substrate by Sgt2, is sufficient to account for the Get3-independence of the insertion reactions for substrates containing the Fis1-TMD in yeast lysate. This is surprising, as the hydrophobicity of Fis1p-TMD is comparable to those of 4AG and 5AG (which were efficiently transferred to Get3), and strongly suggests that another physicochemical property is responsible for TA substrate discrimination during their transfer to Get3. A possible candidate is the helical propensity of the TMD, as secondary structure predictions suggest that the additional Gly/Ser residues in the Fis1-TMD introduce breakages in the helix, and as the substrate binding groove of ATP-bound Get3 appears preorganized for interaction with a helical TMD (Mateja et al., 2015). Regardless of the exact nature of this property, our observations indicate that substrate transfer from Sgt2 to Get3 provides a

strong selection filter against the mitochondrial protein Fis1p, and that a distinct property in the TMD is recognized during this handover event.

Targeting of the Get3•TA complex to the ER and TA insertion into the membrane provides an additional selection filter (Figure 3.9A, Step 3). Our results show that two mechanisms can lead to further rejection of suboptimal substrates at this stage. TA proteins with low hydrophobicity, such as 6AG, dissociate from Get3 much more quickly than those with more hydrophobic TMDs; thus, disassembly of the targeting complex competes effectively with productive targeting and insertion. More importantly, this step provides the major mechanism to reject TA proteins with highly basic CTE, which are inserted into the ER much more slowly than those without (Figure 3.9A and 9C, blue). As the charged CTE compromised both Get3-dependent and Get3-independent TA insertions into the ER, enrichment of basic residues in the CTE provides a general feature that enables TA substrates with relatively hydrophobic TMDs to escape delivery and insertion to the ER. As transporting charges across a hydrophobic environment poses a high energetic barrier, this could provide an effective mechanism to reject substrates using either the phospholipid membrane at the ER and/or translocases that provide no compensation for these charges. Indeed the barrier for transport charges is higher for ER substrates than mitochondrial substrates as the outer membrane of mitochondria has an enrichment of the anionic lipid, cardiolipin (Gebert et al., 2009; van Meer et al., 2008). Finally, a four leucine substitution in the Fis1 TMD could compensate for its charged CTE and re-direct Fis1 to the GET pathway

(Wang et al., 2010), suggesting that TA localization is specified by a balance between multiple physicochemical properties.

The GET pathway uses a variety of molecular strategies to select for the correct substrates and reject suboptimal TAs. Selection during the initial capture utilizes the difference in binding energy of various TAs for Sgt2. Selection during substrate handover to Get3 utilizes an induced-fit mechanism, in which correct substrates enable faster reactions than incorrect substrates. After TA loading onto Get3, these substrates further partition between disassembly from Get3 and productive insertion into ER, with authentic substrates partitioning more favorably into the productive insertion reaction than suboptimal substrates. As this partitioning occurs *after* irreversible ATP hydrolysis on Get3, it is analogous to proofreading mechanisms observed during rejection of near cognate tRNAs by the ribosome (Rodnina and Wintermeyer, 2001a; 2001b). Although each mechanism provides a finite discrimination, the use of multiple, sequential selection steps can generate substantial accuracy despite the small differences that distinguish TA proteins destined to different organelles. This principle has been observed with DNA and RNA polymerases (Sydow and Cramer, 2009), in translation elongation by the ribosome (Ogle and Ramakrishnan, 2005; Rodnina and Wintermeyer, 2001a), and in co-translational protein targeting mediated by the signal recognition particle (Zhang et al., 2010), and may represent a general principle by which key biological processes attain a high degree of fidelity.

Our results also reveal an important role of Sgt2 in the selection and commitment of TA substrates to the GET pathway. Counter-intuitively, differences in binding affinity of different TA substrates to Get3 do not provide a stringent selection mechanism. This is due to the high kinetic stability of the Get3-TA interaction, such that dissociation of the Get3•TA complex ($\tau \sim 1$ hr) is much slower than its subsequent targeting and insertion ($t \sim 5–7$ min). As a result, TA proteins of borderline hydrophobicity that modestly destabilize the Get3•TA complex would not be filtered out of the pathway (Figure 3.9B). Sgt2 could overcome this problem by two mechanisms. First, as Sgt2 forms less stable complexes with TA proteins, a borderline substrate bound to Sgt2 can more readily equilibrate with alternative machineries in the cytosol than if the same substrate were bound to Get3. In addition, Sgt2 poses a higher kinetic barrier for transferring borderline substrates to Get3. Thus, Sgt2 imparts two important selection filters upstream of Get3. This provides, in part, a rationale for the complexity of TA protein loading and substrate handover events in the GET pathway.

Additional mechanisms could further enhance selection accuracy by the GET pathway. A simple extension of our model could include factors that compete with Get3 for receiving substrates from Sgt2, thus introducing a branch point upstream of Get3 that *irreversibly* directs suboptimal substrates from the GET pathway. The mammalian Sgt2 homolog, SgtA, associates with the Bag6 complex. Although the C-terminal domain of Bag6, together with TRC35 and Ubl4A, provides a structural analogue of the Get4/5 complex to mediate TA

substrate transfer to TRC40 (the mammalian Get3 homologue) (Mock et al., 2015), Bag6 also contains additional domains that mediate membrane protein quality control (Hessa et al., 2011). Thus, Bag6 provides a strong candidate to provide such a branch-point that can direct suboptimal substrates from the TRC40/GET pathway and towards quality control machineries (Lee and Ye, 2013; Leznicki and High, 2012). Analogous branches have been suggested by physical interactions between Sgt2 and other factors (Kohl et al.; Wang et al., 2010) but the mechanistic details of these and other machineries could exist in yeast and await discovery.

Materials and Methods

Strains, plasmids and transcripts. Yeast strains used for live-cell imaging are derivatives of W303 (ATCC201238) but were made *TRP1* and *ADE2* by repairing the endogenous auxotrophies. GFP-Fis1-tail constructs were made by PCR amplifying GFP(S65T) which lacks a stop codon, with flanking SpeI and HindIII sites, the C-terminal 102 nt of Fis1 (plus additions for arginine codons and a stop codon included in the 3' oligo) with flanking HindIII and XhoI sites and cloning both fragments into p416ADH. mt-TagBFP is described in (Okreglak and Walter, 2014) and Sec63-tdTomato was a kind gift of Sebastian Schuck, ZMBH, Universität Heidelberg.

A model substrate is comprised of three tandem Strep tags at the N-terminus, a mutant yeast Smt3 in which the Ulp1 cleavage site was removed (a Pro insertion at residue 98 of Smt3), residues 207-222 of Bos1p (SEQTITSINKRVFKDK), various TMDs and CTEs defined in Figure 3.3A, and an opsin tag at the extreme C-terminus (GSMRMNGTEGPNMYMPMSNKTVD). TMD and CTE variants were constructed using Quikchange mutagenesis (Stratagene) or FastCloning (Li et al., 2011). For translation in yeast lysate, the coding sequences for model TA substrates were cloned into pSPBP6 (Siegel and Walter, 1988) under control of the SP6 promoter, and transcribed using a SP6 Megascript kit (Ambion). For coupled transcription-translation *in E. coli* lysate, the substrate coding sequences were cloned into the pCAT vector (Kim

and Swartz, 2001) to replace that of chloramphenicol acetyl transferase. pET29-Sfp-His_6 was a gift from Jun Yin.

Cell imaging. Yeast strains were cultivated in SD –Trp lacking the appropriate nutrients for selection of episomal constructs at 25 ºC at early to mid-log phase (OD_{600} ~ 0.3-0.5). Cells were immobilized on coverslips coated with 0.1 mg/ml concanavalin A (Sigma) and imaged using a Nikon Eclipse Ti equipped with a spinning disk confocal (CSU-X1; Yokogawa), EMCCD camera (iXon3 897; Andor) and a 100X 1.49NA objective. Images were acquired with µManager software (Edelstein et al., 2010) and processed with ImageJ 1.49 (http://rsb.info.nih.gov/ij/).

Translation Extracts. Yeast translation extracts and microsomes were prepared from *Dget3* or *SGT2FLAG*/Δget3 (VDY 57; (Wang et al., 2010) strains as described in (Rome et al., 2013). *E. coli* S30 lysate was prepared as previously (Saraogi et al., 2011b). Coupled transcription-translation in the S30 extract was carried out as described (Saraogi et al., 2011b) except that untagged T7 polymerase and untagged CmRS was used and anti-ssrA oligo was omitted.

Protein expression and purification. Expression and purification of full length Get4/5 and His_6-tagged Get3 were performed as described (Rome et al., 2013). His_6-tagged Sfp was expressed and purified as described (Yin et al., 2006).

Purification of His_6-tagged Sgt2. A hexahistidine tag and TEV protease site were fused to the N-terminus of full length Sgt2 and cloned into pET33b. Proteins were expressed in BL21DE3* at 37ºC for 4 hours after induction with 0.4 mM IPTG. Cell pellets were resuspended in 50 mM Tris-HCl (pH 7.5), 500 mM NaCl, 30 mM imidazole, 5 mM β-mercaptoethanol (β-ME), 1X cOmplete Tablets EDTA free Protease Inhibitor Cocktail (Roche), Benzonase (Novagen), and lysed in 1X BugBuster® (Novagen). Clarified lysates were loaded on Ni Sepharose resin (GE Healthcare) and washed with 30 column volumes of lysis buffer. Proteins were eluted using 50 mM Tris-HCl (pH 7.5), 500 mM NaCl, 300 mM imidazole and dialyzed against 50 mM KHEPES (pH 7.5), 150 mM NaCl and 20% Glycerol. *Purification of untagged Sgt2*. Full length Sgt2 is flanked by N-terminal and C-terminal TEV sites. A His_6-tag was inserted downstream of the C-terminal TEV site. This construct was cloned into pMALC2 as a C-terminal fusion to the MalE gene. Protein was expressed and purified as with His_6-tagged Sgt2 with the following modifications: after affinity purification by Ni-NTA (QIAGEN), protein was dialyzed against 20 mM Tris-HCl (pH 7.5), 20 mM NaCl and 1 mM β-ME. TEV protease was included with partially purified Sgt2 to remove the MBP and His_6 tags. Samples were then incubated with amylose resin to remove MBP and MBP-fusion proteins. The flowthrough was further purified by anion exchange MonoQ 10/100 GL (GE Healthcare) using a gradient of 20 –550 mM NaCl, followed by gel filtration chromatography on a Superdex 200 16/60 (GE Healthcare) in GET Buffer (50 mM KHEPES (pH 7.5), 150 mM KOAc, 5 mM $Mg(OAc)_2$, and 1 mM DTT).

Purification of ybbR-tagged Get3. Amplified DNA encoding wild-type *S. cerevisiae* Get3 was subcloned into pET28-His_6-thrombin-SUMO vector (a gift from André Hoelz) using SalI and NotI restriction sites. For Sfp-mediated labeling, a ybbR tag (DSLEFIASKLA) was inserted between residues S110 and D111 in the His_6-Thrombin-SUMO-Get3 construct through FastCloning (Li et al., 2011). SUMO-Get3 proteins were recombinantly expressed in *E. coli* BL21 DE3* cells grown in LB media for 6-8 hours at 25 °C after induction with 1 mM IPTG when cultures reached an A_{600} ~ 0.3-0.6. The fusion protein was purified first using Ni-NTA affinity chromatography (Qiagen), and incubated with SUMO protease (gift from André Hoelz). The digestion mixture was passed through Ni-NTA to remove His_6-thrombin-SUMO and SUMO protease. Dimeric Get3 was further isolated by gel filtration over Superdex 200 16/60 (GE Healthcare). For ATPase assays, Get3 was further purified over MonoQ 10/100 GL (GE Healthcare) before gel filtration chromatography.

Purification of untagged T7 polymerase. A precision protease site was introduced between the N-terminal His_6-tag and T7 polymerase. After purification of His_6-tagged T7 polymerase via Ni-NTA, the elution was dialyzed overnight against 50 mM Tris-HCl (pH 8.0), 200 mM NaCl, 5% Glycerol, and 10 mM imidazole at 4 ºC in the presence of His_6- tagged precision protease (a gift of Andre Hoelz). The mixture was passed through Ni-NTA to remove the precision protease and further purified over Superdex 200 16/60 (GE Healthcare). Purified T7 polymerase was stored in 50% glycerol at –30 ºC.

Purification of untagged coumarin-tRNA synthetase (CmRS). A precision protease site was introduced between the N-terminal His_6-tag and CmRS (Charbon et al., 2011; Saraogi et al., 2011b). After purification of His_6-tagged CmRS via Ni-Sepharose (GE Healthcare), the elution was dialyzed overnight against 25 mM KHEPES (pH 7.5), 300 mM NaCl, 10% Glycerol, 10 mM β-ME, and 50 mM imidazole at 4 °C in the presence of His_6-tagged precision protease (a gift of Andre Hoelz). The mixture was passed through Ni-Sepharose to remove the precision protease and undigested CmRS. Purified CmRS was stored in 50% glycerol at –30 °C.

Fluorescence labeling

Synthesis and purification of Bodipy FL-CoA. Bodipy FL-CoA was synthesized and purified as described (Yin et al., 2006) with the exception that Bodipy FL maleimide (Life Technologies) was used instead of Alexa Fluor 488 C_5 maleimide. The lyophilized compound was dissolved in DMSO, and dye concentration was quantified after dilution in methanol using ε_{504} = 79,000 $M^{-1}cm^{-1}$.

Labeling of ybbR-Get3 with Bodipy FL-CoA. 30 μM ybbR-Get3 was mixed with 60 μM Bodipy FL-CoA and 12 μM Sfp-His_6 in Sfp labeling buffer (50 mM KHEPES, pH 7.4, 10 mM $MgCl_2$) in a total volume of 800 μL. The reaction mixture was rotated at room temperature for 1 hour. 10 μL 2 M imidazole (pH 7.0) was added before passing the reaction through Ni-NTA to remove Sfp-His_6. Gel filtration through a Sephadex G-25 (Sigma-Aldrich) column was used to

remove excess Bodipy FL-CoA and exchange ybbR-Get3^{BDP} into GET buffer. Translocation and ATPase reactions mediated by ybbR-Get3^{BDP} were performed as described in (Rome et al., 2013).

Purification of Sgt2•TA^{Cm}. 7-hydroxycoumarin was incorporated into TA substrates using the amber suppression system described in (Saraogi et al., 2011b). A TAG codon was introduced four residues upstream of the TMD. Coupled *in vitro* transcription-translation was carried out as described (Saraogi et al., 2011b) in the absence of anti-ssrA oligonucleotide and in the presence of 2 μM recombinantly purified Sgt2, untagged T7, and untagged CmRS. A 5 mL translation reaction was supplemented with 20 mM imidazole (pH 7.5) and batch bound to 0.8 mL NiNTA agarose (Qiagen), and washed with 20 CV of GET Buffer supplemented to a 300 mM KOAc final concentration and 5mM β-ME as the sole reducing agent. Sgt2•TA complex was eluted using GET buffer supplemented with 300 mM imidazole (pH 7.5) and 5mM β-ME as the sole reducing agent. Elutions (10 mL) were concentrated through 10K concentrators (Amicon) and stored at –80 ºC. The presence of His_6-Sgt2 and $Strep_3$-TA was verified by Western blotting. The amount of Sgt2 in the purified complex was quantified by Western blotting and standardized against known amounts of independently purified His_6-Sgt2.

Purification of Get3^{BDP}•TA^{Cm}. Get3^{BDP}•TA^{Cm} complexes were generated by translating TAG-containing TA constructs in the presence of 500 nM Get3^{BDP}. Bos1, 2AG, 3AG, 4AG, 5AG, and Bos1-FisC were synthesized from a 5-10 mL in the presence of 500 nM Get3^{BDP}. Translation reactions were loaded onto a 1 mL

Strep-Tactin Sepharose (IBA Germany) column and washed with 20 CV of GET Buffer. Get3^{BDP} •TA complex was eluted using GET buffer supplemented with 2 mg/mL desthiobiotin. Elutions (10 mL) were concentrated through 10K concentrators (Amicon) and stored at –80 ºC. For 6AG, 500 nM Get3^{BDP} was supplemented in buffers used during washing and elution.

Translocation reactions. To assay overall TA translocation, substrates of interest were translated for 1 hr in *Δget3* lysate with or without recombinant Get3 present (as indicated in the text). Cyclohexamide and *Δget3*-derived microsomes were then added to initiate translocation. Substrates were allowed to translocate for an hour unless translocation time courses were followed. Reactions were quenched by flash freezing in liquid nitrogen following by boiling in SDS buffer and analyzed by SDS-PAGE and autoradiography. The dependence of translocation efficiency on Get3 concentration for Bos1, 2AG, 4AG and Bos1-FisC were fit to Eq 3.1,

$$T_{obsd} = T_{max} \times \frac{[Get3]^h}{[Get3]^h + K_{1/2}^h} \quad , \qquad (3.1)$$

in which T_{obsd} is the observed translocation efficiency (%glycosylated TA) at a particular Get3 concentration, T_{max} is the translocation efficiency at saturating Get3, K_d is the Get3 concentration required for half maximal translocation, and *h* is the hill coefficient. The dependence of translocation efficiency on Get3 concentration for 6AG, Fis1-BosC and Fis1-FisC were fit to a horizontal line. All

curve-fitting was conducted using GraphPad Prism 6 for MacOS, GraphPad Software, San Diego California USA, www.graphpad.com.

Substrate capture by Sgt2. 100 µL S30 translations were carried out for TA substrates of interest in the presence of ^{35}S-methionine and 2 µM His_6-tagged Sgt2 at 30 ºC for 1 hour. Reactions were adjusted to 50 mM KHEPES, pH 7.5, 150 mM KOAc, 5 mM $Mg(OAc)_2$,10% Glycerol, 5 mM β-ME, 20 mM Imidazole (capture buffer), and incubated (with rotation) with 50 µL Ni-NTA agarose equilibrated in capture buffer at 4 ºC for 1 hour. The mixture was loaded into a Mini Bio-Spin Column (Bio-Rad). The resin was washed with 2 mL of capture buffer and eluted with 300 µL capture buffer containing 300 mM imidazole. The load, flowthrough, and elution fractions were analyzed by SDS-PAGE and autoradiography. Images were quantified using ImageQuantTL (GE Healthcare). All capture efficiencies were normalized against that of the internal control (Ctrl or Ctrl+3xStrep) translated and captured in parallel with the substrate of interest).

Fluorescence measurements of TA transfer. Equilibrium titrations of TA transfer between Sgt2 and Get3 were carried out in GET buffer at 25 °C in the presence of 20–50 nM Sgt2•TA^{Cm} complex, 150 nM Sgt2, 150 nM Get4/5, 2 mM ATP, and varying concentrations of $Get3^{BDP}$ in a Fluorolog-3-22 spectrofluorometer (Jobin Yvon). FRET efficiency (E) was calculated according to Eq 3.2,

$$E = 1 - \frac{F_{DA}}{F_D} \quad , \qquad (3.2)$$

in which F_{DA} is the fluorescence in the presence of donor and acceptor, and F_D is the fluorescence of donor in the absence of acceptor.

The Get3 concentration dependence of the transfer reaction was fit to Eq 3.3,

$$E_{obsd} = E_{Max} \times \frac{[Get3]}{K_{1/2}+[Get3]} \quad , \qquad (3.3)$$

in which E_{obsd} is the observed FRET efficiency at a given Get3 concentration, E_{Max} is the FRET efficiency at saturating Get3 concentrations, and $K_{1/2}$ is the concentration of Get3 required to reach half of the maximal FRET.

Time courses of TA transfer from Sgt2 to Get3 were measured using a stopped-flow apparatus (Kintek). Reactions were initiated by mixing equal volumes of ~50nM Sgt2•TA^{Cm} in 150 nM Sgt2 with a mix of 400nM Get3^{BDP}, 400nM Get4/5 and 2 mM ATP. For measurements in the presence of lysate, *Δget3* lysates were spun at 100k rpm in a Beckman TLA 100.1 rotor for 1hr at 4 ºC to remove ribosomes. These reactions were initiated by mixing equal volumes of ~50 nM purified Sgt2•TA^{Cm} complex (supplemented with 100 nM Sgt2) with a mix of 400 nM Get3^{BDP}, 400 nM Get4/5 and 2 mM ATP in ribosome-depleted lysate. Fluorescence decay of the FRET donor was monitored using a 445D40M (Chroma) band pass filter. The data were normalized and fit to Eq 3.4,

$$F_{obsd} = F_e + \Delta F_{fast} \times e^{-k_{fast}t} + \Delta F_{slow} \times e^{-k_{slow}t} \quad , \qquad (3.4)$$

in which F_e is the fluorescence when the reaction reaches equilibrium, ΔF_{fast} and ΔF_{slow} are the amplitudes of the fluorescence changes in the fast and slow

phases, respectively, and k_{fast} and k_{slow} are the rate constants of the fast and slow phases, respectively.

Translocation of the Get3•TA complex. 100 µL S30 translations were carried out for TA substrates of interest in the presence of untagged Sgt2. After translation, the reactions were supplemented with 2 mM ATP, 2 µM Get4/5 and 2 µM Get3 to allow TA transfer to Get3 for 1 hour. Sample was diluted with 2X capture buffer and purified as for Sgt2•TA capture. Elutions were concentrated to ~50 µL and TA concentration wasmeasured by scintillation counting. Samples were normalized to the same number of counts using GET buffer supplemented with 20 mg/mL BSA and 5 mM ATP.

100 µL targeting and translocation reactions were initiated by adding 20 µL of *Δget3* microsomes. At various time points, 10 µL samples were removed from the reaction and quenched by addition of 2XSDS buffer and flash freezing in liquid nitrogen. Samples were analyzed by SDS-PAGE and autoradiography. The time course of translocation was fit to Eq 3.5,

$$\%translocation = T + (A - T)e^{-k_{obsd}t} , \quad (3.5)$$

in which *T* is the %translocation at the end of the reaction, A is the translocation at t = 0, and k_{obsd} is the apparent rate constant of the translocation reaction.

In a given translocation reaction, the observed rate constant (k_{obsd}) and endpoint (*T*) of the reaction are contributed by the rate constants of productive insertion (k_{insert}) and nonproductive reactions ($k_{nonproductive}$) according to Eqs 3.6-7,

$$k_{obsd} = k_{insert} + k_{nonproductive} , \quad (3.6)$$

$$k_{insert} = k_{obsd} \times \frac{T}{100} \quad . \qquad (3.7)$$

The values of k_{insert} and $k_{nonproductive}$ were obtained by solving Eqs 3.6-7.

Kinetic stability of the Get3•TA complex. Dissociation rate constants of Get3•A complexes were measured by chasing 20–50 nM preformed $Get3^{BDP}$•TA^{Cm} complexes with a 10-fold excess of unlabeled Get3. The time course of loss of FRET was monitored and fit to Eq 3.8,

$$F = F_e + (A - F_e)e^{-k_{obsd}t} \qquad (3.8)$$

in which F is the observed donor fluorescence at a particular time, F_e is the donor fluorescence when the reaction is complete, and k_{obsd} is the dissociation rate constant for the Get3•TA complex.

.

Figures

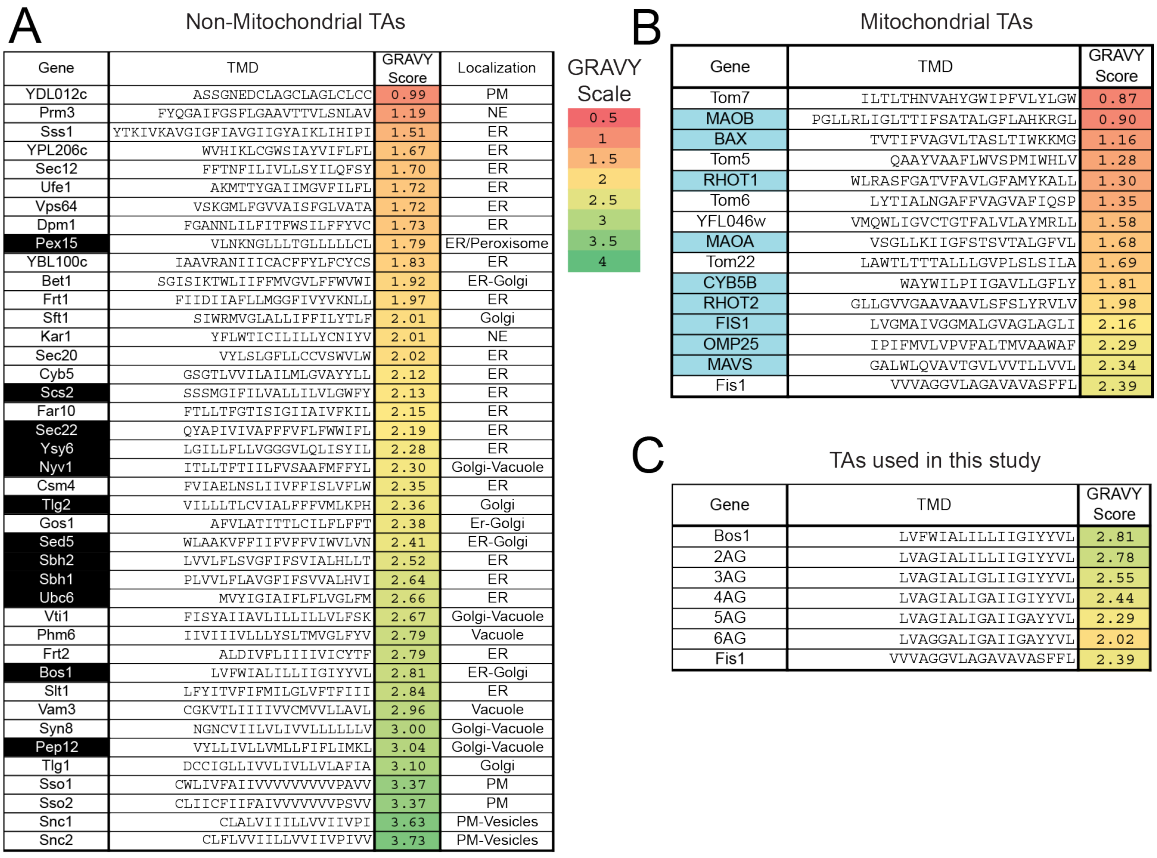

Gene	TMD	GRAVY Score	Localization
YDL012c	ASSGNEDCLAGCLAGLCLCC	0.99	PM
Prm3	FYQGAIFGSFLGAAVTTVLSNLAV	1.19	NE
Sss1	YTKIVKAVGIGFIAVGIIGYAIKLIHIPI	1.51	ER
YPL206c	WVHIKLCGWSIAYVIFLFL	1.67	ER
Sec12	FFTNFILIVLLSYILQFSY	1.70	ER
Ufe1	AKMTTYGAIIMGVFILFL	1.72	ER
Vps64	VSKGMLFGVVAISFGLVATA	1.72	ER
Dpm1	FGANNLILFITFWSILFFYVC	1.73	ER
Pex15	VLNKNGLLLTGLLLLLCL	1.79	ER/Peroxisome
YBL100c	IAAVRANIIICACFFYLFCYCS	1.83	ER
Bet1	SGISIKTWLIIFFMVGVLFFWVWI	1.92	ER-Golgi
Frt1	FIIDIIAFLLMGGFIVYVKNLL	1.97	ER
Sft1	SIWRMVGLALLIFFILYTLF	2.01	Golgi
Kar1	YFLWTICILILLYCNIYV	2.01	NE
Sec20	VYLSLGFLLCCVSWVLW	2.02	ER
Cyb5	GSGTLVVILAILMLGVAYYLL	2.12	ER
Scs2	SSSMGIFILVALLILVLGWFY	2.13	ER
Far10	FTLLTFGTISIGIIAIVFKIL	2.15	ER
Sec22	QYAPIVIVAFFFVFLFWWIFL	2.19	ER
Ysy6	LGILLFLLVGGGVLQLISYIL	2.28	ER
Nyv1	ITLLTFTIILFVSAAFMFFYL	2.30	Golgi-Vacuole
Csm4	FVIAELNSLIIVFFISLVFLW	2.35	ER
Tlg2	VILLLTLCVIALFFFVMLKPH	2.36	Golgi
Gos1	AFVLATITTLCILFLFFT	2.38	Er-Golgi
Sed5	WLAAKVFFIIFVFFVIWVLVN	2.41	ER-Golgi
Sbh2	LVVLFLSVGFIFSVIALHLLT	2.52	ER
Sbh1	PLVVLFLAVGFIFSVVALHVI	2.64	ER
Ubc6	MVYIGIAIFLFLVGLFM	2.66	ER
Vti1	FISYAIIAVLILLILLVLFSK	2.67	Golgi-Vacuole
Phm6	IIVIIIVLLLYSLTMVGLFYV	2.79	Vacuole
Frt2	ALDIVFLIIIIVICYTF	2.79	ER
Bos1	LVFWIALILLIIGIYYVL	2.81	ER-Golgi
Slt1	LFYITVFIFMILGLVFTFIII	2.84	ER
Vam3	CGKVTLIIIIVVCMVVLLAVL	2.96	Vacuole
Syn8	NGNCVIILVLIVVLLLLLLV	3.00	Golgi-Vacuole
Pep12	VYLLIVLLVMLLFIFLIMKL	3.04	Golgi-Vacuole
Tlg1	DCCIGLLIVVLIVLLVLAFIA	3.10	Golgi
Sso1	CWLIVFAIIVVVVVVVVVPAVV	3.37	PM
Sso2	CLIICFIIFAIVVVVVVVVPSVV	3.37	PM
Snc1	CLALVIIILLVVIIVPI	3.63	PM-Vesicles
Snc2	CLFLVVIILLVVIIVPIVV	3.73	PM-Vesicles

Gene	TMD	GRAVY Score
Tom7	ILTLTHNVAHYGWIPFVLYLGW	0.87
MAOB	PGLLRLIGLTTIFSATALGFLAHKRGL	0.90
BAX	TVTIFVAGVLTASLTIWKKMG	1.16
Tom5	QAAYVAAFLWVSPMIWHLV	1.28
RHOT1	WLRASFGATVFAVLGFAMYKALL	1.30
Tom6	LYTIALNGAFFVAGVAFIQSP	1.35
YFL046w	VMQWLIGVCTGTFALVLAYMRLL	1.58
MAOA	VSGLLKIIGFSTSVTALGFVL	1.68
Tom22	LAWTLTTTALLLGVPLSLSILA	1.69
CYB5B	WAYWILPIIGAVLLGFLY	1.81
RHOT2	GLLGVVGAAVAAVLSFSLYRVLV	1.98
FIS1	LVGMAIVGGMALGVAGLAGLI	2.16
OMP25	IPIFMVLVPVFALTMVAAWAF	2.29
MAVS	GALWLQVAVTGVLVVTLLVVL	2.34
Fis1	VVVAGGVLAGAVAVASFFL	2.39

Gene	TMD	GRAVY Score
Bos1	LVFWIALILLIIGIYYVL	2.81
2AG	LVAGIALILLIIGIYYVL	2.78
3AG	LVAGIALIGLIIGIYYVL	2.55
4AG	LVAGIALIGAIIGIYYVL	2.44
5AG	LVAGIALIGAIIGAYYVL	2.29
6AG	LVAGGALIGAIIGAYYVL	2.02
Fis1	VVVAGGVLAGAVAVASFFL	2.39

Figure 3.1

List and hydrophobicity analysis of the TMDs of ER (**A**) and mitochondrial (**B**) TAs, as well as the model substrates used in this study (Burri and Lithgow, 2004; Kalbfleisch et al., 2007) (**C**). Grand average of hydropathy (GRAVY) scores are color ramped for each substrate as indicated by the scale bar. For (B), human mitochondrial TAs are highlighted in blue. Abbreviations: PM, plasma membrane; NE, nuclear envelope.

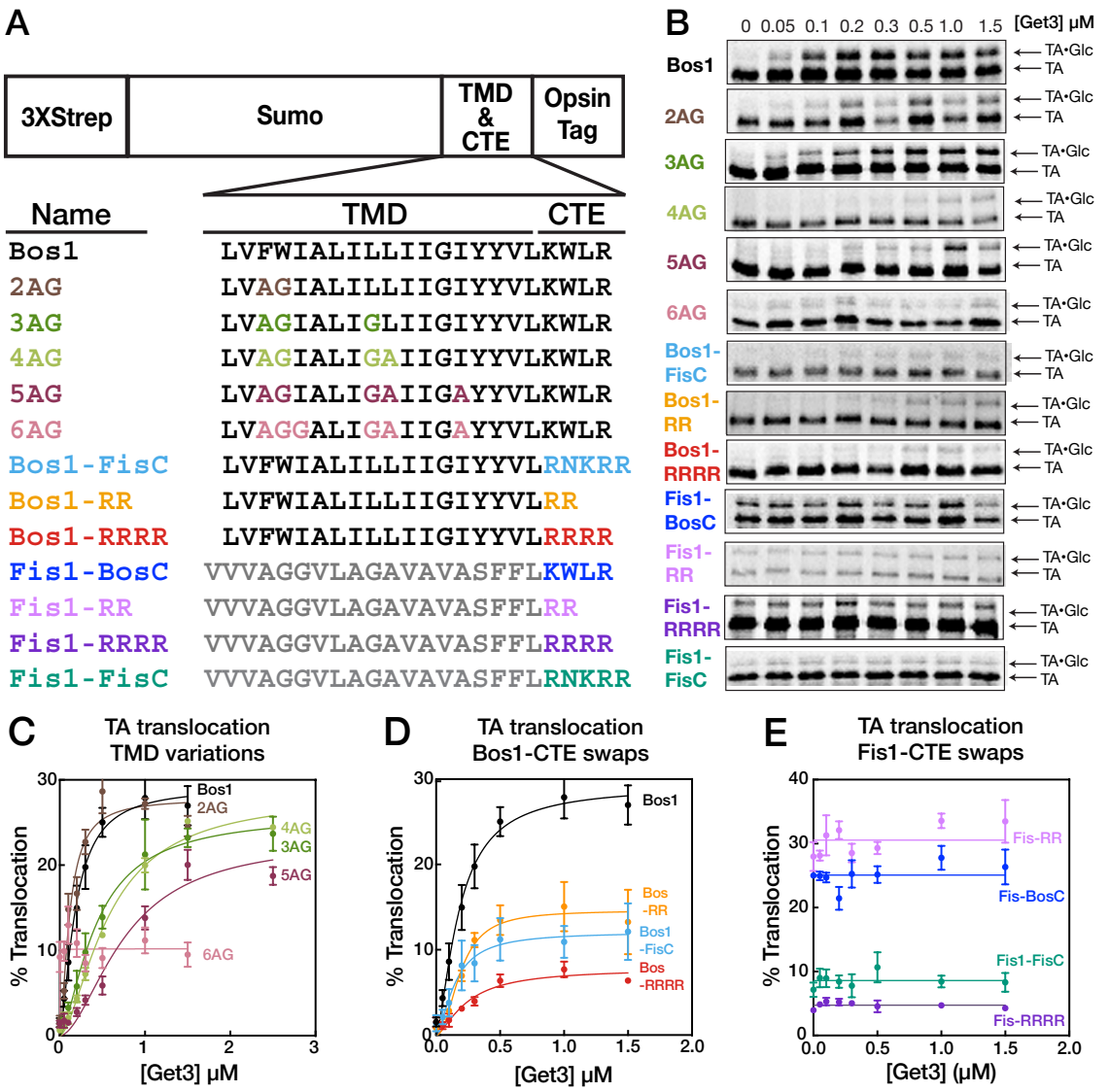

Figure 3.2

TAs are targeted to the ER based on TMD hydrophobicity and C-terminal basic residues. (**A**) Nomenclature and schematic of the model substrates used in this work. The sequences of the TMD and CTE are indicated below. (**B**) Overall targeting and translocation of model TA substrates into ER microsomes. TAs are translated in a *Δget3* yeast lysate and presented to *Δget3* microsomes in the presence of indicated concentrations of purified Get3. (**C-E**) Quantification of

the translocation of TAs for TMD variants **(C)**, CTE variants with Bos1 TMD (**D**), and CTE variants with Fis1 TMD (**E**). The data for Bos1, 2AG, 3AG, 4AG, 5AG, Bos1-FisC, Bos1-RR, and Bos1-RRRR were fit to Eq. 3.1, and the results are summarized in Table 3.1. The data for 6AG, Fis1-BosC, Fis1-FisC, Fis1-RR, and Fis1-RRRR were fit to horizontal lines with y =10 ± 0.5, y = 25 ± 0.6, y = 9 ± 0.5, y = 31 ± 0.7, and y = 5 ± 0.2 %, respectively. Values are reported as mean ± S.E.M, with n = 3-6.

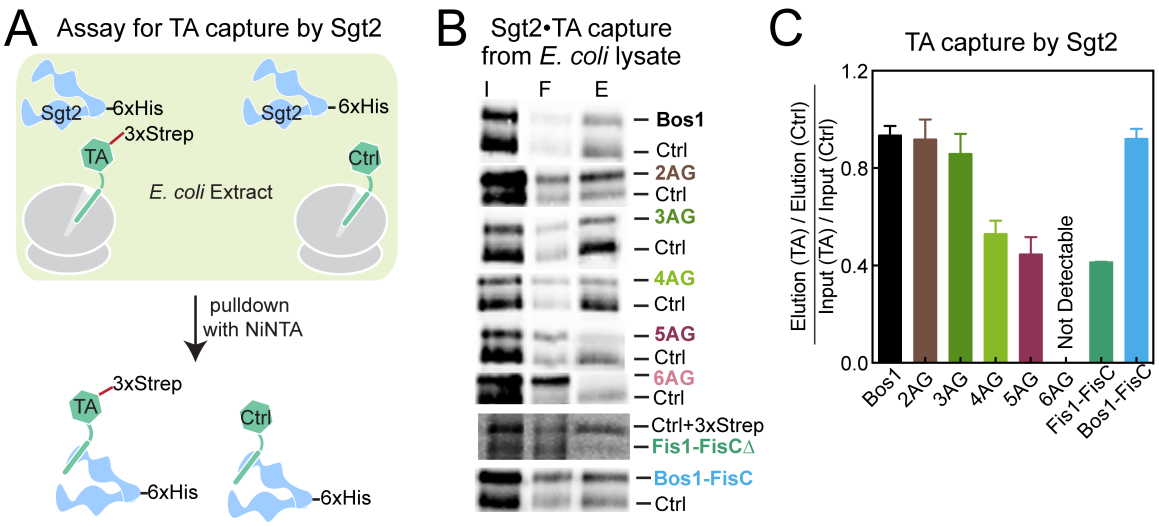

Figure 3.3

Sgt2 discriminates TAs on the basis of TMD hydrophobicity. (**A**) Schematic of Sgt2•TA capture assay. As an internal control, all TAs were translated and pulled down in parallel with Bos1 (Ctrl+3xStrep) or Bos1 lacking the N-terminal 3xStrep tag (Ctrl). (**B**) Autoradiogram of Sgt2•TA pulldowns. I, F, and E denote input, flowthrough, and elution, respectively. (**C**) Quantification of the experiments in (**B**). All the quantifications for the TA of interest were normalized against Ctrl or

Bos1 Ctrl. Normalized TA capture efficiencies were 0.93 ± 0.04, 0.92 ± 0.08, 0.56±0.08, 0.53±0.09, 0.44 ± 0.07, 0, 0.413±0.002 and 0.92±0.04 for Bos1, 2AG, 3AG, 4AG, 5AG, 6AG, Fis1-FisC, and Bos1-FisC, respectively. Values are reported as mean ± S.E.M, with n = 3-7

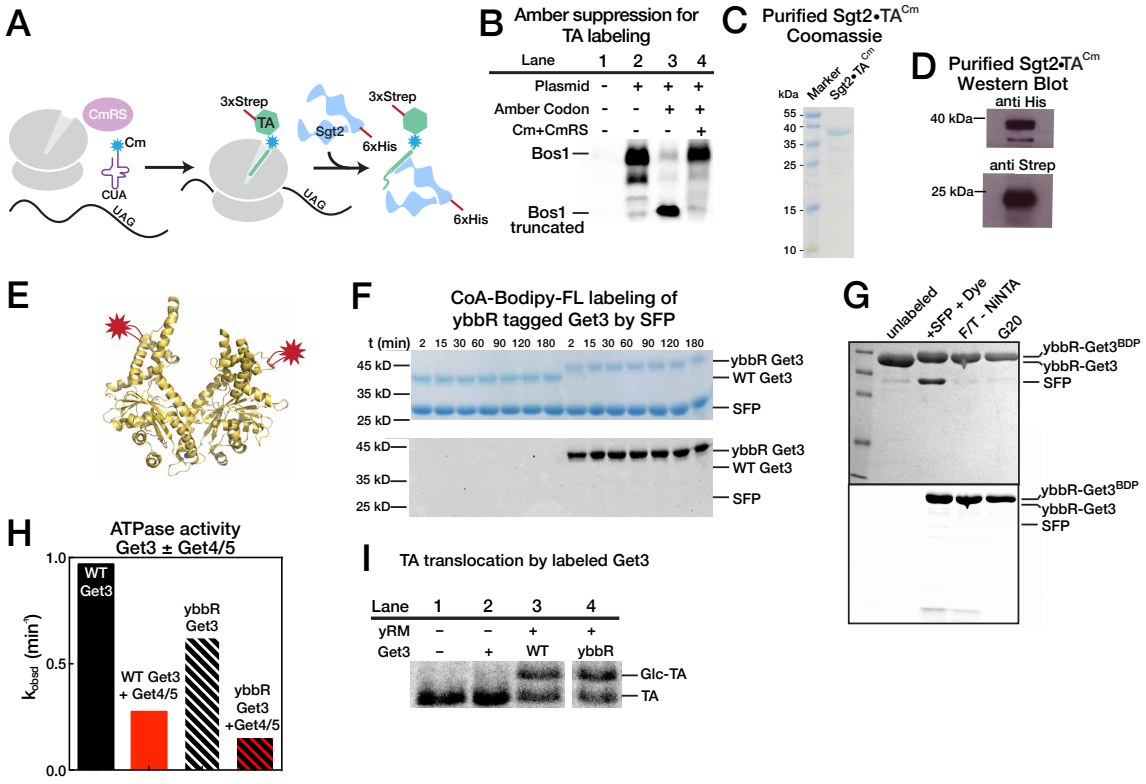

Figure 3.4

A fluorescence assay to monitor TA transfer from Sgt2 to Get3. (**A**) Scheme of TA labeling with the non-natural amino acid Cm using amber suppression technology in *E. coli* lysate. (**B**) Assessment of amber suppression efficiency. Bos1 was translated in the presence of ^{35}S-methionine without (lane 2) or with (lane 3-4) an amber codon four residues before the TMD. Lane 4 shows the suppression reaction in the presence of CmRS and Cm. (**C**) Coomassie stained SDS PAGE gel of a purified Sgt2•TA^{Cm} complex. (**D**) Western blot analysis of

purified Sgt2•TA^{Cm} complex. Sgt2 was His_6 tagged and TA was $strep_3$-tagged. (**E**) Location of the ybbR tag (for labeling) on the structure of Get3 (PDB: 3H84). (**F**) Coomassie-stain (top) and in-gel fluorescence (bottom) of Sfp-mediated conjugation of CoA-BODIPY-FL to the Get3 ybbR tag. (**G**) Labeling and purification of labeled Get3. Top, coomassie-stains; bottom, in-gel fluorescence. (**H**) ATPase assay of labeled ybbR tagged Get3. **(I)** Translocation assay of labeled ybbR tagged Get3. Values are reported as mean ± S.E.M., with n = 3.

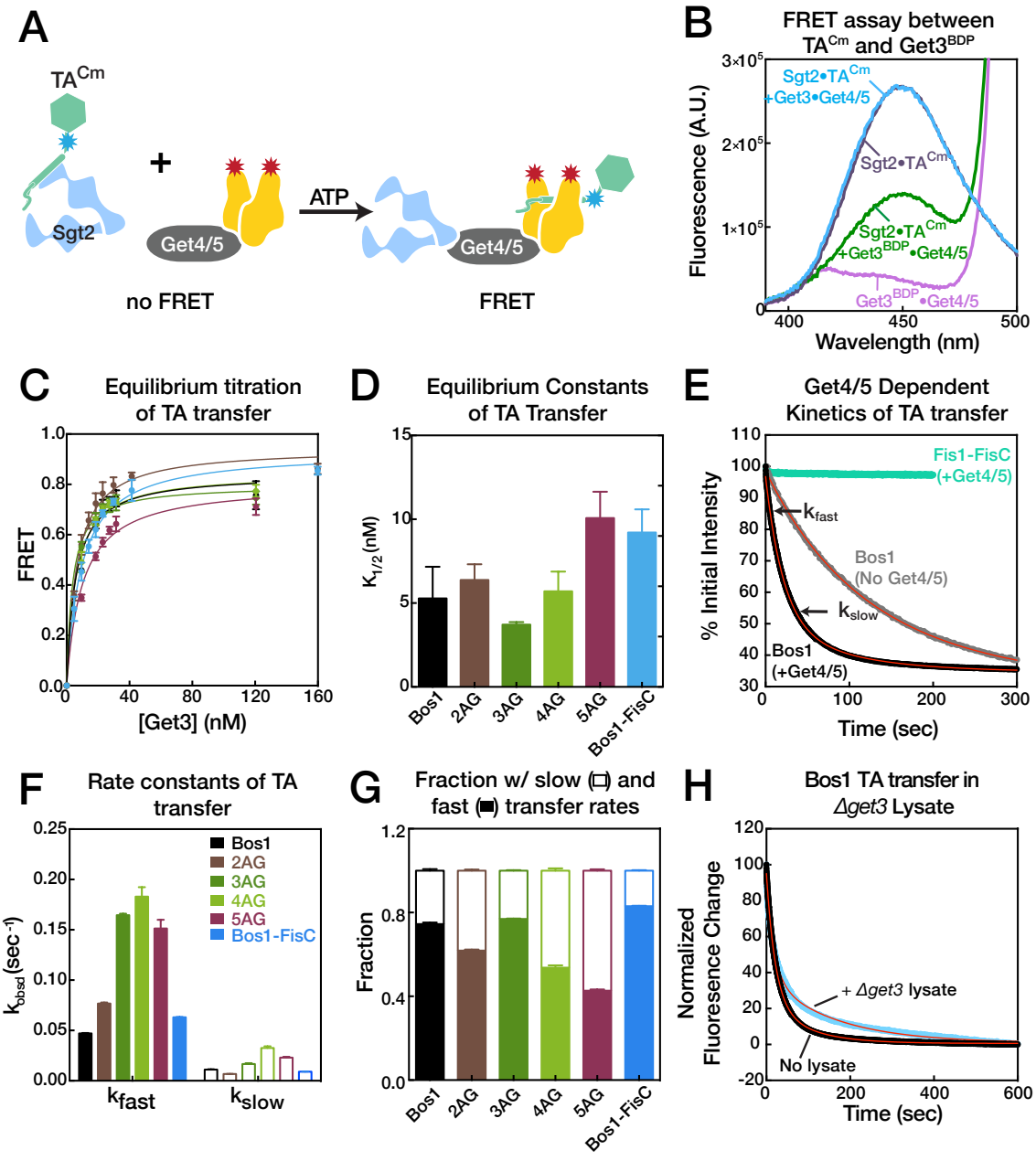

Figure 3.5

Equilibrium and kinetics of TA transfer from Sgt2 to Get3. (**A**) Scheme depicting the FRET assay for TA transfer from Sgt2 to Get3. Purified Sgt2•TA^{Cm} complex is presented to Get3^{BDP}•Get4/5 complex in the presence of ATP. Loading of TA^{Cm} onto Get3^{BDP} results in gain of FRET between the dye pair. (**B**)

Characteristic fluorescence emission spectra for purified Sgt2•TA^{Cm} complex (purple; donor fluorescence), Sgt2•TA^{Cm} incubated with unlabeled Get3, Get4/5 and ATP (blue; donor fluorescence corrected for environmental sensitivity), $Get3^{BDP}$ and Get4/5 (acceptor fluorescence), and Sgt2•TA^{Cm} complex incubated with $Get3^{BDP}$, Get4/5 and ATP (donor fluorescence in the presence of acceptor). (**C**) Dependence of the equilibrium of TA transfer reactions on Get3 concentration. All reactions used ~50 nM Sgt2•TA^{Cm} complexes supplemented with 150 nM Sgt2, 150 nM Get4/5, 2 mM ATP, and indicated concentrations of $Get3^{BDP}$. The data were fit to Eq 3.3, and the values are reported in **(D)** and Table 3.2. (**D**) Summary of the Get3 concentrations required for 50% complete TA transfer ($K_{1/2}$ values), derived from the data in **(C)**. Values are reported as mean ± S.E.M., with n = 3. (**E**) Time course of Bos1 transfer from Sgt2 to Get3, measured using a Kintek stopped flow apparatus with (black) and without Get4/5 (gray), and Fis1-FisC transfer with Get4/5 (green). The data were fit (red line) to Eq 3.4, and the derived values are summarized in parts F-G and Table 3.2. **(F, G)** Summary of observed rate constants (part F) and relative amplitudes **(**part G**)** of the TA transfer reaction for various substrates. Values are reported as mean ± S.E.M., with n = 5. (**H**) TA transfer of Bos1 from Sgt2 to Get3 in the presence (blue) and absence (black) of a ribosome depleted yeast lysate. The time courses were fit to Eq 3.4 and gave k_{fast} and k_{slow} values of 0.05 ± 0.001 s^{-1} and 0.006 ± 0.0002 s^{-1}, respectively, for the reaction in the presence of lysate.

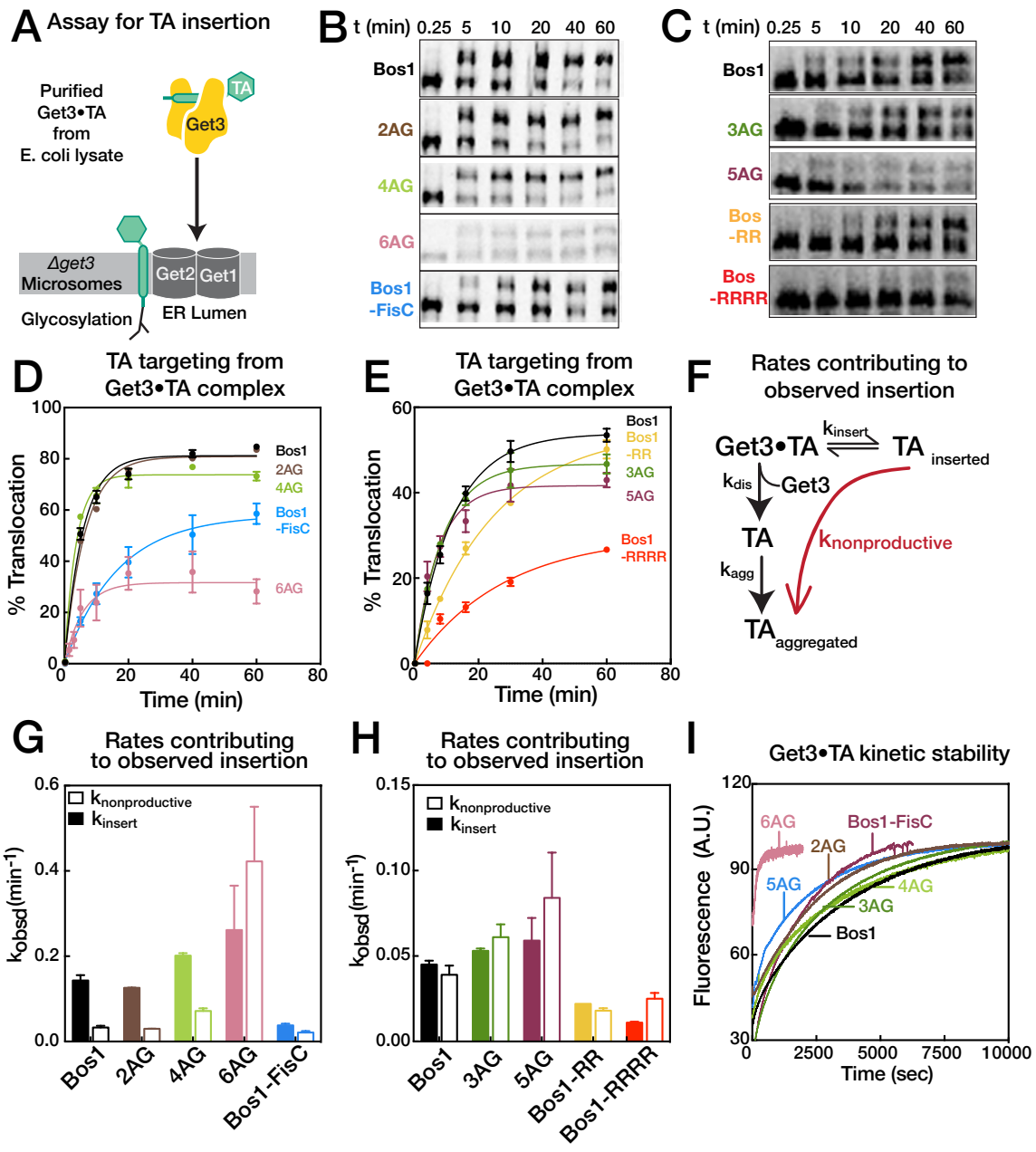

Figure 3.6

Targeting and insertion of the Get3·TA complex into the ER membrane is limited by basic residues in the CTE. (**A**) Schematic of the TA targeting and insertion reaction reported in Figure 3.6. Get3•TA complexes generated and purified from *E. coli* lysate were presented to *Δget3* microsomes. Insertion was

monitored by glycosylation of the opsin tag on TA substrates in the ER lumen. (**B-C**) Autoradiogram of insertion reactions carried out in parallel. Different microsome preparations gave different insertion efficiencies for Bos1 in (B) and (C), but did not affect the comparison of the substrates of interest with Bos1 assayed in the same experiment. (**D-E**) Quantification of the insertion reactions shown in B and C, respectively. The data were fit to Eq 3.5. (**F**) Schematic of the molecular events during the insertion reaction. Productive TA insertion (k_{insert}) must compete with nonproductive processes (collectively termed $k_{nonproductive}$), including reversal of the targeting reaction, disassembly of the Get3•TA complex (k_{dis}) and aggregation of TA substrates (k_{agg}). (**G-H**) Summary of the rate constants of competing events, defined by part F and Eq 3.6-7, that contribute to the observed rate constants and efficiencies of the targeting/insertion reactions in part C. The rate constants in G and H were derived from the data in Figure 3.6D and E, respectively (see also Table 3.3). (I) The kinetic stability of Get3•TA complexes (k_{dis} defined in part D) measured by pulse-chase experiments as described under Experimental Procedures. The data were fit to Eq 3.8 and dissociation rate constants are summarized in Table 3.3.

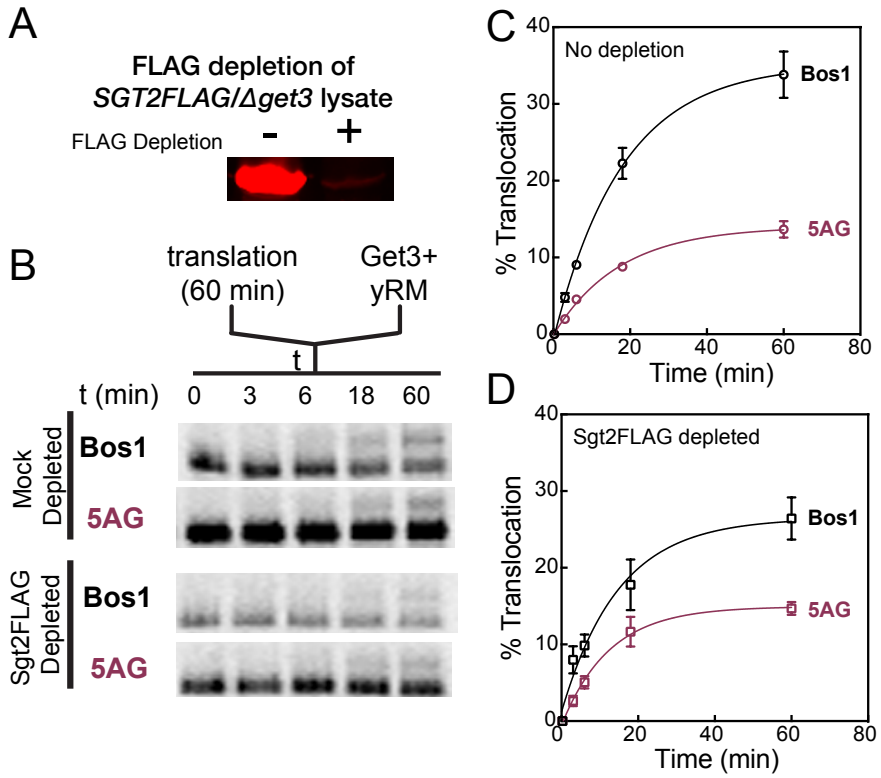

Figure 3.7

Effect of Sgt2 depletion on the targeting and insertion of Bos1 and 5AG. (A) Western blot of undepleted and depleted Δget3/SGT2FLAG lysate. (B) Autoradiogram of Bos1 and 4AG translocation into ER microsomes in Δget3 lysate mock depleted with FLAG resin (top) and Δget3/SGT2FLAG lysate depleted with FLAG resin to remove Sgt2. Reactions were carried out in the presence of 1 μM Get3. (C-D) Quantitation of the results in (B) for mock depleted (part C) and Sgt2-depleted lysate (part D). The data were fit to Eq. 3.5, and the results are summarized in Table 3.4.

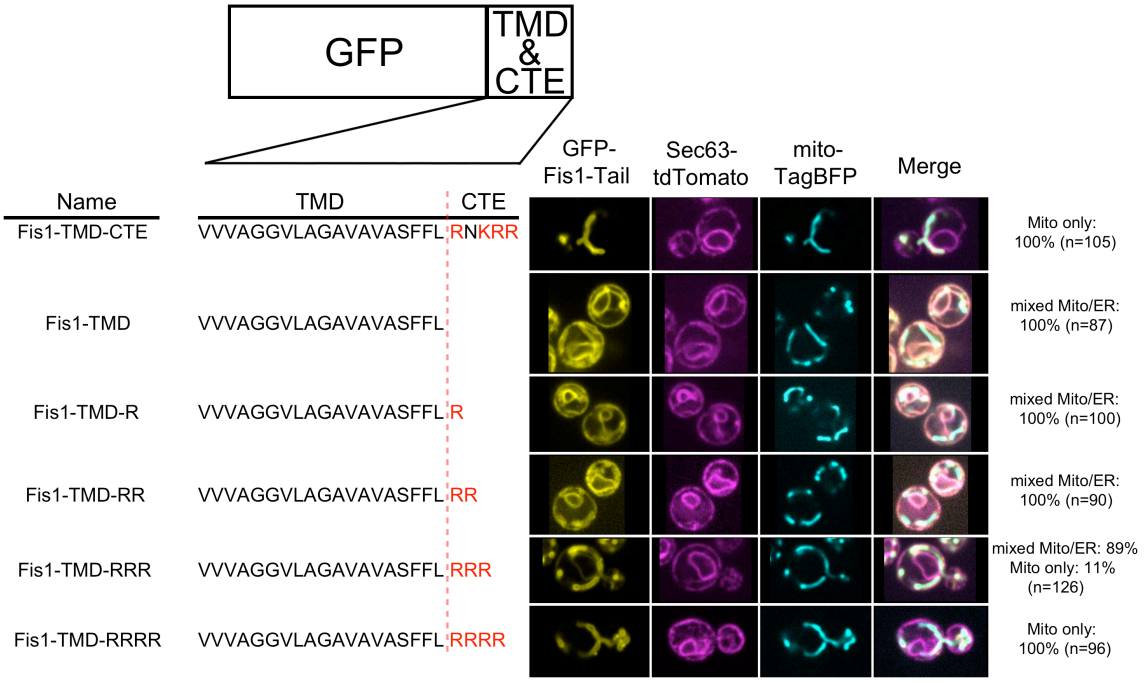

Figure 3.8

Mitochondrial selection for TA protein targeting is imparted by the net charge of its C-terminal element. Nomenclature and schematic of the constructs used for live-cell imaging of cells expressing GFP-tagged Fis1 tail constructs are shown on the left. Medial focal planes are shown on the right, with ER marked by Sec63-tdTomato and mitochondria by mitochondrially targeted TagBFP. Quantification denotes % of cells in each category (mixed Mito/ER or Mito only).

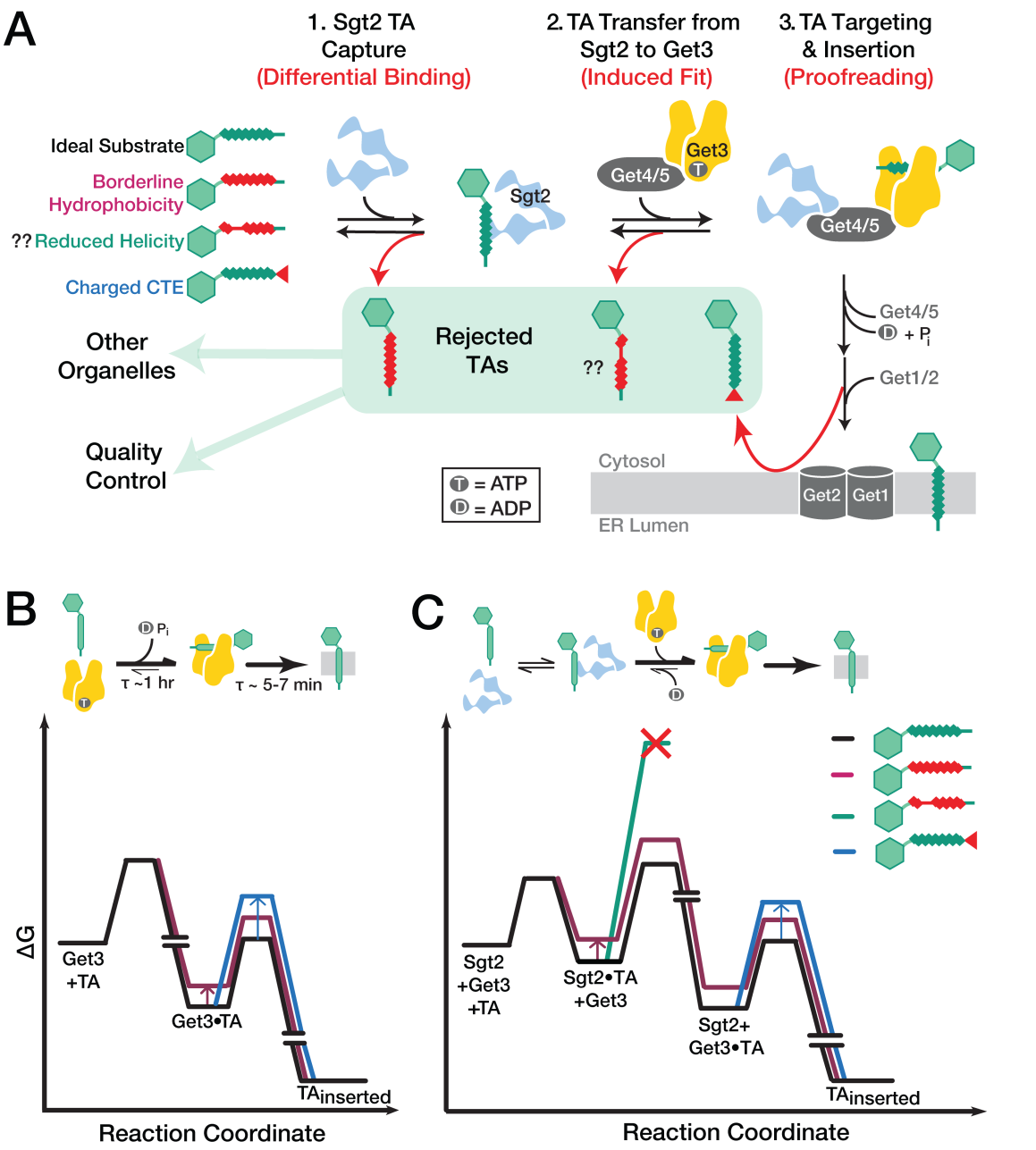

Figure 3.9

(A) Model of sequential TA selection by the GET pathway. Step 1: TAs are captured by Sgt2. TA substrates with less hydrophobic TMDs (red coil) are rejected. Step 2: Get4/5 mediated TA transfer from Sgt2 to ATP-bound Get3. Substrates with reduced helical propensity are rejected. Step 3: after

hydrolyzing ATP and dissociating from Get4/5, the Get3•TA complex associates with the membrane receptors Get1 and Get2 that mediate TA insertion. TAs enriched in basic residues at the extreme C-termini (red tail) are rejected at this step. (B-C) Free energy profiles for TA capture and insertion without (B) and with (C) Sgt2 in the GET pathway. The free energy profiles for a good substrate (Bos1) are indicated in black, for a borderline hydrophobic substrate (5AG) are in maroon, for a substrate with reduced helical propensity in the TMD are in green, and that for a substrate with a charged CTE (Bos1-FisC) are in blue. Reaction schemes for each pathway are represented above the respective free energy profile.

Table 3.1: Summary of kinetic parameters for TA targeting and translocation *Δget3* lysate. Related to Figure 3.2.

Substrate	$K_{1/2}$ (μM)	Hill Coefficient	T_{max} (%)
Bos1	0.18 ± 0.03	1.5 ± 0.3	29 ± 2.3
2AG	0.11 ± 0.02	1.6 ± 0.4	28 ± 1.8
3AG	0.42 ± 0.06	1.5 ± 0.2	26 ± 1.5
4AG	0.57 ± 0.06	1.6 ± 0.2	28 ± 1.6
5AG	0.76 ± 0.16	1.8 ± 0.4	23 ± 1.8
Bos1-FisC	0.15 ± 0.06	1.6 ± 0.8	12 ± 2
Bos-RR	0.19 ± 0.04	2.1 ± 0.8	15 ± 1.4
Bos-RRRR	0.24 ± 0.07	1.5 ± 0.5	8 ± 1.1

Table 3.2: Summary of kinetic parameters for TA transfer. Related to Figure 3.5.

Substrate	$K_{1/2}$ (nM)	FRET endpoint	k_{fast} (s^{-1})	$Fraction_{fast}$	k_{slow} (s^{-1})	$Fraction_{slow}$
Bos1 (No Get4/5)	N.D.	N.D.	0.0094 ± $7x10^{-5}$	0.76 ± 0.03	0.0030 ± $1x10^{-4}$	0.24 ± 0.03
Bos1	5.6 ± 1	0.84 ± 0.03	0.047 ± $4x10^{-4}$	0.75 ± 0.007	0.011 ± $4x10^{-4}$	0.25 ± 0.007
2AG	6.4 ± 0.5	0.94 ± 0.02	0.077 ± $1x10^{-3}$	0.62 ± 0.005	0.007 ± $1x10^{-4}$	0.38 ± 0.005
3AG	3.7 ± 0.5	0.80 ± 0.01	0.164 ± $2x10^{-3}$	0.77 ± 0.002	0.017 ± $8x10^{-4}$	0.23 ± 0.002
4AG	5.7 ± 0.6	0.84 ± 0.02	0.183 ± $9x10^{-3}$	0.54 ± 0.011	0.033 ± $2x10^{-3}$	0.46 ± 0.011

5AG	10 ± 1	0.80 ± 0.02	0.151 ± $9x10^{-3}$	0.43 ± 0.006	0.023 ± $8x10^{-4}$	0.57 ± 0.006
Bos1FisC	9.3 ± 0.6	0.93 ± 0.02	0.063 ± $3x10^{-4}$	0.83 ± 0.002	0.009 ± $1x10^{-4}$	0.17 ± 0.002

Table 3.3: Summary of translocation rate constants. Related to Figure 3.6.

Substrate	k_{obsd} (min^{-1})	Translocation endpoint (%)	k_{insert} (min^{-1})	$k_{nonproductive}$ (min^{-1})	k_{dis} (min^{-1})
Bos1	0.18 ±0.02	81.2 ± 0.5	0.14±0.01	0.033±0.004	$1.8x10^{-2}$ ± $3.4x10^{-5}$
2AG	0.16±0.0003	80.8 ± 0.2	0.126 ± 0.001	0.030 ± 0.0002	$2.3x10^{-2}$ ± 5.2 x 10^{-5}
4AG	0.273 ± 0.0003	74 ± 2	0.20 ± 0.006	0.072 ± 0.006	$1.7x10^{-2}$ ± $6.3x10^{-5}$
6AG	0.7 ± 0.2	36 ± 4	0.3 ± 0.1	0.4 ± 0.1	$2.0x10^{-1}$ ± $2.5x10^{-3}$
Bos1-FisC	0.59 ± 0.007	58.4 ± 4.6	0.38 ± 0.004	0.02 ± 0.003	$2.9x10^{-2}$ ± $3.0x10^{-5}$
Bos1	0.085 ± 0.008	53.8 ± 2.1	0.045 ± 0.002	0.039 ± 0.005	
3AG	0.11 ± 0.008	46.7 ± 2.4	0.053 ± 0.001	0.06 ± 0.008	$2.6x10^{-2}$ ± $6.3x10^{-5}$
5AG	0.14 ± 0.4	41.9 ± 2.3	0.06 ± 0.01	0.08 ± 0.03	$3.4x10^{-2}$ ± $1x10^{-4}$
Bos1-RR	0.04 ± 0.002	54.8 ±2.1	0.0221 ± 0.0001	0.018 ± 0.002	Not determined
Bos1-RRRR	0.04 ± 0.004	30.1 ± 1.7	0.011 ± 0.0006	0.025 ± 0.003	Not determined

** Values are reported as mean ± S.E.M., with n=2.

Table 3.4: Summary of rate constants of TA translocation without preincubation with Get3. Related to Figure 3.7.

	TA	Endpoint	k_1 (min^{-1})
Δget3 Mock depleted	Bos1	35.5 ± 1.8	0.053 ± 0.007
	5AG	14.1 ± 0.6	0.057 ± 0.006
Δget3/SGT2FLAG FLAG depleted	Bos1	26.1 ± 2.2	0.076 ± 0.017
	5AG	15.1 ± 1.0	0.075 ± 0.013

Acknowledgments. We thank Bil Clemons, Michael Rome, Kuang Shen, Xin Zhang, and members of the Shan and Clemons labs for critical discussions and comments on the manuscript, and the Dougherty lab for use of HPLC. This work was supported by NIH grant GM107368 and Gordon and Betty Moore Foundation Grant GBMF2939 to S.S., NIH grants R01GM32384 & U01GM098254 to P.W., NIH training grant 5T32GM007616-33 to M.R, and the Leukemia and Lymphoma Society fellowship to V.O. P.W. is an Investigator of the Howard Hughes Medical Institute.

References

Akopian, D., Dalal, K., Shen, K., Duong, F., and Shan, S.-O. (2013a). SecYEG activates GTPases to drive the completion of cotranslational protein targeting. J Cell Biol *200*, 397–405.

Akopian, D., Shen, K., Zhang, X., and Shan, S.-O. (2013b). Signal Recognition Particle: An Essential Protein-Targeting Machine. Annu. Rev. Biochem. *82*, 693–721.

Alberts, B. (2008). Molecular Biology of the Cell (Garland Pub).

Beilharz, T. (2003). Bipartite Signals Mediate Subcellular Targeting of Tail-anchored Membrane Proteins in Saccharomyces cerevisiae. Journal of Biological Chemistry *278*, 8219–8223.

Borgese, N., Gazzoni, I., Barberi, M., Colombo, S., and Pedrazzini, E. (2001). Targeting of a tail-anchored protein to endoplasmic reticulum and mitochondrial outer membrane by independent but competing pathways. Molecular Biology of the Cell *12*, 2482–2496.

Borgese, N., Brambillasca, S., and Colombo, S. (2007). How tails guide tail-anchored proteins to their destinations. Current Opinion in Cell Biology *19*, 368–375.

Borgese, N., Colombo, S., and Pedrazzini, E. (2003). The tale of tail-anchored proteins. J Cell Biol *161*, 1013–1019.

Bozkurt, G., Stjepanovic, G., Vilardi, F., Amlacher, S., Wild, K., Bange, G., Favaloro, V., Rippe, K., Hurt, E., Dobberstein, B., et al. (2009). Structural insights into tail-anchored protein binding and membrane insertion by Get3. Proc. Natl. Acad. Sci. U.S.a. *106*, 21131–21136.

Burri, L., and Lithgow, T. (2004). A complete set of SNAREs in yeast. Traffic *5*, 45–52.

Chang, Y.W., Lin, T.W., Li, Y.C., Huang, Y.S., Sun, Y.J., and Hsiao, C.D. (2012). Interaction Surface and Topology of Get3-Get4-Get5 Protein Complex, Involved in Targeting Tail-anchored Proteins to Endoplasmic Reticulum. Journal of Biological Chemistry *287*, 4783–4789.

Chappie, J.S., Acharya, S., Leonard, M., Schmid, S.L., and Dyda, F. (2010). G domain dimerization controls dynamin's assembly-stimulated GTPase activity. Nature *465*, 435–440.

Charbon, G., Brustad, E., Scott, K.A., Wang, J., Løbner-Olesen, A., Schultz, P.G., Jacobs-Wagner, C., and Chapman, E. (2011). Subcellular Protein Localization by Using a Genetically Encoded Fluorescent Amino Acid. ChemBioChem *12*, 1818–1821.

Chartron, J.W., VanderVelde, D.G., Rao, M., and Clemons, W.M. (2012a). Get5 Carboxyl-terminal Domain Is a Novel Dimerization Motif That Tethers an Extended Get4/Get5 Complex. Journal of Biological Chemistry *287*, 8310–8317.

Chartron, J.W., Clemons, W.M., Jr, and Suloway, C.J. (2012b). The complex process of GETting tail-anchored membrane proteins to the ER. Current Opinion in Structural Biology *22*, 217–224.

Chartron, J.W., Gonzalez, G.M., and Clemons, W.M.J. (2011). A Structural Model of the Sgt2 Protein and Its Interactions with Chaperones and the Get4/Get5 Complex. J. Biol. Chem. *286*, 34325–34334.

Chartron, J.W., Suloway, C.J.M., Zaslaver, M., and Clemons, W.M.J. (2010). Structural characterization of the Get4/Get5 complex and its interaction with Get3. Proc. Natl. Acad. Sci. U.S.a. *107*, 12127–12132.

Chartron, J.W., VanderVelde, D.G., and Clemons, W.M., Jr (2012c). Structures of the Sgt2/SGTA Dimerization Domain with the Get5/UBL4A UBL Domain Reveal an Interaction that Forms a Conserved Dynamic Interface. CellReports *2*, 1620–1632.

Chen, Y., Pieuchot, L., Loh, R.A., Yang, J., Kari, T.M.A., Wong, J.Y., and Jedd, G. (2014). Hydrophobic handoff for direct delivery of peroxisome tail-anchored proteins. Nat Commun *5*.

Claessen, J.H.L., Mueller, B., Spooner, E., Pivorunas, V.L., and Ploegh, H.L. (2010). The Transmembrane Segment of a Tail-anchored Protein Determines Its Degradative Fate through Dislocation from the Endoplasmic Reticulum. Journal of Biological Chemistry *285*, 20732–20739.

Cremo, C.R., Neuron, J.M., and Yount, R.G. (1990). Interaction of myosin subfragment 1 with fluorescent ribose-modified nucleotides. A comparison of vanadate trapping and SH1-SH2 cross-linking. Biochemistry *29*, 3309–3319.

Cross, B.C.S., Sinning, I., Luirink, J., and High, S. (2009). Delivering proteins for export from the cytosol. Nature Publishing Group *10*, 255–264.

Eccleston, J.F., Petrovic, A., Davis, C.T., Rangachari, K., and Wilson, R.J.M.I. (2006). The kinetic mechanism of the SufC ATPase: the cleavage step is accelerated by SufB. Journal of Biological Chemistry *281*, 8371–8378.

Edelstein, A., Amodaj, N., Hoover, K., Vale, R., and Stuurman, N. (2010). Computer control of microscopes using μManager. Curr Protoc Mol Biol *Chapter 14*, Unit14.20.

Emanuelsson, O., and Heijne, von, G. (2001). Prediction of organellar targeting signals. Biochim. Biophys. Acta *1541*, 114–119.

Gasper, R., Meyer, S., Gotthardt, K., Sirajuddin, M., and Wittinghofer, A. (2009). It takes two to tango: regulation of G proteins by dimerization. Nat Rev Mol Cell Biol *10*, 423–429.

Gebert, N., Joshi, A.S., Kutik, S., Becker, T., McKenzie, M., Guan, X.L., Mooga, V.P., Stroud, D.A., Kulkarni, G., Wenk, M.R., et al. (2009). Mitochondrial Cardiolipin Involvedin Outer-Membrane Protein Biogenesis: Implications for Barth Syndrome. Current Biology *19*, 2133–2139.

Ghaemmaghami, S., Huh, W.-K., Bower, K., Howson, R.W., Belle, A., Dephoure, N., O'Shea, E.K., and Weissman, J.S. (2003). Global analysis of protein expression in yeast. Nature *425*, 737–741.

Goerke, A.R., and Swartz, J.R. (2009). High-level cell-free synthesis yields of proteins containing site-specific non-natural amino acids. Biotechnol. Bioeng. *102*, 400–416.

Gristick, H.B., Rao, M., Chartron, J.W., Rome, M.E., Shan, S.-O., and Clemons, W.M. (2014). Crystal structure of ATP-bound Get3-Get4-Get5 complex reveals regulation of Get3 by Get4. Nature Structural &Amp; Molecular Biology *21*, 437–442.

Habib, S.J., Vasiljev, A., Neupert, W., and Rapaport, D. (2003). Multiple functions of tail-anchor domains of mitochondrial outer membrane proteins. FEBS Letters *555*, 511–515.

Hegde, R.S., and Keenan, R.J. (2011). Tail-anchored membrane protein insertion into the endoplasmic reticulum. Nature Publishing Group *12*, 787–798.

Heijne, von, G. (1985). Signal sequences: the limits of variation. Journal of Molecular Biology.

Hessa, T., Sharma, A., Mariappan, M., Eshleman, H.D., Gutierrez, E., and Hegde, R.S. (2011). Protein targeting and degradation are coupled for elimination of mislocalized proteins. Nature *475*, 394–397.

Hu, J., Li, J., Qian, X., Denic, V., and Sha, B. (2009). The Crystal Structures of Yeast Get3 Suggest a Mechanism for Tail-Anchored Protein Membrane Insertion. PLoS ONE *4*, e8061.

Hunter, W.B. (2009). Medium for development of bee cell cultures (Apis mellifera: Hymenoptera: Apidae). In Vitro Cell.Dev.Biol.-Animal *46*, 83–86.

Jewett, M.C., and Swartz, J.R. (2004). Mimicking theEscherichia coli cytoplasmic environment activates long-lived and efficient cell-free protein synthesis. Biotechnol. Bioeng. *86*, 19–26.

Jonikas, M.C., Collins, S.R., Denic, V., Oh, E., Quan, E.M., Schmid, V., Weibezahn, J., Schwappach, B., Walter, P., Weissman, J.S., et al. (2009). Comprehensive Characterization of Genes Required for Protein Folding in the Endoplasmic Reticulum. Science *323*, 1693–1697.

Kalbfleisch, T., Cambon, A., and Wattenberg, B.W. (2007). A Bioinformatics Approach to Identifying Tail-Anchored Proteins in the Human Genome. Traffic *8*, 1687–1694.

Kiekebusch, D., Michie, K.A., Essen, L.-O., Löwe, J., and Thanbichler, M. (2012). Localized Dimerization and Nucleoid Binding Drive Gradient Formation by the Bacterial Cell Division Inhibitor MipZ. Molecular Cell *46*, 245–259.

Kim, D.M., and Swartz, J.R. (2001). Regeneration of adenosine triphosphate from glycolytic intermediates for cell-free protein synthesis. Biotechnol. Bioeng. *74*, 309–316.

Kohl, C., Tessarz, P., Malsburg, von der, K., Zahn, R., Bukau, B., and Mogk, A. Cooperative and independent activities of Sgt2 and Get5 in the targeting of tail-anchored proteins. Biological Chemistry *392*.

Kubota, K., Yamagata, A., Sato, Y., Goto-Ito, S., and Fukai, S. (2012). Get1 Stabilizes an Open Dimer Conformation of Get3 ATPase by Binding Two Distinct Interfaces. Journal of Molecular Biology *422*, 366–375.

Kutay, U., Ahnert-Hilger, G., Hartmann, E., WIEDENMANN, B., and Rapoport, T.A. (1995). Transport route for synaptobrevin via a novel pathway of insertion into the endoplasmic reticulum membrane. The EMBO Journal *14*, 217–223.

Kutay, U., Hartmann, E., and Rapoport, T.A. (1993). A class of membrane proteins with a C-terminal anchor. Trends Cell Biol. *3*, 72–75.

Kyte, J., and Doolittle, R.F. (1982). A simple method for displaying the hydropathic character of a protein. Journal of Molecular Biology *157*, 105–132.

Lee, J.-G., and Ye, Y. (2013). Bag6/Bat3/Scythe: A novel chaperone activity with diverse regulatory functions in protein biogenesis and degradation. Bioessays *35*, 377–385.

Leipe, D.D., Wolf, Y.I., Koonin, E.V., and Aravind, L. (2002). Classification and

evolution of P-loop GTPases and related ATPases. Journal of Molecular Biology *317*, 41–72.

Leznicki, P., and High, S. (2012). SGTA antagonizes BAG6-mediated protein triage. Proc Natl Acad Sci USA *109*, 19214–19219.

Li, C., Wen, A., Shen, B., Lu, J., Huang, Y., and Chang, Y. (2011). FastCloning: a highly simplified, purification-free,sequence- and ligation-independent PCR cloningmethod. BMC Biotechnology *11*, 92.

Mariappan, M., Li, X., Stefanovic, S., Sharma, A., Mateja, A., Keenan, R.J., and Hegde, R.S. (2010). A ribosome-associating factor chaperones tail-anchored membrane proteins. Nature *466*, 1120–1124.

Mariappan, M., Mateja, A., Dobosz, M., Bove, E., Hegde, R.S., and Keenan, R.J. (2011). The mechanism of membrane-associated steps in tail-anchored protein insertion. Nature *477*, 61–66.

Marty, N.J., Teresinski, H.J., Hwang, Y.T., Clendening, E.A., Gidda, S.K., Sliwinska, E., Zhang, D., Miernyk, J.A., Brito, G.C., Andrews, D.W., et al. (2014). New insights into the targeting of a subset of tail-anchored proteins to the outer mitochondrial membrane. Front. Plant Sci. *5*, 426.

Mateja, A., Paduch, M., Chang, H.-Y., Szydlowska, A., Kossiakoff, A.A., Hegde, R.S., and Keenan, R.J. (2015). Protein targeting. Structure of the Get3 targeting factor in complex with its membrane protein cargo. Science *347*, 1152–1155.

Mateja, A., Szlachcic, A., Downing, M.E., Dobosz, M., Mariappan, M., Hegde, R.S., and Keenan, R.J. (2009). The structural basis of tail-anchored membrane protein recognition by Get3. Nature *461*, 361–366.

Mock, J.-Y., Chartron, J.W., Zaslaver, M., Xu, Y., Ye, Y., and Clemons, W.M., Jr. (2015). Bag6 complex contains a minimal tail-anchor–targeting module and a mock BAG domain. Proc Natl Acad Sci USA *112*, 106–111.

Ogle, J.M., and Ramakrishnan, V. (2005). Structural insights into translational fidelity. Annu. Rev. Biochem. *74*, 129–177.

Okreglak, V., and Walter, P. (2014). The conserved AAA-ATPase Msp1 confers organelle specificity to tail-anchored proteins. Proc Natl Acad Sci USA *111*, 8019–8024.

Pedrazzini, E. (2009). Tail-Anchored Proteins in Plants. J. Plant Biol. *52*, 88–101.

Peluso, P., Shan, S.-O., Nock, S., Herschlag, D., and Walter, P. (2001). Role of SRP RNA in the GTPase Cycles of Ffh and FtsY †. Biochemistry *40*, 15224–15233.

Randall, L.L., and Hardy, S.J. (1995). High selectivity with low specificity: how SecB has solved the paradox of chaperone binding. Trends in Biochemical Sciences *20*, 65–69.

Rapaport, D. (2003). Finding the right organelle. EMBO Reports *4*, 948–952.

Rodnina, M.V., and Wintermeyer, W. (2001a). Fidelity of aminoacyl-tRNA selection on the ribosome: kinetic and structural mechanisms. Annu. Rev. Biochem. *70*, 415–435.

Rodnina, M.V., and Wintermeyer, W. (2001b). Ribosome fidelity: tRNA discrimination, proofreading and induced fit. Trends in Biochemical Sciences *26*, 124–130.

Rome, M.E., Chio, U.S., Rao, M., Gristick, H., and Shan, S.-O. (2014). Differential gradients of interaction affinities drive efficient targeting and recycling in the GET pathway. Proc Natl Acad Sci USA *111*, E4929–E4935.

Rome, M.E., Rao, M., Clemons, W.M., and Shan, S.-O. (2013). Precise timing of ATPase activation drives targeting of tail-anchored proteins. Proc Natl Acad Sci USA *110*, 7666–7671.

Rothblatt, J.A., and Meyer, D.I. (1986). Secretion in yeast: reconstitution of the translocation and glycosylation of alpha-factor and invertase in a homologous cell-free system. Cell *44*, 619–628.

Saraogi, I., Akopian, D., and Shan, S.-O. (2011a). A tale of two GTPases in cotranslational protein targeting. Protein Science *20*, 1790–1795.

Saraogi, I., Zhang, D., Chandrasekaran, S., and Shan, S.-O. (2011b). Site-Specific Fluorescent Labeling of Nascent Proteins on the Translating Ribosome. J. Am. Chem. Soc. *133*, 14936–14939.

Schuldiner, M., Metz, J., Schmid, V., Denic, V., Rakwalska, M., Schmitt, H.D., Schwappach, B., and Weissman, J.S. (2008). The GET Complex Mediates Insertion of Tail-Anchored Proteins into the ER Membrane. Cell *134*, 634–645.

Shan, S.-O., Schmid, S.L., and Zhang, X. (2009). Signal Recognition Particle (SRP) and SRP Receptor: A New Paradigm for Multistate Regulatory GTPases. Biochemistry *48*, 6696–6704.

Shao, S., and Hegde, R.S. (2011). Membrane Protein Insertion at the Endoplasmic Reticulum. Annu. Rev. Cell Dev. Biol. *27*, 25–56.

Siegel, V., and Walter, P. (1988). The affinity of signal recognition particle for presecretory proteins is dependent on nascent chain length. The EMBO Journal *7*, 1769–1775.

Stefanovic, S., and Hegde, R.S. (2007). Identification of a Targeting Factor for Posttranslational Membrane Protein Insertion into the ER. Cell *128*, 1147–1159.

Stefer, S., Reitz, S., Wang, F., Wild, K., Pang, Y.Y., Schwarz, D., Bomke, J., Hein, C., Lohr, F., Bernhard, F., et al. (2011). Structural Basis for Tail-Anchored Membrane Protein Biogenesis by the Get3-Receptor Complex. Science *333*, 758–762.

Suloway, C.J.M., Chartron, J.W., Zaslaver, M., and Clemons, W.M.J. (2009). Model for eukaryotic tail-anchored protein binding based on the structure of Get3. Proc. Natl. Acad. Sci. U.S.a. *106*, 14849–14854.

Suloway, C.J., Rome, M.E., and Clemons, W.M., Jr (2011). Tail-anchor targeting by a Get3 tetramer: the structure of an archaeal homologue. The EMBO Journal *31*, 707–719.

Sydow, J.F., and Cramer, P. (2009). RNA polymerase fidelity and transcriptional proofreading. Current Opinion in Structural Biology *19*, 732–739.

van Meer, G., Voelker, D.R., and Feigenson, G.W. (2008). Membrane lipids: where they are and how they behave. Nature Publishing Group *9*, 112–124.

Wang, F., Brown, E.C., Mak, G., Zhuang, J., and Denic, V. (2010). A Chaperone Cascade Sorts Proteinsfor Posttranslational Membrane Insertion into the Endoplasmic Reticulum. Molecular Cell *40*, 159–171.

Wang, F., Chan, C., Weir, N.R., and Denic, V. (2014). The Get1/2 transmembrane complex is an endoplasmic-reticulum membrane protein insertase. Nature *512*, 441–444.

Wang, F., Whynot, A., Tung, M., and Denic, V. (2011a). The Mechanism of Tail-Anchored Protein Insertion into the ER Membrane. Molecular Cell *43*, 738–750.

Wang, Q., Liu, Y., Soetandyo, N., Baek, K., Hegde, R., and Ye, Y. (2011b). A Ubiquitin Ligase-Associated Chaperone Holdase Maintains Polypeptides in Soluble Statesfor Proteasome Degradation. Molecular Cell *42*, 758–770.

Wereszczynski, J., and McCammon, J.A. (2012). Nucleotide-dependent mechanism of Get3 as elucidated from free energy calculations. Proc Natl Acad Sci USA *109*, 7759–7764.

Whitley, P., Grahn, E., Kutay, U., Rapoport, T.A., and Heijne, von, G. (1996). A 12-residue-long polyleucine tail is sufficient to anchor synaptobrevin to the endoplasmic reticulum membrane. J. Biol. Chem. *271*, 7583–7586.

Wu, C., Amrani, N., Jacobson, A., and Sachs, M.S. (2007). The Use of Fungal In Vitro Systems for Studying Translational Regulation. In Methods in Enzymology,

(Elsevier), pp. 203–225.

Yabal, M., Brambillasca, S., Soffientini, P., Pedrazzini, E., Borgese, N., and Makarow, M. (2003). Translocation of the C Terminus of a Tail-anchored Protein across the Endoplasmic Reticulum Membrane in Yeast Mutants Defective in Signal Peptide-driven Translocation. Journal of Biological Chemistry *278*, 3489–3496.

Yamagata, A., Mimura, H., Sato, Y., Yamashita, M., Yoshikawa, A., and Fukai, S. (2010). Structural insight into the membrane insertion of tail-anchored proteins by Get3. Genes to Cells *15*, 29–41.

Yin, J., Lin, A.J., Golan, D.E., and Walsh, C.T. (2006). Site-specific protein labeling by Sfp phosphopantetheinyl transferase. Nat Protoc *1*, 280–285.

Zhang, X., Rashid, R., Wang, K., and Shan, S.O. (2010). Sequential Checkpoints Govern Substrate Selection During Cotranslational Protein Targeting. Science *328*, 757–760.

Zhang, X., and Shan, S.-O. (2014). Fidelity of Cotranslational Protein Targeting by the Signal Recognition Particle. Annu. Rev. Biophys. *43*, 381–408.

Zhang, X., Kung, S., and Shan, S.-O. (2008). Demonstration of a Multistep Mechanism for Assembly of the SRP·SRP Receptor Complex: Implications for the Catalytic Role of SRP RNA. Journal of Molecular Biology *381*, 581–593.

Zhang, X., Schaffitzel, C., Ban, N., and Shan, S.-O. (2009). Multiple conformational switches in a GTPase complex control co-translational protein targeting. Proc Natl Acad Sci USA *106*, 1754–1759.

Zheng, N., and Gierasch, L.M. (1996). Signal sequences: the same yet different. Cell *86*, 849–852.